2017

Mechanical and structural contributions of extracellular matrix constituents to vascular mechanics

BOSTON UNIVERSITY

COLLEGE OF ENGINEERING

Dissertation

MECHANICAL AND STRUCTURAL CONTRIBUTIONS OF EXTRACELLULAR MATRIX CONSTITUENTS TO VASCULAR MECHANICS

by

JEFFREY M. MATTSON

B.S., Rensselaer Polytechnic Institute, 2009
M.S., University of Delaware, 2011

Submitted in partial fulfillment of the

requirements for the degree of

Doctor of Philosophy

2017

Approved by

First Reader ____
Katherine Yanhang Zhang, Ph.D.
Associate Professor of Mechanical Engineering
Associate Professor of Materials Science and Engineering
Associate Professor of Biomedical Engineering

Second Reader ____
Elise F. Morgan, Ph.D.
Professor of Mechanical Engineering
Professor of Materials Science and Engineering
Professor of Biomedical Engineering

Third Reader ____
Bela Suki, Ph.D.
Professor of Biomedical Engineering
Professor of Materials Science and Engineering

Fourth Reader ____
Michael B. Albro, Ph.D.
Assistant Professor of Mechanical Engineering
Assistant Professor of Materials Science and Engineering

"Discovery is to see what everybody else has seen, and to think what nobody else has thought." – Albert Szent-Györgyi, M.D., Ph.D.

DEDICATION

To my supportive wife, parents, brother, and sister-in-law.

ACKNOWLEDGMENTS

Many thanks to my advisor, Professor Katherine Yanhang Zhang, who helped me grow professionally as well as personally. Katherine perfected the balance of letting me challenge myself to conduct independent research while keeping me on the path towards progress. She provided the necessary motivation at key points during my development and always served as a reminder for the awe-inspiring capacity of learning the hidden language of natural phenomena.

I would also like to honorably thank my dissertation committee for their service and advice throughout my education: Professors Elise Morgan, Bela Suki, and Michael Albro. Thank you Raphael Turcotte and Dr. Tarik Haydar for your collaboration and training me to use the multiphoton microscope. Thank you Marina Nicolas Chueca for pointing out the lack of existing research characterizing vena cava structure and mechanics. Thank you Joann Buczk-Thomas for training me how to do the DMB assay. Thank you Dr. Katya Ravid for the T32 funding and multidisciplinary group meetings.

Additionally, thank you to my labmates for joining me on this journey and engaging in thoughtful discussions: Sella Yunjie Wang, Xunjie Yu, Haiyue Li, Ming-Jay Chow, Shahrokh Zeinali-Davarani, Bin Xu, Hyung Jin Sun, Jacob Hahn, and John Burns.

MECHANICAL AND STRUCTURAL CONTRIBUTIONS

OF EXTRACELLULAR MATRIX CONSTITUENTS

TO VASCULAR MECHANICS

JEFFREY M. MATTSON

Boston University, College of Engineering, 2017

Major Professor: Katherine Yanhang Zhang, Ph.D., Associate Professor of Mechanical Engineering, Associate Professor of Materials Science and Engineering, Associate Professor of Biomedical Engineering

ABSTRACT

Elastic and collagen fibers are the major load-bearing extracellular matrix (ECM) constituents of the vascular wall. Elastic fibers accommodate repeated cycles of extension and recoil that occur during pulsatile blood flow at lower levels of strain, whereas the recruitment of collagen fibers at higher levels of strain leads to nonlinear stiffening that protects blood vessels from overextension. Glycosaminoglycans (GAGs) provide a structural basis for multiple biological functions, such as the organization of ECM and the regulation of cell growth factors. There exists a complex interdependence of ECM compositional, structural, and mechanical properties. The overall goal of the research is to study the biomechanical and structural roles of different ECM constituents in vascular mechanics through coupled mechanical testing, advanced optical imaging, and microstructure-based constitutive modeling.

Arteries function differently than veins in the circulatory system, however in several treatment options veins are subjected to sudden elevated arterial pressure. Our study improves the understanding of elastin and collagen fiber contribution to ECM

mechanics of different vessel types. Our research demonstrates that ECM fiber distribution, recruitment, and content each play an important role in vascular function, and the important structural and functional differences between arteries and veins that should be taken into account when considering treatment options. While elastin and collagen have received extensive consideration, little is known about the biomechanical roles of GAGs in blood vessels. The mechanics of tissue with low GAG content can be indirectly affected by the interaction of GAGs with collagen fibers, which is one of the primary contributors to arterial mechanics. Our study suggests that that the interaction between GAGs and other ECM constituents plays an important role in the mechanics of the arterial wall, and GAGs should be considered in addition to elastic and collagen fibers when studying arterial function. A structure-based constitutive model was then developed to successfully predict arterial mechanics considering the contribution of GAGs to fiber recruitment. Building upon previous research, ongoing work is presented to study the fundamental yet clinically relevant structural-mechanical behavior of arterial ECM in diabetes using an integrated experimental and modeling approach.

TABLE OF CONTENTS

LIST OF TABLES

LIST OF FIGURES

CHAPTER 1 INTRODUCTION

1.1 Objectives

The extracellular matrix (ECM) in the vascular wall is largely composed of elastic and collagen fibers, as well as ground substance including glycosaminoglycans (GAGs), which together compose the ECM interspersed among organized layers of cells to form lamellar structures. The elastic fibers are essential to accommodate deformations encountered during physiological function of arteries, which undergo repeated cycles of extension and recoil. The extensibility and the ultimate stiffness of the tissue in the stiffened region are highly associated with the content and distribution of collagen fibers. GAGs constitute only a minor component of vascular tissue, however previous studies have demonstrated that these macromolecules are of enormous importance in influencing vascular properties such as viscoelasticity, permeability, hemostasis, etc. The pathogenesis of many cardiovascular diseases has been associated with loss of organization and function of the ECM. The mechanical and structural contributions of ECM constituents are not fully understood. This knowledge is essential for understanding the mechanisms of vascular remodeling and disease progressions. The main goal of this dissertation is to advance the current understanding of the microstructure of elastin, collagen, and GAGs in the ECM and provide insights how these constituents work in conjunction to provide the passive mechanical behavior of large central blood vessels.

1.2 Cardiovascular Diseases and ECM Remodeling

Cardiovascular diseases are the leading cause of death in the western world. It is responsible for 40 percent of all the deaths in the United States, more than all forms of cancer combined ("Disease Statistics - NHLBI, NIH," 2012). While cardiovascular disease is a broad term used to describe a range of diseases that affect heart and blood vessels, arteriosclerosis or hardening of the arteries is presented in many of these diseases, particularly diabetes. The ECM of the vascular wall plays an important role in the pathogenesis of arteriosclerosis. The prevailing concept is that elastin and collagen are the primary load-bearing components of vascular tissue. The carbohydrate-protein macromolecules of the interstitial matrix, GAGs, are of particular interest since these macromolecules affect mechanical properties of other soft tissues, but are only recently gaining attention in the vascular wall. Pathogenesis of vascular diseases, including diabetes, hypertension, atherosclerosis, stenosis, and aneurysms has been associated with ECM disorders in structure and function. Such understandings are much needed in order to incorporate quantitative information from future advances in vascular biology, medical imaging, and biomechanics.

As a result of vascular diseases, changes in the pressure/flow conditions, or local injuries to the tissue, the mechanical properties of blood vessels can change significantly. Due to the seriousness of cardiovascular diseases, improvements to diagnosis and treatments of the clinical conditions are desirable. Balloon angioplasty of narrowed arteries is a common surgical procedure to restore blood flow in narrowed arteries. However, this palliative treatment can result in tears in the intima (Sohn et al., 1994) and understanding how the damage can change vascular mechanics is important. Finally bypass surgeries can utilize a variety of grafts ranging from a patient's own saphenous vein, synthetic material grafts, or one made from decellularized tissue (Quint et al., 2011). Being able to more closely replicate the structure and mechanical properties of healthy blood vessels allows for a higher rate of success in bypass surgeries. As these examples show, a strong understanding of how the organization and composition of the ECM affects the mechanical properties of the vascular wall can be beneficial to identifying and treating vascular ailments and plays an important role in clinical and tissue engineering fields.

1.3 Structure of the Vascular Wall

The vascular wall consists of three layers: the intima, media, and adventitia (Figure 1.1). The intimal layer is closest to the lumen, composed of a layer of endothelial cells, and important for providing hemocompatibility with blood (Wagenseil and Mecham, 2009). The media is composed of vascular smooth muscle cells, collagen and elastic fibers, and proteoglycans made up of GAGs attached to a core protein. The adventitia consists primarily of fibroblast cells and large crimped collagen fiber bundles, which play an important role in preventing vascular rupture at high pressures (Burton, 1954).

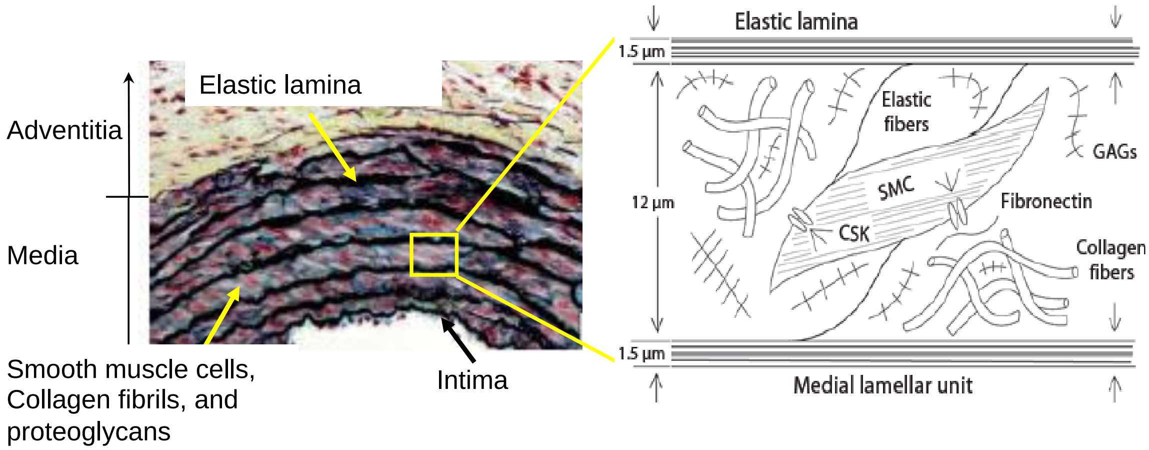

Figure 1.1. Left: Histological image showing intima, media, and adventitia in vascular wall. Right: Schematic drawing of normal medial lamellar unit consisting of paired elastic laminae (at the top and bottom) with an embedded smooth muscle cell (SMC) as well as collagen fibers, elastic fibers, adhesion molecules (fibronectin), and GAGs (Humphrey, 2012).

The structural proteins elastin and collagen account for ~50% of the dry weight of the vessel (O'Connell et al., 2008), and are essential to accommodate deformations encountered during physiological functions. GAGs constitute only a minor component of vascular tissue (2%–5% by dry weight) as compared to cartilage (50% by dry weight), however these macromolecules are of enormous importance in influencing vascular properties such as viscoelasticity, thrombosis, permeability, lipid metabolism, and hemostasis of the arterial wall (G. S. Berenson et al., 1984; Camejo, 1982; Wight, 1989).

1.4 Outline of the Research

In Chapter 2, the experimental techniques used in this research are introduced, including histology, assays, biaxial tensile testing, and multiphoton microscopy.

In Chapter 3, we compared the structure and mechanics of porcine aorta and vena cava. Equibiaxial tensile tests were performed to study the differences of elastic properties between the central artery and central vein. The resulting mechanics were then paired with histology, assays, and multiphoton microscopy to establish structure-function relationships of elastin and collagen contributions to vascular mechanics.

In Chapter 4, we investigated the role of GAGs in porcine thoracic aorta. Planar biaxial tensile and stress relaxation tests were conducted before and after enzymatic GAG depletion. The mechanics were again paired with structural analysis to consider the role of GAGs in addition to elastin and collagen in elastic and viscoelastic vascular mechanics.

In Chapter 5, we modeled the contribution of GAGs to fiber recruitment in arterial mechanics. The experimental data from Chapter 4 were used to determine the microstructure-based constitutive model parameters based on untreated aorta samples. The model was then used to successfully predict the stress-stretch behavior of GAG depleted aorta based on measured changes to ECM fiber orientation and recruitment.

In Chapter 6, we extended our experimental expertise from the porcine animal model to human aorta of diabetic, hypertensive and age-matched control donors to understand the role of elastin, collagen, and GAGs in vascular remodeling during the normal aging process compared to changes due to diabetes and hypertension.

In Chapter 7, conclusions and outlook of future work are presented.

CHAPTER 2 EXPERIMENTAL METHODS

2.1 Overview

This chapter gives an introduction to the experimental techniques used in this research, including histology, biochemical assays, biaxial tensile testing, and multiphoton microscopy.

2.2 Histology

Histology studies were performed to assess the overall structural composition of blood vessels. Samples were fixed in 10% formalin buffer (Fisher Scientific, Waltham MA) and then imbedded in paraffin. Sections of approximately 6 µm in thickness were obtained and stained with either Movat’s pentachrome or Alcian blue (Figure 2.1). Movat’s pentachrome stains collagen yellow, elastin black, smooth muscle cells red, and GAGs blue. Alcian blue stains GAGs blue.

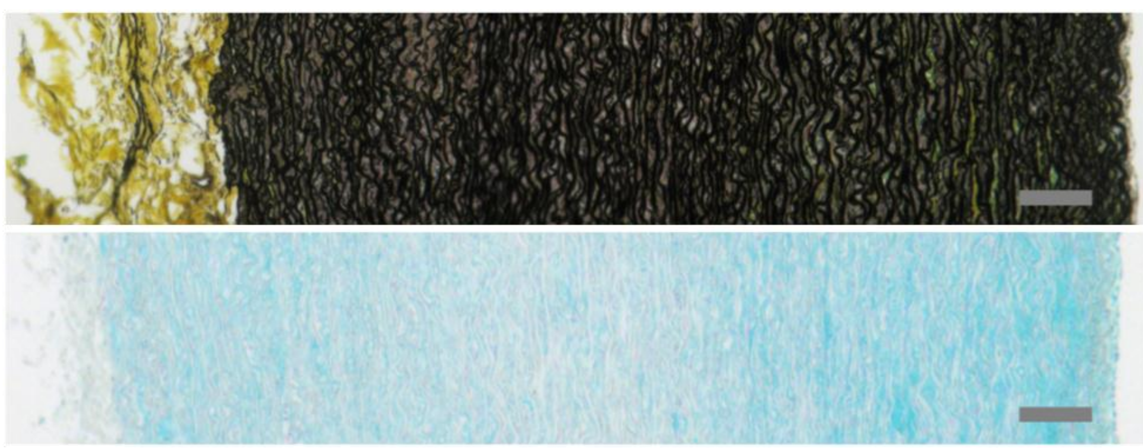

Figure 2.1. Examples of histology stains of aorta with adventitia on the left and intima on the right. Top: Movat’s pentachrome. Bottom: Alcian Blue. Scale bars are 100µm.

2.3 Biochemical assays

Biochemical assays allow quantification of elastin and collagen content. Samples were analyzed using a Sircol collagen assay kit following manufacture instructions (Biocolor Ltd.). The Sircol collagen kit uses a quantitative dye-binding method and absorbance was measured using a SpectraMax M5 plate reader (Molecular Devices) at a 540 nm wavelength. Collagen content was expressed as µg of collagen/mg of wet tissue weight. Elastin content was measured using Fastin elastin assay kit (Biocolor Ltd.). Following manufacture's protocols, our assays measured soluble tropoelastins and insoluble elastin that was solubilized into α-elastin polypeptides. The optical density was measured at 513 nm using the microplate reader. Elastin content was also expressed as µg of elastin/mg of wet tissue weight.

2.4 Biaxial Tensile Testing

To fully characterize anisotropic biological tissue, a custom designed biaxial tensile testing device was used to mechanically test the tissue samples following protocols described previously (Chow et al., 2013; Grashow et al., 2006; Zou and Zhang, 2011). Briefly, tissue deformation, stretch, was measured by tracking four carbon marker dots on the tissue during a tension control protocol using a custom LabVIEW program (Figure 2.1). Samples were hooked on each edge and connected to the linear positioners with sutures. A plane stress state is assumed since the thickness of the sample was small compared to the length and width. Soft biological tissues are also considered to be incompressible so that the volume of the sample is preserved during loading.

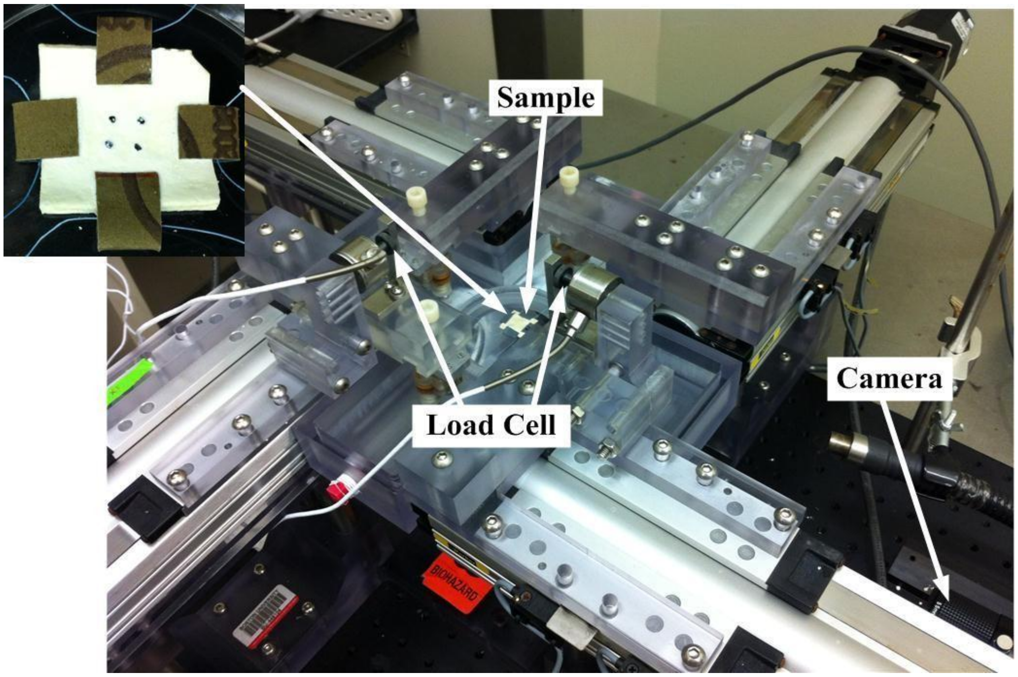

Figure 2.1. Picture of the biaxial tensile tester showing the sample mounted to the linear positioners with the sutures looped through the sandpaper fold glued to each side.

2.4.1 Biaxial Tensile Test

A preload of 5 ± 0.050 N/m was applied in order to straighten the sutures connecting the tissue to the device. Samples were loaded with 10 s half-cycles at 50 N/m until a consistent preconditioning response was achieved. Then the samples were subjected to equibiaxial and nonequibixial loading conditions to characterize the anisotropic mechanical behavior. The last cycle of a synchronized biaxial response was used for data analysis. Cauchy stresses were calculated as:

$$\sigma_1 = \frac{F_1\lambda_1}{tL_{o2}}, and \quad \sigma_2 = \frac{F_2\lambda_2}{tL_{o1}}$$

where F is the applied load, λ is the stretch, L_o is the initial length, and t is the thickness of the tissue. The subscripts 1 and 2 correspond to the longitudinal and circumferential directions.

2.4.2 Stress Relaxation Test

For stress relaxation tests, immediately following the last quasi-static equibiaxial cycle, tension was reapplied with a 2 s rise time and held at a constant stretch for 900 s. This cyclic tension followed by stress relaxation protocol was repeated 3 to 4 times to achieve a consistent response (Zou and Zhang, 2011). To quantify stress relaxation, normalized stress relaxation curves are obtained by normalizing to the peak stress averaged with 20 data points from the beginning of the stress relaxation test (+/- 10ms) to produce a better representation of the peak stress. Percent stress relaxation is taken as the decrease in normalized value for the end of the test at 900s.

2.5 Multiphoton Microscopy

To understand the contribution of collagen and elastin fibers to the structure and function of the vascular wall, mechanical loading was paired with multiphoton imaging of tissue (Figure 2.2) following methods detailed by Chow et al. (Chow et al., 2014). Briefly, a mode-locked Ti:sapphire laser (Maitai-HP, excitation wavelength 800 nm, 100 fs pulse width, 80 MHz repetition rate, Spectra-Physics, Santa Clara, CA) was used to generate second-harmonic generation from collagen (417/80 nm) and two-photon-excited fluorescence from elastin (525/45 nm) in the vascular wall. Each sample was imaged with a field-of-view of 360 μm at nine locations spread over an area of 1 cm^2 to obtain the average structural properties of the sample (i.e. to minimize local artefact). Samples were imaged from both the adventitial and medial surfaces to assess adventitial collagen as well as medial collagen and elastin. Due to signal strength differences, the average power was consistently set to 40 mW for the media and 25 mW for the adventitia. The adventitial side was imaged to a depth of 60 μm, whereas the medial side was imaged to a depth of 40 μm and maximum intensity projections of the Z-stacks were made. Images were cropped from 360x360 μm^2 to 110x110 μm^2 regions with optimal fiber coverage, which were used for analysis. All samples were imaged with the circumferential direction of the tissue aligned horizontally. Thus, fibers oriented at 0° and ±90° are in the circumferential (C) and longitudinal (L) anatomic directions of the blood vessel, respectively.

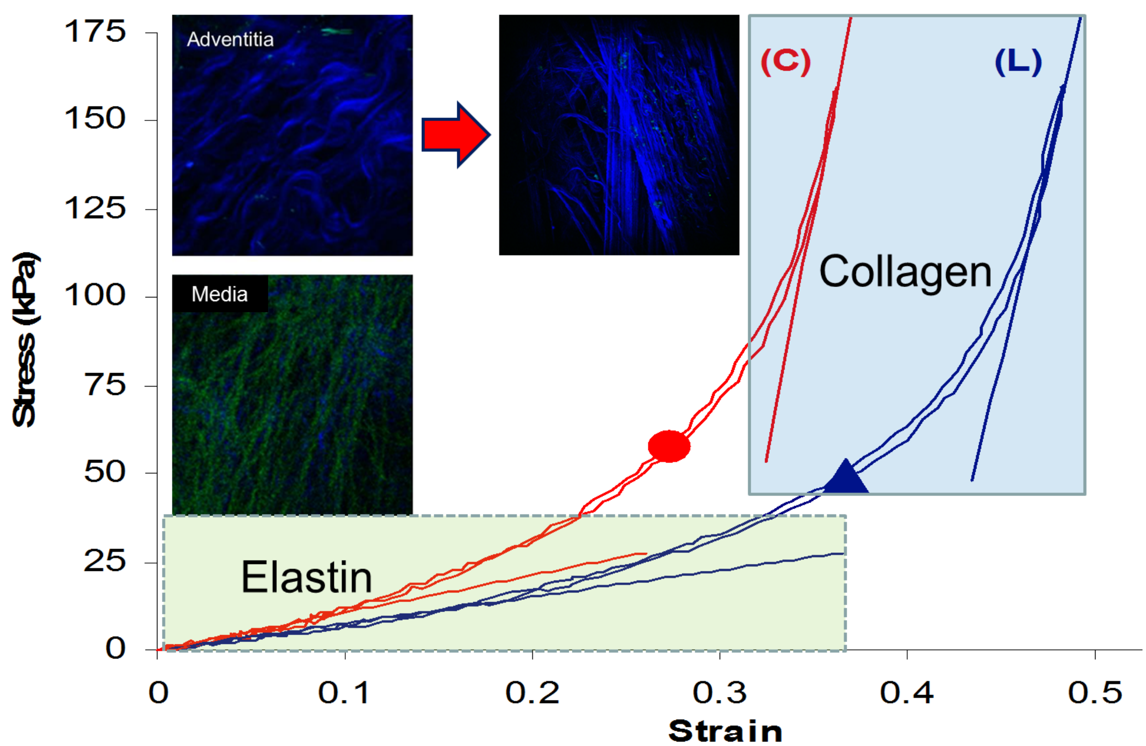

Figure 2.2. Representative biaxial stress-strain curves of the vascular wall with inset multiphoton images of medial elastin (green) and collagen (blue) at low levels of strain and adventitial collagen (blue) being recruited at higher levels of strain. Images are 110x110 μm^2, (C) = circumference, (L) = longitude.

CHAPTER 3 COMPARISON OF AORTA AND VENA CAVA EXTRACELLULAR MATRIX STRUCTURE AND BIAXIAL MECHANICAL PROPERTIES

3.1 Overview

Elastic and collagen fibers are well-known to be the major load-bearing extracellular matrix (ECM) constituents of the vascular wall. Elastic fibers accommodate repeated cycles of extension and recoil that occur during pulsatile blood flow at lower levels of strain, whereas the recruitment of collagen fibers at higher levels of strain leads to nonlinear stiffening that protects blood vessels from overextension. Arteries function differently than veins in the circulatory system, however in several treatment options veins are subjected to sudden elevated arterial pressure. It is important to understand the fundamental structure and function differences between a vein and an artery. Our research compared the relationship between biaxial mechanical function and ECM structure of porcine thoracic aorta and inferior vena cava. Physiologically, aorta is subject to higher, cyclical transmural pressure (76–114 mmHg) than vena cava, which is a capacitance vessel that stores blood at non-pulsatile pressures of <30 mmHg. Findings suggest that aorta contains slightly more elastin than collagen due to the cyclical extensibility, but vena cava contains almost four times more collagen than elastin to maintain integrity without the need for cyclical extensibility. Furthermore, multiphoton imaging of vena cava showed longitudinally oriented elastin and circumferentially oriented collagen that is recruited at supraphysiologic stress, but low levels of strain. These structural observations support the functional finding that vena cava is highly anisotropic with the longitude being more compliant and the circumference stiffens substantially at low levels of strain. Overall, our research demonstrates how elastic and collagen fibers contribute to the mechanical and structural properties of blood vessels. Specifically, fiber distributions and recruitment should be considered in addition to relative collagen and elastin amounts. Also, the importance of accounting for the structural and functional differences between arteries and veins should be taken into account when considering disease treatment options.

3.2 Introduction

Vein graft failure is a common finding in patients following coronary artery bypass graft (CABG) surgery. Thrombosis or the development of a blood clot, neointimal hyperplasia characterized by thickening of the innermost layer of a vein or artery, and atherosclerosis are the three progressive stages that lead to stenosis or occlusion of the graft. Within 5 years after CABG surgery, about 30–50% patients develop vein graft failure and require repeated surgery (Desai et al., 2010). Vein graft failure has a huge economic effect on health care resources, and a devastating effect on the patient. Understanding the mechanisms of venous graft failure is predicated upon elucidating the structural and functional mismatch between arteries and veins. From the biomechanical point of view, the proliferative structural remodeling of a vein graft occurs in order to maintain the wall stresses at its biologically preset level. Following implantation, the vein graft, which has been subjected to an internal pressure of 10 mmHg, is immediately subjected to arterial pressure (100 mmHg) and increaseas in flow as well as wall stresses. Previous research has shown that the abrupt increase of mechanical wall stresses and flow fields in the vein graft activate various cellular and intracellular signaling molecules, which stimulate vascular smooth muscle cells in the media to be synthetic and migratory, accelerating the progression of neointimal hyperplasia (John, 2009; Miyake et al., 2008). The relationship between biological remodeling and mechanical function is obviously causal. However the significant structural and functional differences between veins and arteries are not well understood.

It is important to understand that the veins and arteries are very different in both function and structure. Both arteries and veins have three layers: tunica intima, media, and adventitia. The thinnest layer is the innermost layer, the tunica intima, which is made up of a single layer of endothelial cells and its main purpose is to provide hemocompatibility with the blood. In arteries the thickest layer is the tunica media, i.e., the middle layer of the vessel wall. The tunica media layer contains smooth muscle cells that are embedded in a matrix of elastic lamella, collagen fibers, as well as aqueous ground substance matrix containing proteoglycans. Arteries tend to have a thicker tunica media layer in order to accommodate the pulsatile blood flow. However veins have a relatively thin tunica media layer. The outermost layer in the vessels is the tunica adventitia or tunica externa, which provides structural stability of the vessels. It is consists primarily of a dense network of type I collagen fibers. The structural difference between arteries and veins are obvious. However the differences between the biomechanical roles of ECM constituents, such as elastin and collagen, in controlling arterial and venous function is underrecognized.

The overall goal of this study was to evaluate the relationship between extracellular matrix (ECM) structure and biaxial mechanical properties for aorta and inferior vena cava. In contrast to many studies of aorta mechanics, only limited prior study concerning biaxial mechanical properties of inferior vena cava (Lee et al., 2013; McGilvray et al., 2010) has been performed, despite 60–80% of blood volume being localized in veins (Monos et al., 1995). Uniaxial tests (Alastrué et al., 2008; Rossmann, 2010; Silver et al., 2003) have been used to determine the mechanical properties of veins, but these results are inadequate for fully characterizing the anisotropic behavior of vena cava. Vena cava grafts and stents are relevant to leimyosarcoma, complications from liver transplants, and aortocaval fistulas from ruptured atherosclerotic abdominal aortic aneurysms (Alkhalili et al., 2016; Huang et al., 2015; Ng et al., 2015; Wachtel et al., 2015).Improved understanding of vein mechanics will aid in the development of tissue engineered autologous and non-autologous vena grafts. Findings from this study will help us understand the fundamental structure-function relationship between ECM fiber distribution and recruitment with the complex nonlinear and anisotropic vascular behavior.

3.3 Materials and Methods

3.3.1 Sample Preparation

Porcine (12–24 months, 160–200 pounds) descending thoracic aortas and inferior vena cavas were obtained from a local abattoir and cleaned of loose connective/fatty tissue. Duplicate square samples (~20x20 mm) were cut from 3 of each blood vessel type, for a total of 6 aorta samples and 6 vena cava samples. Samples were cut with one edge parallel to the longitudinal direction and the other edge parallel to the circumferential direction of the blood vessel.

3.3.2 Histology

Movat's pentachrome stain was used to compare the overall structural composition of aorta and vena cava. Refer to Chapter 2.2 for details.

3.3.3 Biochemical assays

For the elastin and collagen assays, adjacent tissue from each blood vessel next to where biaxial samples were cut was used. Refer to Chapter 2.3 for further details.

3.3.4 Biaxial Tensile Test

Refer to Chapter 2.4 and 2.4.1 for the biaxial tensile testing protocol. For this experiment, samples were subjected to a 400 N/m equibiaxial loading condition to characterize the anisotropic mechanical behavior.

3.3.5 Multiphoton Microscopy

Refer to Chapter 2.5 for multiphoton microscopy imaging. Vena cava in this experiment was imaged with a Carl Zeiss LSM 710 NLO microscope system equipped with a Coherent Chameleon Vision–S tunable femtosecond IR pulse laser with an excitation wavelength of 800nm. Power was tuned to approximately 11% of 1900mW, not including attenuation from the optics. Each sample was imaged with a field-of-view of 425 μm at five locations spread over an area of 1 cm^2. The other settings were matched to those of the custom multiphoton microscope used to image aorta. Aorta samples were imaged from 0 to 40% equibiaxial strain in 5% increments. Vena cava samples were imaged at 0%, 5%, and 10% equibiaxial strain, then 10C-20L, and 10C-30L due to the higher degree of anisotropy. The images were then used in the analysis of fiber straightening and recruitment in response to mechanical loading.

3.3.6 Imaging analysis

Fiber orientation and frequency of fiber angle were determined from two-dimensional fast Fourier transform analysis using the Directionality plug-in in FIJI (fiji.sc/Fiji, Ashburn, VA) following the developer's instructions. Adventitial collagen fiber waviness was quantified with NeuronJ (imagescience.org/meijering/software/neuronj) by measuring the end-to-end distance (L_o) and total fiber length (L_f), to define a straightness parameter:

$$P_s = L_o / L_f$$

which is equal to 1 for a straight line (Chow et al., 2014).

3.3.7 Statistical Analysis

Blood vessel thickness, collagen and elastin assay results, stress-stretch data, and straightness parameter are summarized and plotted with mean ± standard error of the mean. Two-tailed independent t-tests were used for analysis with $p<0.05$ considered as statistically significant.

3.4 Results

Movat's histological stain revealed some interesting differences between aorta and vena cava (Figures 3.1a–c). In aorta, collagen (yellow) is most visible in the adventitia, but also exists throughout the media where elastin (black) is most prominent. In vena cava, collagen is visible throughout the thickness, however elastin appears to be discontinuous. As discussed later, the scattered appearance of elastin is due to looking at the cross section of longitudinal elastin. Smooth muscles cells (red) are also visible in the aorta media, but are less apparent in the vena cava. Glycosaminoglycans (blue) can be seen in parts of the aorta media, especially towards the inner third of the wall. The adventitia-media boundary is also more obvious in aorta than it is in vena cava. Additionally, the average aorta thickness (1.32±0.086 mm) was almost twice as much as vena cava (0.66±0.072 mm). Collagen and elastin assay results confirm that collagen:elastin ratio is lower in aorta 1:1.5 and higher in vena cava ~4:1 (Figure 3.1d).

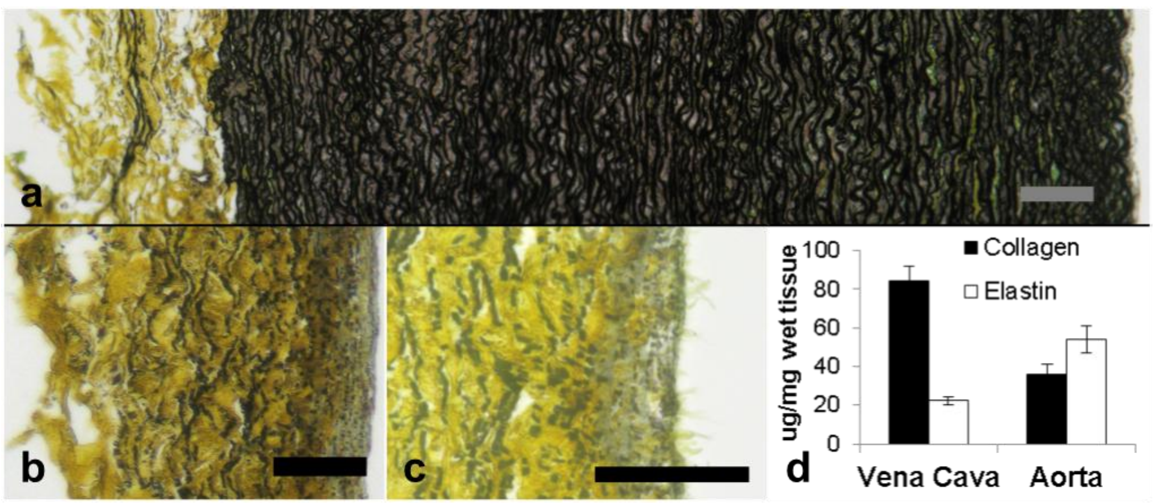

Figure 3.1. Movat's stain of aorta (a) and vena cava (b, c) from adventitia (left) to intima (right). Scale bars are 100 µm. The adventitia is primarily collagen (yellow) and media is mostly elastin (black) with smooth muscle (red), collagen, and GAGs (blue). Collagen and elastin assay results (d) show vena cava is primarily collagen (collagen: 84±8, elastin: 22±2), but aorta has more elastin (collagen: 36±5, elastin: 54±7).

The average equibiaxial stress-stretch curves demonstrate marked differences in anisotropy between aorta and vena cava (Figure 3.2a). Both aorta and vena cava show a stiffer circumference than the longitude, however much greater anisotropy was observed in vena cava. At 200 kPa, the average vena cava circumference does not stretch much beyond 1.06, whereas the average longitude stretches to 1.30. In contrast, average aorta circumference and longitude stretch to the range of 1.19 to 1.22 at 200 kPa.

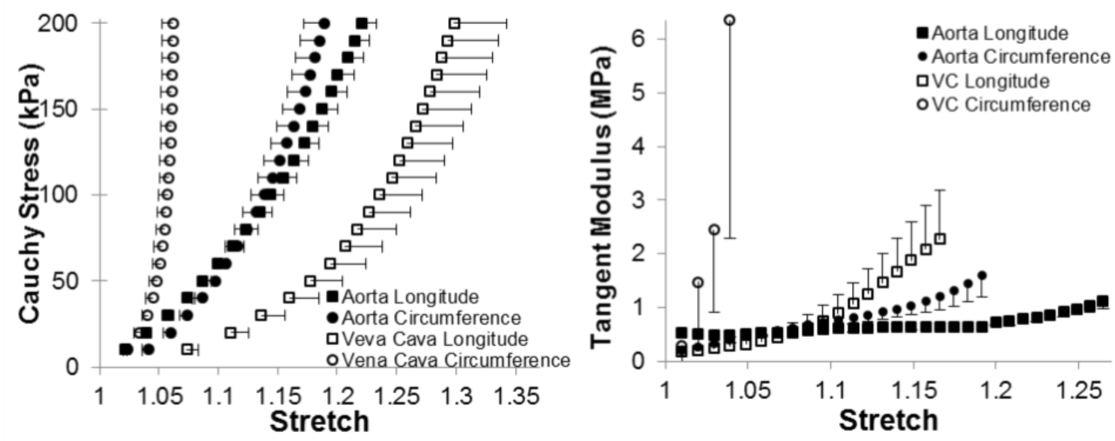

Figure 3.2. Average stress-stretch curves (a) for equibiaxial tests of aorta and vena cava with the vena cava being more anisotropic than aorta due to a stiffer circumference and more compliant longitude. Tangent modulus (b) was determined by fitting a 6th order polynomial in 0.1 increments of stretch up to the largest value that all samples experienced for each curve.

A detailed exploration of the structural differences between aorta and vena cava was made possible by using a multiphoton microscope. Figure 3.3 shows the organization of elastin (green) and collagen (blue) in the medial and adventitial layers of the two vascular types. Overall, the ECM fibers in aorta appear to be more uniformly distributed than vena cava. The elastin fibers in vena cava show an obvious longitudinally orientation, whereas medial and adventitial collagen fibers are predominantly circumferentially oriented. It is also noticed that the vena cava adventitial collagen seems to have a tighter crimp than aorta. Looking specifically at multiphoton images of vena cava at different levels of strain, adventitial collagen clearly begins straightening with 5% strain and is fully recruited at 10% strain (Figure 3.4). Additionally, medial collagen can be seen crimped at 0%, but straighter at 5% and straight at 10% strain. Elastin fibers are longitudinally oriented, and show minimal visual changes.

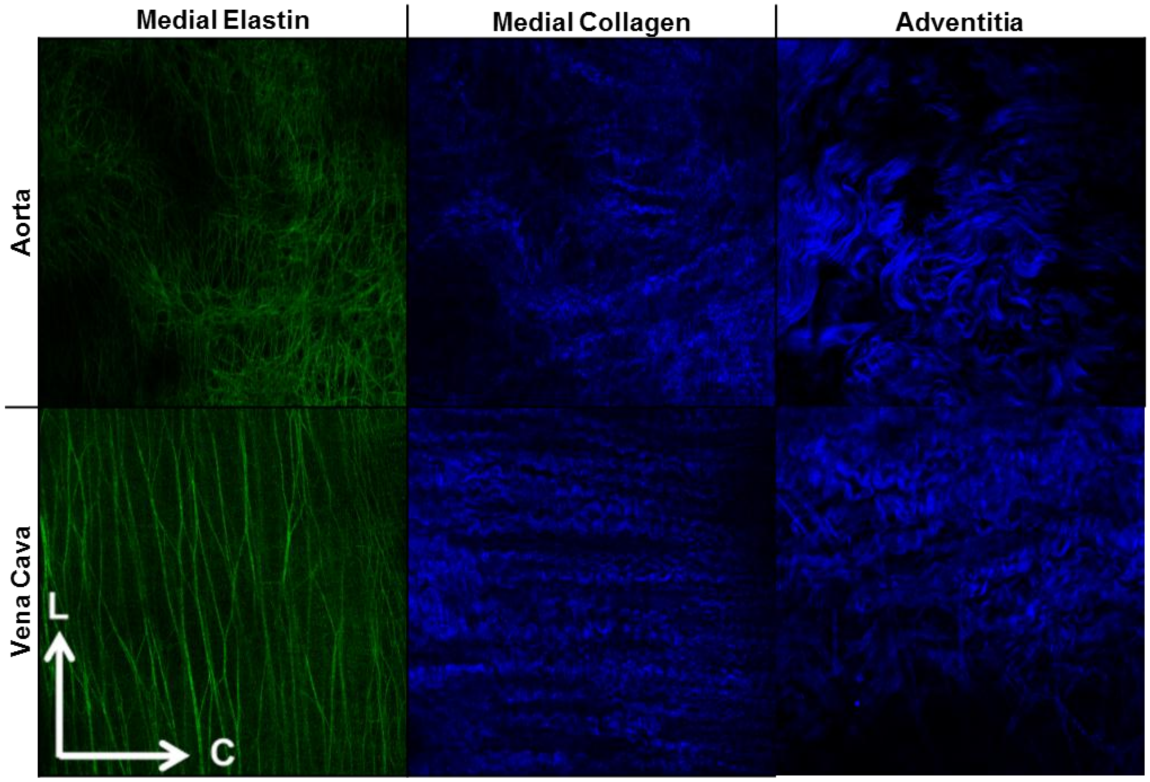

Figure 3.3. Multiphoton images of unstretched media and adventitia for both aorta and vena cava. In vena cava, elastin (green) is generally longitudinally oriented and medial collagen (blue) is generally circumferentially oriented, but medial fibers are more uniformly distributed in aorta. Adventitial collagen (blue) is wavy, but straightens with stretch. Circumferential (C) and longitudinal (L) directions are at 0° and ±90°, respectively. Images are 425µm x 425µm.

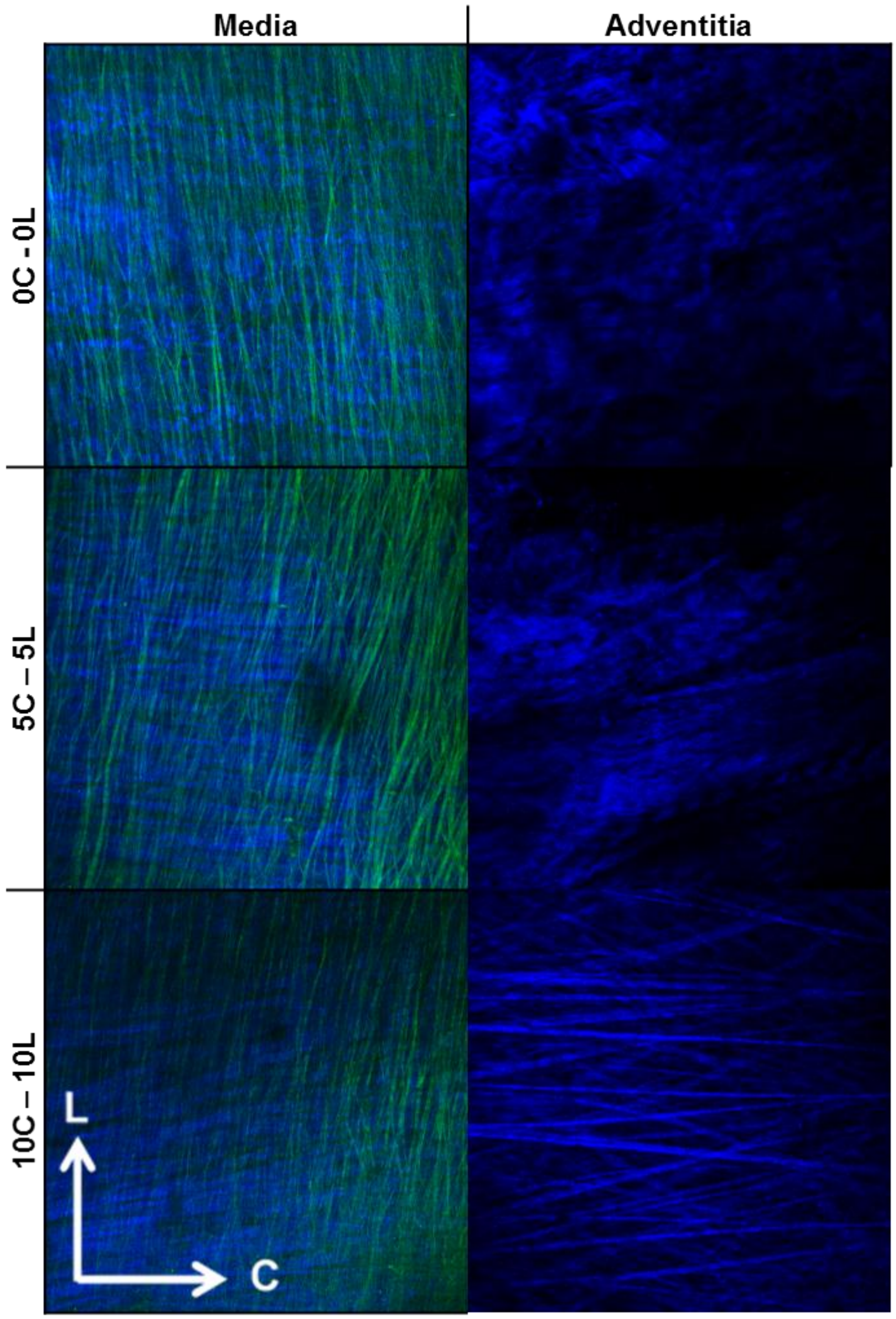

Figure 3.4. Multiphoton images of vena cava, where the numbers represent grip-to-grip strain for circumferential (C) and longitudinal (L) directions at 0° and ±90°, respectively. Elastin (green) is generally longitudinally oriented and medial and adventitial collagen (blue) are generally circumferentially oriented. Collagen is wavy at 0C-0L, but straightens with stretch. Images are 425μm x 425μm.

Straightness parameter (P_s) was used to quantify the waviness of adventitial collagen in aorta and vena cava (Figure 3.5), which did not show significant difference at unstretched (zero equibiaxial strain) state. However, the vena cava adventitial collagen fibers are significantly straighter at 5% and 10% equibiaxial strain than aorta ($p<0.05$). Vena cava was not stretched further due to the very stiff circumference (Figure 3.2). The fibers at 10% equibiaxial strain are essentially straight (P_s=0.98±0.0016). Aorta adventitial collagen did not reach that level until at about 40% strain (P_s=0.99±0.0080).

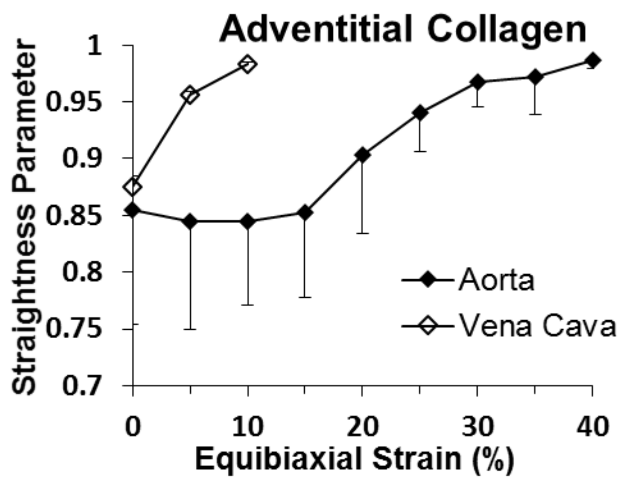

Figure 3.5. Straightness parameter (P_s) for adventitial collagen. The straightness parameter of a straight line is equal to 1. Vena cava adventitial collagen fibers are recruited immediately with stretch and fully straightened by 10% strain, whereas aorta fibers show a delayed recruitment beginning between 15–20% strain. These findings agree with the mechanics where the circumferential direction of vena cava becomes very stiff at low levels of strain.

Figure 3.6 further compares distributions of aorta and vena cava ECM fibers with mechanical loading. The aortic elastin is relatively uniformly distributed, whereas the vena cava elastin is longitudinally oriented. Overall the distribution of elastin fibers shows minimal changes with increasing strain. Both medial and adventitial collagen fibers show preferential distributions in the circumferential direction within the 10%

strain range. Vena cava becomes more circumferentially aligned with increasing strain.

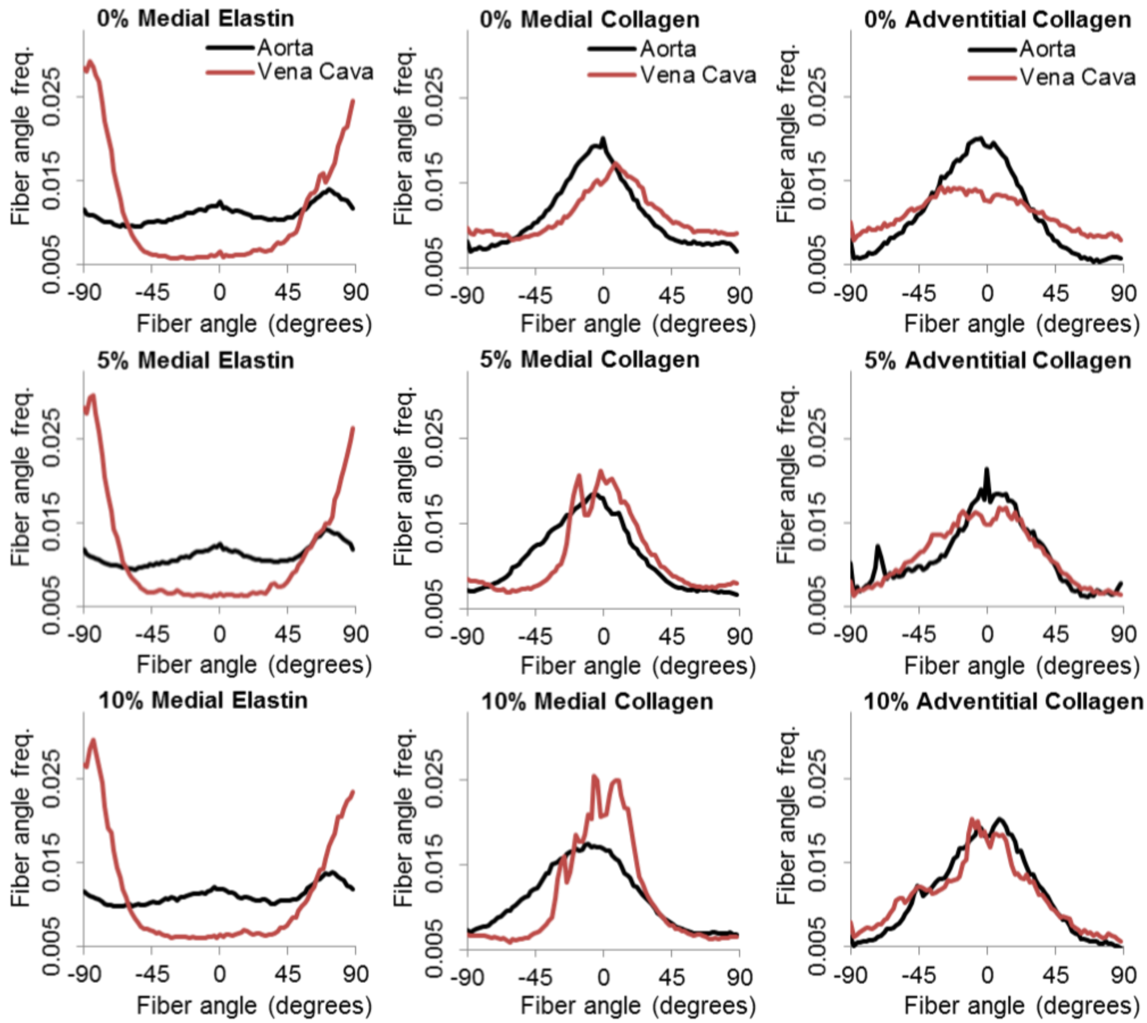

Figure 3.6. Fiber distributions, where the numbers represent grip-to-grip strain for circumferential (C) and longitudinal (L) directions at 0° and ±90°, respectively. The most striking difference is the longitudinally oriented elastin in vena cava. Aorta collagen fibers are more circumferentially aligned than in vena cava when unloaded, but with stretch, vena cava collagen fibers become more circumferentially aligned.

To study fiber reorientation with deformation, the vena cava was subjected to 10%C-20%L and 10%C-30%L nonequibiaxial strain, where C and L represents the circumferential and longitudinal directions, respectively (Figure 3.7). Minimum changes were observed in elastin fibers. However the circumferentially oriented medial and adventitial collagen fibers show wider distributions, suggesting that the circumferentially orientated fibers begin to shift towards the longitudinal direction in response to the large longitudinal deformation.

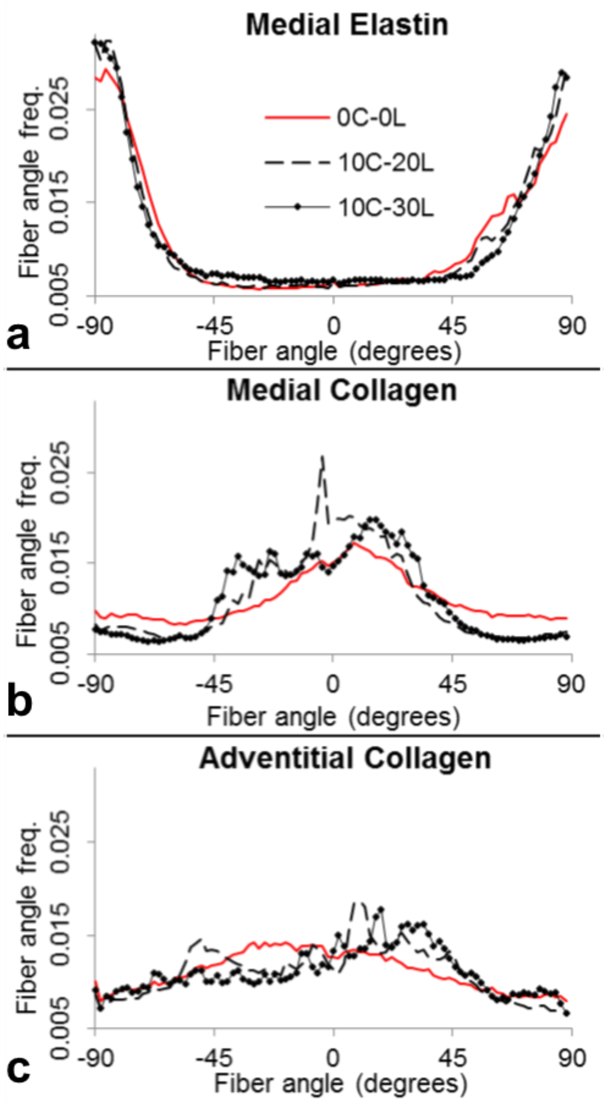

Figure 3.7. Vena cava fiber distributions, where the numbers represent grip-to-grip strain for circumferential (C) and longitudinal (L) directions at 0° and ±90°, respectively. The circumference was only stretched to 10% strain because of the high degree of anisotropy. Medial elastin (a) remains longitudinally oriented with stretch and becomes more so with greater stretch in the longitudinal direction. Medial Collagen (b) becomes more circumferential with stretch, but the distribution widens with fibers shifting more longitudinally with greater longitudinal stretch. Adventitial collagen (c) behaves similarly to medial collagen.

3.5 Discussion

Aorta and vena cava have different functions in the circulatory system. Our study revealed fundamental differences in ECM composition, fiber distribution and recruitment between aorta and vena cava. Moreover, these structural characteristics correlate very well with their biaxial stress-strain mechanical behavior. Whereas the arterial wall is subjected to a pulsatile transmural pressure of approximately 76–114 mmHg (Kim and Baek, 2011), mechanical loads borne by veins are quite different. Blood pressure in veins is not pulsatile, but steady and much lower than the arterial pressure. Veins are capacitance vessels with greater compliance at low pressure but very stiff at supra-physiologic values (>30mmHg transmural pressure) (Lee et al., 2013). However, other mechanical loads caused by the surrounding organs or due to individual movements and breathing, requires more compliance in the longitudinal direction (Alastrué et al., 2008).

Arterial wall mechanics in response to pulsatile blood flow from the heart is understood to play a significant role in cardiovascular disease. The mechanical properties of veins are less extensively studied, perhaps due to the lower blood pressure involved. However vein mechanics are of many clinical interests (Desch and Weizsäcker, 2007). For example, certain biomechanical changes to osmotic pressure, hypertrophy, and reduced compliance of the veins might contribute to the development and maintenance of arterial hypertension (Safar and London, 1985). Also, in deep vein thrombosis, a clot can form, dislodge, and move to the lungs or heart causing a pulmonary embolism or heart attack (Alastrué et al., 2008). A solution is to install a filter in the inferior vena cava, which is a situation where increased understanding of mechanics would benefit the surgical procedure and outcome. Additionally, vein mechanics should be considered for tissue engineered constructs, as well as for arterio-venous fistulas, which are important for successful dialysis treatment (Lee et al., 2013). Vein grafts are often used to treat cardiovascular diseases such as in arteries and they remodel to new conditions (Owens et al., 2015). In vein segments grafted into arteries, exposure to the high pulsatile pressure load leads to significant wall remodeling within a few days of grafting. An inflammatory response, neointima development, collagen and elastin turnover, cellular proliferation and apoptosis occurs, reducing the differences in elastic properties between arteries and veins at similar loading levels (Dobrin et al., 1989; Lu et al., 2014; Lüscher et al., 1992). It is assumed that at least a part of biomechanical changes developing in the grafted vein wall is a physiological adaptation mechanism that normalizes the extremely high circumferential stress. Interestingly, experimental evidence supports the idea that certain morphological and biochemical alterations of grafted veins are reversible (Davies et al., 1999; Fann et al., 1990; Seidel et al., 1984).

Collagen and elastin assay results show vena cava is primarily collagen, but aorta has more elastin (Figure 3.1d). Adventitia generally comprises 60 to 75% of vena cava and 10% of aorta, with the media of vena cava not being as clearly defined as in aorta because there are no internal/external elastic lamina (Humphrey, 2002). Our finding of a ~4:1 collagen:elastin ratio in vena cava and 1:1.5 in thoracic aorta are in agreement with previous studies. The collagen:elastin ratio was reported to be ~5:1 in saphenous vein and ~1.5:1 in canine abdominal aorta (Humphrey, 2002) and thoracic aorta has been found to have more elastin than abdominal aorta (Sokolis, 2007). Elastin fibers in the large elastic arteries such as aorta are essential for its cyclical extensibility. However vena cava contains much more collagen than elastin mainly to maintain integrity without the need to sustain cyclic loading.

The striking differences in both mechanics and structure between aorta and vena cava are interesting. There is a marked difference in elastin alignment between aorta and vena cava. Elastin has remarkably long half-life and can elongate up to 150% of its original length (Humphrey, 2002). In terms of a structure-function relationship, we are reminded that aorta experiences repeated multi-axial cyclic extension from pulsatile blood flow. Therefore, it makes sense that aorta would have a rather uniformly oriented elastin. Elastin in vena cava, however, is longitudinally oriented. Longitudinal elastin has also been found in porcine jugular veins (Sokolis, 2013). One possible reason for longitudinally oriented elastin in veins maybe to handle the extension due to breathing (Alastrué et al., 2008), since the torso elongates during inhalation and imposes a longitudinal stretch on the vena cava.

The large anisotropy seen in the vena cava shows strong correlation between ECM fiber structure and mechanical function of blood vessels. The unique distribution of elastin in vena cava results in a compliant longitudinal stress-strain behavior (Figure 3.2a). With the absence of elastin in the circumferential direction and tighter crimp in the adventitial collagen of vena cava (Figure 3.3), the stress-strain curve shows a rapid stiffening behavior at lower levels of stretch.

In contrast, aorta shows much less anisotropy than vena cava (Figure 3.2a). The tangent modulus is in the range of 0.2 to 1.6 MPa for aorta and 0.2 to 6.4 MPa for vena cava (Figure 3.2b). It is important to note that such measurements were based on tissue level experiments, and may not be revealed from local measurements. For example, Akhtar et al. used nanoindentation to compare the mechanical properties across the thickness of ferret aorta and vena cava (Akhtar et al., 2009). For aorta, the elastic modulus linearly decreased from ~30 MPa at the adventitia to ~8 MPa at the intimal surface. For vena cava, the modulus was ~35 MPa at the adventitia and intima, but ~20 MPa in the medial layer. Differences may be due to the distribution of ECM components and cells. In addition to difference between the percentage that adventitia comprises aorta versus vena cava, it is also worth noting that medial collagen is generally considered to be mainly type III and the adventitia mainly the stiffer type I collagen.

Collagen undergoes continuous turnover during a lifetime. There is also evidence that faster loading rates in aorta can lead to a shorter half-life (~22 days) compared to a less demanding mechanical environment (Gineyts et al., 2000; Humphrey et al., 2009, 2014) such as the vena cava. The wavy collagen fibers seen in the aorta is correlated with the wide range of *in vivo* strains for aorta (Humphrey et al., 2014; Wagenseil and Mecham, 2009). However for vena cava, collagen is deposited in the vessel wall in the absence of pulsatile motion experienced by aorta. The very stiff circumference of the vena cava can be related to the fact that collagen straightens and stiffens at lower levels of strain because it experiences lower levels of strain *in vivo* while it is being deposited.

With higher strain, vena cava collagen reveals a narrower circumferential distribution due to fiber straightening with circumferential alignment. At 0% strain, aorta has relatively more circumferentially oriented collagen than vena cava. At 5% strain, aorta and vena cava have a similar proportion of collagen in the circumferential direction, but at 10% strain, vena cava actually has proportionally more circumferentially-aligned medial collagen (Figure 3.6). More circumferentially oriented collagen at higher strains correlates well with the very stiff circumference of the vena cava, especially considering the earlier recruitment (Figures 3.4 and 3.5).

Additionally, aorta has more elastin to contribute at lower levels of strain, especially in the circumferential direction, and thus a delayed recruitment for collagen at higher levels of strain that compliments the observed nonlinear stiffening (Chow et al., 2014). For example, the straightness parameter (Figure 3.5) is not significantly different ($p=0.50$) at 0% strain between aorta (0.85 ± 0.10) and vena cava (0.87 ± 0.010). However, the adventitial collagen of vena cava becomes significantly straighter ($p<0.05$) with the first 5% increase in strain (0.96 ± 0.0028), but aorta has delayed recruitment and only becomes that straight beyond 25% strain (0.94 ± 0.035)

However, when vena cava is stretched two and three times as much in the longitude compared to the circumference, the fibers begin to reorient towards the longitudinal direction (Figure 3.7). The longitudinal elastin peaks become higher and the medial and adventitial collagen peaks around the circumference become more widely distributed as fibers begin to shift towards the longitude.

3.6 Summary

This study establishes several new fundamental concepts for understanding the differences of aorta and vena cava at the structural and functional levels. In summary, aorta contains less collagen than elastin, but vena cava contains almost four times more collagen than elastin. In vena cava, the elastin is longitudinally oriented and the collagen becomes more circumferentially oriented and straightens at low levels of strain. These structural observations support the functional finding that vena cava is more anisotropic than aorta because the circumference stiffens substantially at low levels of strain. Importantly, these findings should be put in context with the fact that physiologic pressure in vena cava is much lower than aorta. Overall, this study improves the understanding of elastin and collagen fiber contribution to ECM mechanics of blood vessel. Specifically, it points to the need to consider fiber distributions and waviness in addition to relative collagen and elastin amounts. When comparing the mechanics of vena cava to aorta, it is important to remember that ECM fiber distribution, recruitment, and content each play an important role in arterial function. Individual traits (e.g., more collagen = stiffer) may be obvious, but combining them (e.g., more collagen with different distribution and recruitment may or may not = stiffer) to form the big picture is less obvious and warrants investigation. Finally, this study demonstrates the importance to account for the structural and functional difference between arteries and veins when considering disease treatment options such as using a vein graft for an artery, which creates a mismatch between vein wall mechanics and artery loading conditions.

CHAPTER 4 GLYCOSAMINOGLYCANS CONTRIBUTE TO EXTRACELLULAR MATRIX FIBER RECRUITMENT AND ARTERIAL WALL MECHANICS

4.1 Overview

Elastic and collagen fibers are well-known to be the major load-bearing extracellular matrix (ECM) components of the arterial wall. Despite the important mechanical role of glycosaminoglycans (GAGs) in other tissues such as cartilage, GAGs are only recently gaining attention in mechanical studies of arterial tissue. The goal of this study was to study the mechanical and structural contributions of GAGs to the arterial wall. Biaxial tensile testing was paired with multiphoton microscopic imaging of elastic and collagen fibers in order to establish the structure-function relationships of porcine thoracic aorta before and after enzymatic GAG removal. Removal of GAGs results in an earlier transition point of the nonlinear stress-strain curves ($p<0.05$). However, stiffness was not significantly different after GAG removal treatment, indicating earlier but not absolute stiffening. Multiphoton microscopy showed that when GAGs are removed, the adventitial collagen fibers are straighter and recruited at lower levels of strain, in agreement with the mechanical change. The amount of stress relaxation also decreased in GAG depleted arteries ($p<0.05$). These findings suggest that the interaction between GAGs and other ECM constituents plays an important role in the mechanics of the arterial wall, and GAGs should be considered in addition to elastic and collagen fibers when studying arterial function.

4.2 Introduction

The wall of an artery contains elastic and collagen fibers, as well as ground substance including glycosaminoglycans (GAGs). Together they compose the extracellular matrix (ECM) interspersed among organized layers of cells. Elastic fibers are essential to accommodate deformations encountered during physiological function of arteries, which undergo repeated cycles of extension and recoil, while the extensibility of the tissue are associated with the collagen fibers. Studies of the structural components and mechanics of arterial ECM generally focus on elastic and collagen fibers while GAGs are often neglected, most likely because of their relatively low content (2–5% by dry weight) in arterial tissue (Wight, 1980). Recent studies showed that GAGs influence viscoelasticity as well as residual stress, which plays an important role in arterial homeostasis (Azeloglu et al., 2008; Wight, 1980). GAGs have also been hypothesized to contribute to mechanosensing, which can be disrupted under pathological conditions that can lead to wall delamination (Roccabianca et al., 2014; Sara Roccabianca et al., 2014). Additionally, the mechanical interactions of GAGs with elastic and collagen fibers are not fully understood. The swelling pressure of inflated GAGs imposes tensile loading of the fiber network, which in turn entangles/restrains the GAGs within the ECM, as well as provide shear stiffness to the ECM and help maintain ECM organization (Maroudas, 1976; Takahashi et al., 2014; Zhu et al., 1996). Taken together the above observations call for a more in depth understanding of GAGs contribution to aorta mechanics and cardiovascular diseases such as diabetes, atherosclerosis, aneurysm, and hypertension for which altered ECM is a hallmark.

GAGs are long, unbranched chains of repeating disaccharide units that are classified into four groups: chondroitin sulfate/dermatan sulfate (previously chondroitin sulfate B), heparan sulfate, keratan sulfate, and hyaluronan. Sulfated GAGs have a high affinity for water molecules and are negatively charged, which attract cations and thus water to maintain osmotic equilibrium as well as repulse each other to serve as a mechanism for resisting compression and shear (Cavalcante et al., 2005). GAGs bound to a core protein form proteoglycans (PGs), which aggregate by attaching to hyaluronan, the only non-sulfated GAG.

PGs are found in different locations in the arterial wall, which may indicate differences in function of each PG family that is classified by the types of GAGs that comprise them (Camejo et al., 1998; Dingemans et al., 2000). The majority of PGs are believed to reside in the media and can associate with elastin, collagen, cells, or be found in interstitial space (Halper, 2014). Of the total amount of GAGs in the thoracic aorta of various species, chondroitin sulfate is the most abundant at 40–56%, with the remainder being 4–30% dermatan sulfate, 9–32% heparan sulfate, and 4–24% hyaluronan (Aikawa et al., 1984). Chondroitin/dermatan sulfate forms collagen fiber-associated, non-aggregating decorin and biglycan PGs, as well as versican, a large interstitial PG that aggregates along hyaluronan and can interact with elastin (Humphrey, 2012). Heparan sulfate is found on perlecan, a cell-associated PG that also aggregates along hyaluronan and interacts with the fibrillin of elastic fibers (Hayes et al., 2011).

It has long been speculated that the elastic fibers of healthy central arteries contribute at lower levels of strain, whereas collagen fibers are recruited at higher levels to create nonlinear passive mechanical behavior (Burton, 1954). Our recent studies using multiphoton microscopy demonstrate an interesting sequential engagement of elastic and collagen fibers in response to mechanical loading (Chow et al., 2014; Turcotte et al., 2016). Such intrinsic interrelation between elastic and collagen fibers is essential for an artery to function normally. The contribution of GAGs to arterial mechanics is only recently gaining attention (Roccabianca et al., 2014). Due to the unique presence and properties of GAGs in the arterial wall, they may play a role in engaging the ECM fibers in the arterial wall and thus indirectly affect its biomechanical function.

To understand the role of GAGs in the passive mechanical behavior of thoracic aorta, biaxial tensile and stress relaxation tests were performed to characterize the elastic and viscoelastic properties of untreated tissue and treated tissue with GAGs enzymatically removed. Multiphoton microscopy was performed to study the structural organization of elastic and collagen fibers in the arterial wall when GAGs are absent. Mechanical testing was paired with multiphoton microscopy to establish insightful structure-function understandings.

4.3 Materials and Methods

4.3.1 Sample Preparation

Descending porcine thoracic aortas (n=3) were obtained (12–24 months, 160–200 pounds) from a local abattoir and cleaned of loose connective/fatty tissue. Approximately 20 mm sized square samples (n=6, 2 from each aorta) were cut so that one edge is parallel to the longitudinal direction and the other edge is parallel to the circumferential direction of the artery.

4.3.2 Enzymatic GAG Removal Treatment

To enzymatically remove GAGs in arterial tissue, a protocol adapted from Lovekamp et al. (Lovekamp et al., 2006) was used by adding heparinase to the treatment. Briefly, samples were treated in 100 mM ammonium acetate buffer, pH 7.0, 2–5 U/mL hyaluronidase, 0.025 U/mL chondroitinase ABC, 0.25 U/mL heparinase (Sigma Aldrich #H3506, C3667, H3917, St. Louis, MO) and gently agitated for 24 hours at 37°C to remove GAGs. Samples were then rinsed and mechanically tested in 150 mM phosphate buffered saline (PBS).

4.3.3 Histology

Histology studies were performed on tissue sections with and without GAGs removal. Alcian blue and Movat's pentachrome stains were used to evaluate the efficiency of GAG removal treatment and to inspect the structure of the remaining ECM components, respectively. Refer to Chapter 2.2 for the histology protocol.

4.3.4 Biaxial Tensile Test

Refer to Chapter 2.4 and 2.4.1 for details. For this experiment, samples were subjected to a set of equibiaxial and non-equibiaxial loading conditions, 200C-400L, 300C-400L, 400C-400L, 400C-300L, and 400C-200L N/m to characterize the anisotropic mechanical behavior, where C and L represents the circumferential and longitudinal directions, respectively.

True strains were calculated as:

$$\varepsilon_1 = \ln \lambda_1, \varepsilon_2 = \ln \lambda_2$$

where λ is the stretch.

4.3.5 Stress Relaxation Test

Refer to Chapter 2.4.2 for the stress relaxation protocol. For this experiment, immediately following the cycle for 400C-400L N/m, this tension was reapplied with a 2 s rise time and held at a constant stretch for 900 s.

4.3.6 Multiphoton Microscopy

To understand the contribution of GAGs to the structure and function of the arterial wall, and the interaction of GAGs and other ECM constituents, mechanical loading was paired with multiphoton imaging of tissue with GAGs removed following methods detailed in Chapter 2.5. Samples were imaged from 0 to 40% equibiaxial strain in 5% increments. These images were then used in the analysis of fiber straightening and recruitment in response to mechanical loading. To examine the effect of GAG removal on fiber mobility/reorientation, treated samples were imaged at equal and non-equibiaxial deformation of 30C-30L, 15C-30L, and 30C-15L where the numbers represent grip-to-grip percentile strain.

4.3.7 Imaging analysis

Fiber orientation, frequency of fiber angle, was determined from two-dimensional fast Fourier transform analysis using the Directionality plug-in in FIJI (fiji.sc/Fiji, Ashburn, VA) following the developer's instructions. To quantify fiber reorientation, fiber ratio was quantified by calculating the ratio of circumferential (0°±20°) to longitudinal (±90°±20°) fibers at each level of stretch. Fiber mobility was then determined by dividing the fiber ratio of unequal stretch by the ratio of equal stretch.

Comparisons were made between treated samples and our previously published untreated samples published (Chow et al., 2014).

Adventitial collagen fiber waviness was quantified with NeuronJ (imagescience.org/meijering/ software/neuronj) by measuring the end-to-end distance (L_o) and total fiber length (L_f), to define a straightness parameter:

$$P_s = L_o / L_f$$

which is equal to 1 for a straight line (Chow et al., 2014).

This manual tracing method cannot be applied to the more intricate elastic and collagen fiber network in the media. Therefore, fractal analysis was also used as a broad measure of fiber recruitment following the protocol described by Chow *et al*. (Chow et al., 2014). Briefly, a box counting protocol of ImageJ gives a fractal dimension that is a measure of self-similarity of an image. The fractal number, D, can be approximated as:

$$D \approx \log(N_r)/\log(r)$$

where r is the box size and N_r is the number of boxes required to cover the image with the box size of r. To limit sensitivity of variation between samples, results are expressed as the absolute value of $(D - D_o)/D_o$, where D and D_o are the average fractal number for the deformed and undeformed state, respectively.

4.3.8 Statistical Analysis

Stress-strain data, transition point, initial and stiff slopes, axial cross-coupling, percent stress relaxation, straightness parameter, and fractal analysis are summarized and plotted with mean ± standard error of the mean. Two-tailed paired t-tests were used for analysis with $p<0.05$ considered as statistically significant.

4.4 Results

We first validated the efficiency of the GAG removal treatment and its impact on ECM fiber integrity. Histology images show effective GAG removal and that the collagen and elastic fibers remain intact (Figures 4.1 and 4.2). Alcian blue stains GAGs in blue, which were observed throughout the thickness of the untreated tissue. Effective GAG removal was confirmed by the absence of blue staining in the treated tissue (Figure 4.1). Movat’s stain also results in GAGs appearing blue in untreated tissue, as well as staining elastic fibers in black, collagen fibers in yellow, and smooth muscle in red. The fibers remain intact after treatment, however more empty spaces are observed in the treated tissue (5.1% for treated vs. 0.8% for untreated). Here empty spaces were quantified in the Movat’s histology stain images of the medial layer using ImageJ by minimizing the brightness, then making the image binary and using the “analyze particles” feature (Tan and Sanderson, 2014). Note that empty spaces are not quantified for the adventitial layer due to the more prevalent white spaces in the tissue.

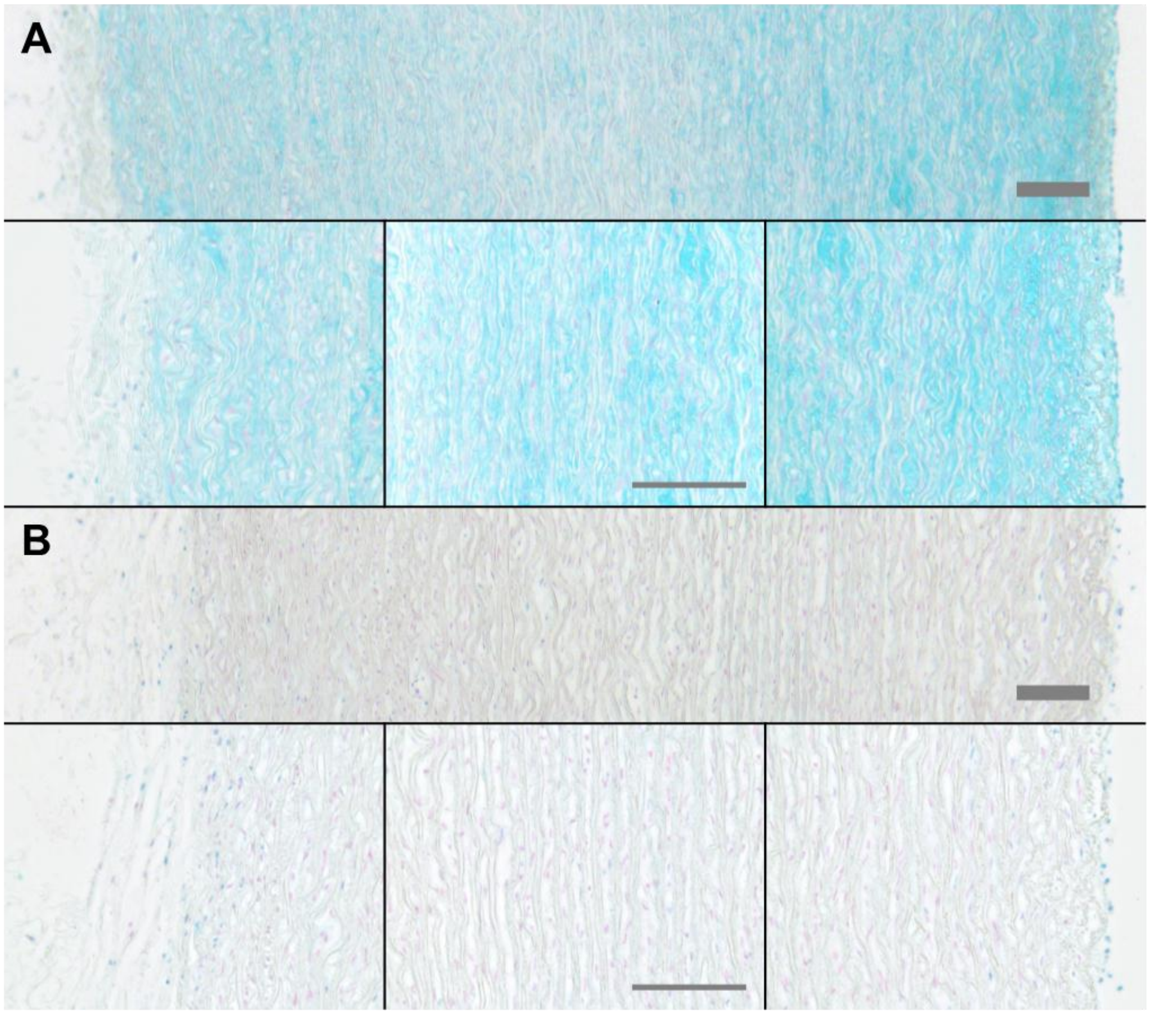

Figure 4.1. Alcian Blue stain of aorta from adventitia (left) to intima (right) for untreated (A) and treated (B) tissue. In untreated tissue, GAGs (blue) appear throughout the thickness, but slightly more concentrated towards the intima. Treated tissue shows effective enzymatic GAG removal demonstrated by the lack of blue staining. All scale bars are 100 µm.

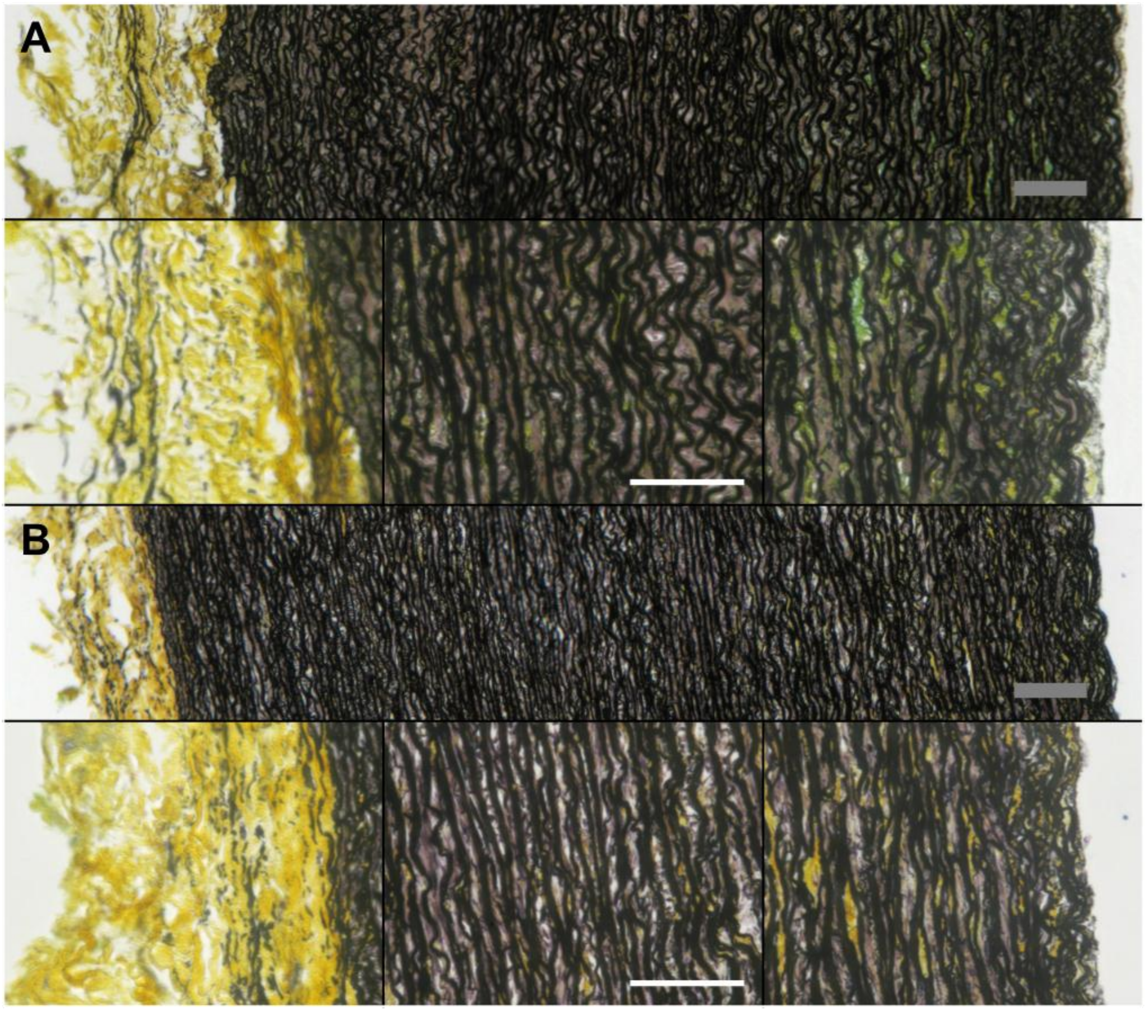

Figure 4.2. Movat's stain of aorta from adventitia (left) to intima (right) for untreated (A) and treated (B) tissue. The adventitia is primarily collagen (yellow) and media is mostly elastin (black) with smooth muscle (red), collagen, and GAGs (blue, untreated). Tissue structure remains visibly intact after treatment, noting that fibers appear straighter after treatment with more white space between elastin. All scale bars are 100 µm.

We then evaluated the impact of GAG removal on the biomechanical function of arteries. Averaged stress-strain curves of samples before and after removing GAGs are shown in Figure 4.3. To quantify the changes in mechanical properties due to GAG removal, initial and stiff slopes were determined by linear fit to the regions of stress-strain curves from 0–20 kPa and 180–200 kPa, respectively. Transition stress/strain was then calculated as the intersection of the bilinear curve fit to the initial and stiff regions of the stress-strain curves (Chow et al., 2011). For treated samples, the transition points of the circumferential (p=0.04) and longitudinal (p=0.002) directions are at significantly lower strain measurements, indicating earlier stiffening behavior of the arterial wall. However, the initial and stiff slopes for each direction are not significantly different after treatment (Figure 4.4, all p>0.1), suggesting GAG removal results in earlier stiffening, but not absolute stiffening.

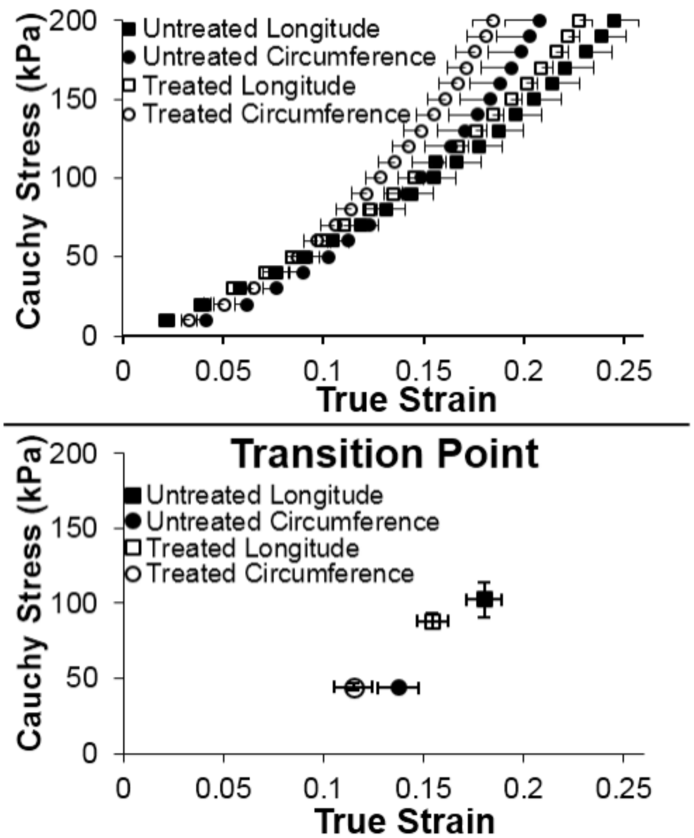

Figure 4.3. Average stress-strain curves for equibiaxial tests of untreated aorta and after GAG removal treatment. Treated samples have transition points at significantly lower strain (p<0.05), indicating earlier fiber recruitment.

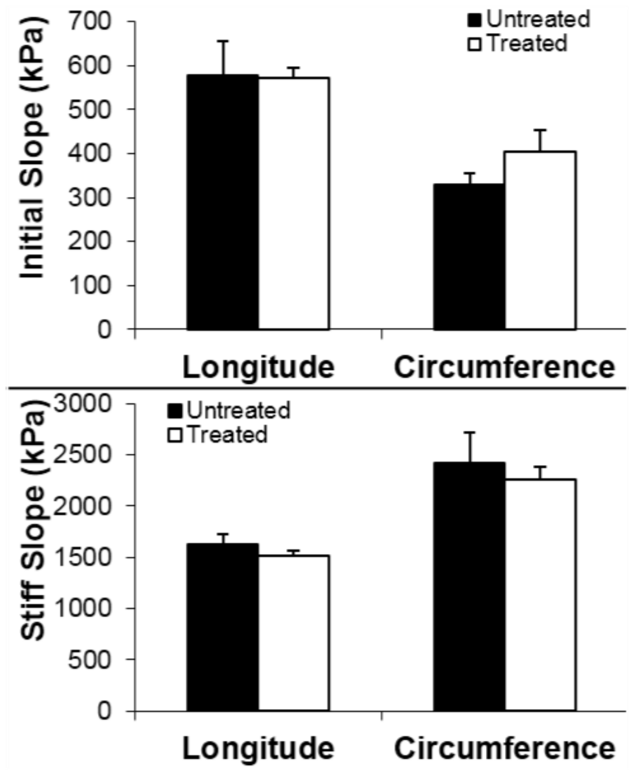

Figure 4.4. Despite lower transition points, the initial and stiff slopes did not significantly change ($p>0.1$), suggesting that straighter fibers are recruited at lower strains and result in earlier, but not absolute stiffening.

Non-equibiaxial testing showed similar results to equibiaxial testing, with treated samples stiffening at lower strains than untreated samples (Figure 4.5). To examine the effect of GAG removal on mechanical coupling between material axes, axial cross-coupling was quantified by dividing the peak stretch for each non-equibiaxial tension condition (λ) by the peak stretch for the equibiaxial tension condition (λ_{eq}) for that sample (Sacks and Chuong, 1998), since non-equibiaxial tension loading would result in a larger stretch in the direction with higher tension. It appears that after GAG removal, there were minimal changes to axial cross-coupling (Figure 4.5), which suggests that GAG removal does not affect fiber mobility under non-equibiaxial loading.

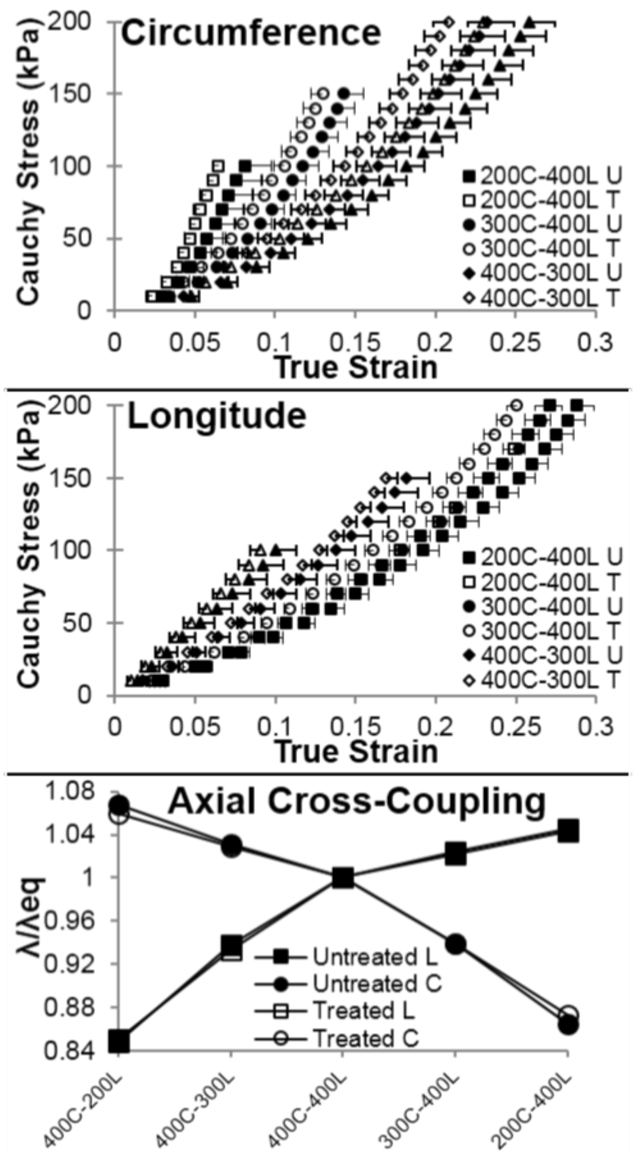

Figure 4.5. Non-equibiaxial mechanical testing data for each anatomical direction before and after treatment, and axial cross- coupling. At all loading conditions, treated samples showed earlier stiffening. However, there were minimal changes to axial cross-coupling, which was quantified by dividing the peak stretch for each non-equibiaxial loading condition (λ) compared to the peak stretch for the equibiaxial loading condition (λ_{eq}) for that sample.

Stress relaxation tests were performed to examine the contribution of GAGs to the viscoelastic behavior of arteries. Removing GAGs significantly reduce the per cent stress relaxation from 8.766±0.007% to 7.140±0.005% (p=0.01) and 9.900±0.014% to

7.830±0.008% (p=0.03) in the longitudinal and circumferential directions, respectively (Figure 4.6).

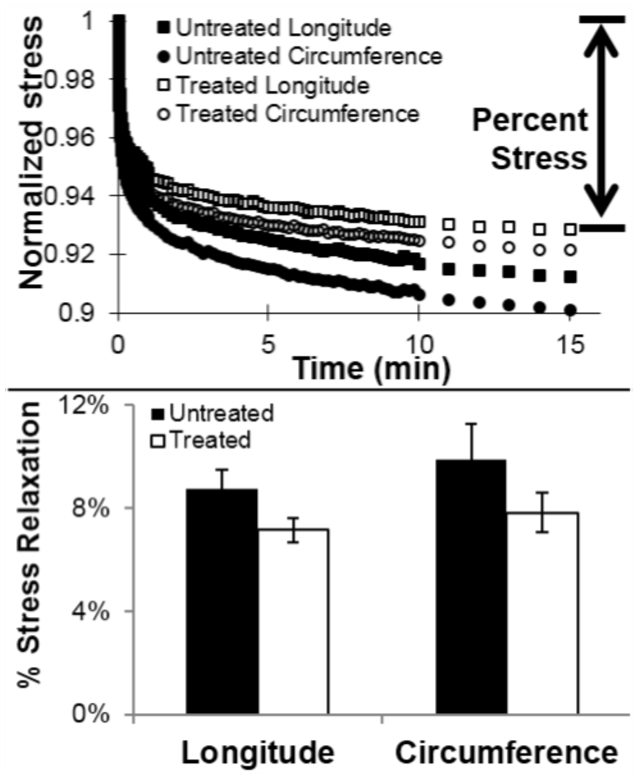

Figure 4.6. Removing GAGs significantly ($p<0.05$) reduced the per cent stress relaxation from 8.77±0.01% to 7.14±0.004% and 9.90±0.01% to 7.83±0.01% in the longitudinal and circumferential directions, respectively.

Multiphoton imaging enabled us to visualize the structural changes in elastin, medial collagen and adventitial collagen fiber networks. GAGs are closely associated with elastin and collagen fibers, thus removal of GAGs may affect the orientation/recruitment of these two major ECM components, which dominate the mechanical function of the arterial wall. Large bundles of collagen fibers were observed in the adventitial layer (Figure 4.7). The medial collagen fibers appeared as a network of rather finer fibers. Upon mechanical stretching, both adventitial and medial collagen fibers became noticeably straightened. Minimal changes in elastin fiber network with mechanical stretch were observed.

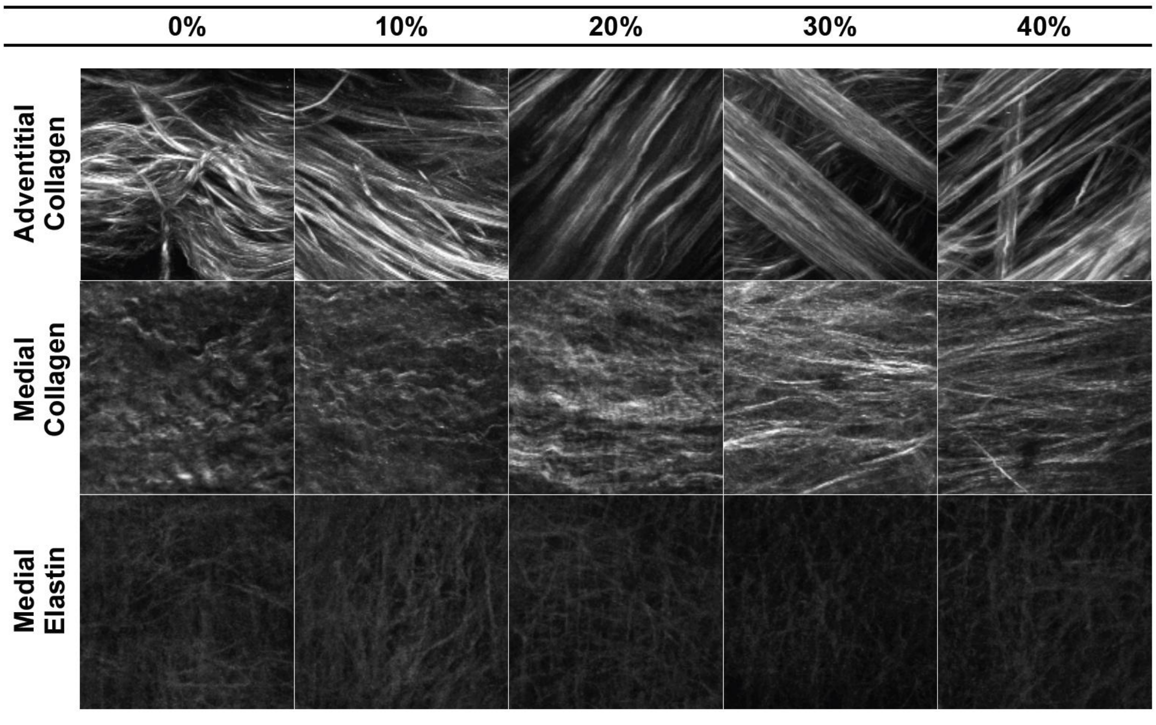

Figure 4.7. Fibers at different levels of equibiaxial stretch, where the numbers represent grip-to-grip strain for circumferential (C) and longitudinal (L) directions at 0° and ±90°, respectively. Equibiaxial stretch demonstrates fiber recruitment. Images are 110µm x 110µm.

The fiber orientation was plotted from 0% to 40% equibiaxial strain in 10% increments (Figure 4.8). The appearance of multiple peaks in adventitial collagen corresponds with the existence of fiber bundles/families in the adventitial layer. These peaks become more evident with fiber straightening due to increased biaxial strain. The medial collagen fibers are predominantly circumferentially oriented and becomes more so with increased strain. Medial elastin shows minimal changes in fiber distribution with mechanical loading.

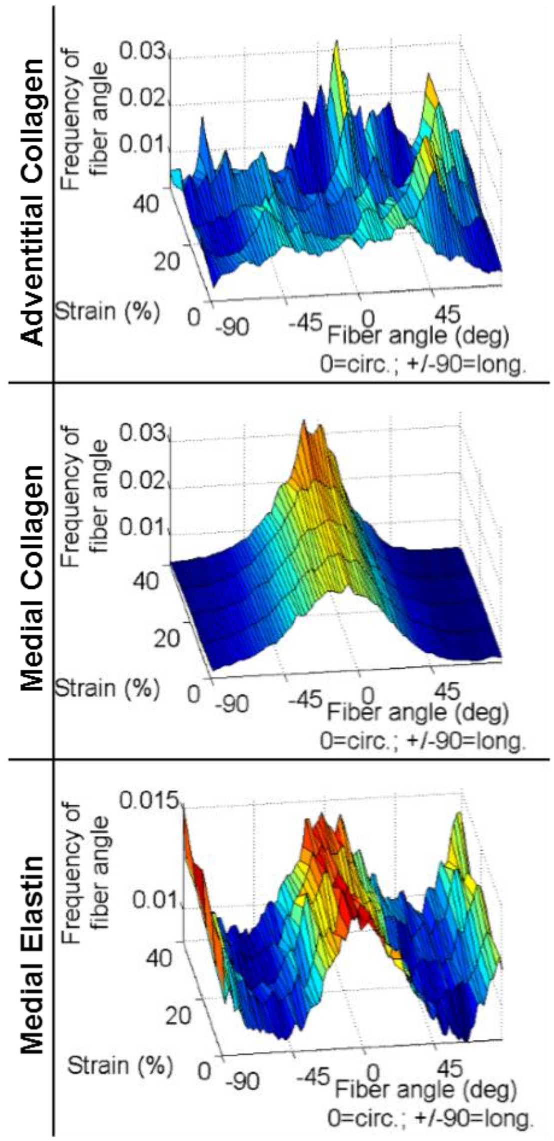

Figure 4.8. Fiber distributions during equibiaxial strain of treated tissue with GAGs removed. Adventitial collagen shows many peaks, indicating multiple fiber bundles that become more prominent with increased strain. Medial collagen becomes slightly more circumferentially aligned and medial elastin shows little changes suggesting that elastin is recruited at all levels of stretch.

To quantify fiber reorientation/mobility, fiber ratio was quantified by calculating the ratio of circumferential (0°±20°) to longitudinal (±90°±20°) fibers at each level of stretch. Fiber mobility was then determined by dividing the fiber ratio of unequal stretch by the ratio of equal stretch. Comparisons were made between treated samples and previously published untreated samples (Chow et al., 2014). The fiber mobility analysis suggests that both untreated and treated tissue shows more fiber mobility towards the circumferential than longitudinal direction for adventitial and medical collagen fiber networks, as demonstrated in Figure 4.9. GAG removal results in minimal changes to fiber reorientation under non-equibiaxial deformation (p>0.2).

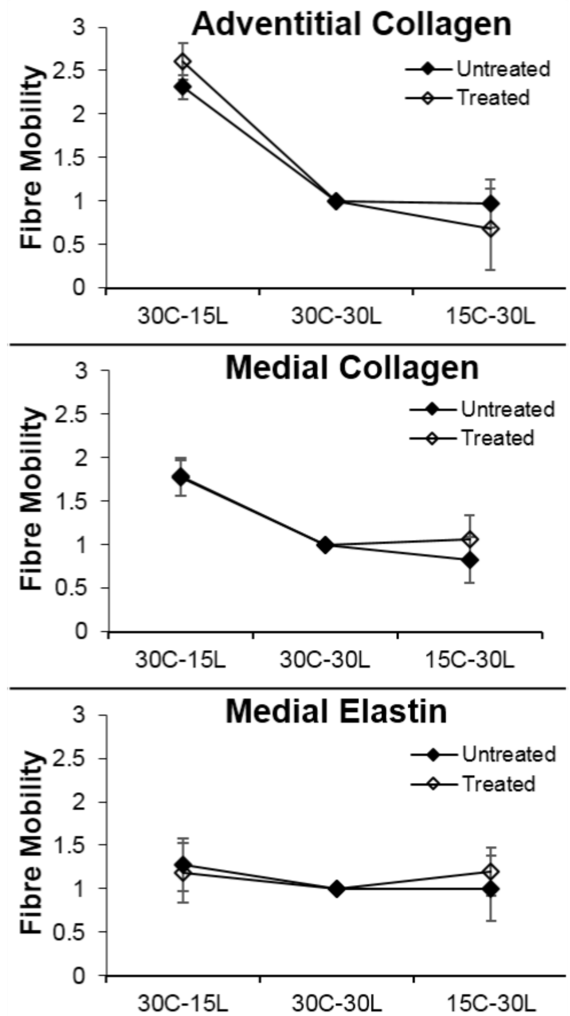

Figure 4.9: Circumferential to longitudinal fiber ratios for non-equibiaxial strain were divided by the same sample's ratio for equibiaxial strain to quantify fiber mobility. Fiber mobility greater than 1 indicates circumferential fiber reorientation and less than 1 indicates longitudinal fiber reorientation. Both untreated and treated tissue show similar behavior, indicating no change to fiber mobility.

Waviness of adventitial collagen fibers was quantified with the straightness parameter (Figure 4.10). At 0% strain, the straightness parameter for adventitial collagen fibers of tissue with GAGs removed (P_s=0.920±0.005) was significantly higher than for untreated tissue (P_s=0.855±0.017) from Chow *et al*. (Chow et al., 2014). While delayed collagen fiber engagement behavior, i.e., fibers do not show significant straightening until around 20% strain, was observed in the adventitial collagen from untreated tissue, this behavior is absent from the treated tissue. With GAG removal, the initially straightened collagen fibers show a less evident but continuous straightening process with increased mechanical strain.

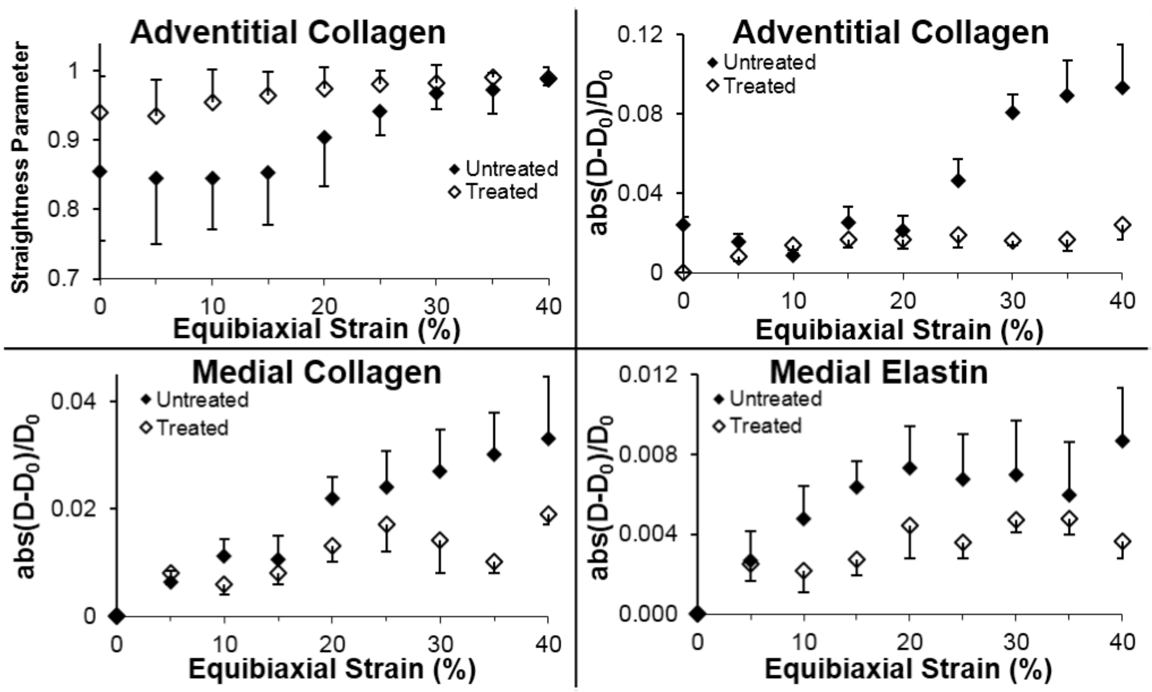

Figure 4.10. Straightness parameter for adventitial collagen and fractal analysis for all three fiber types. The straightness parameter of a straight line is equal to 1. GAG removal treatment results in straighter adventitial collagen fibers compared to untreated tissue at all levels of strain from the 0% unloaded state until being fully straightened. Fractal analysis indicates that for untreated tissue, adventitial collagen begins recruitment at 20% strain, but medial fibers begin recruitment at the onset of stretching. For treated tissue, all fibers are recruited at earlier strains and show less changes after.

Fractal analysis further revealed that the treated samples show smaller changes in fiber recruitment. These results are consistent with the finding that the ECM fibers appear to be straighter and are engaged earlier than the untreated tissue. For the untreated tissue, our earlier study (Chow et al., 2014) reported an interesting sequential elastin and collagen fiber recruitment, which suggests an intrinsic structural and functional interrelation among ECM constituents. Briefly, elastin is recruited early and then plateaus at about 20% strain, medial collagen is continuously recruited, and adventitial collagen has a delayed recruitment around 20% strain (Chow et al., 2014). With GAG removal, however, in general such sequential trend in fiber recruitment disappears, and all fibers are recruited early and have small changes afterward (Figure 4.10).

4.5 Discussion

GAGs/PGs serve many functions in development, maintenance, and repair of a variety of tissues (Couchman and Pataki, 2012; Halper, 2014). Furthermore, GAG content begins decreasing with age after the first 40 years of life, as well as with pathologies such as osteoarthritis (Maroudas, 1976; Tovar et al., 1998). An increase in GAG depleting enzymes such as those used in this study are also noted in conditions such as hyperglycemia and hyperlipidemia that are prevalent in diabetes and atherosclerosis (Baker et al., 2010, 2009; Wang et al., 2009). Building upon our prior research on ECM mechanics, the present study integrates biomechanical characterization and multiphoton imaging to explore how GAGs contribute to the structural and biomechanical integrity of arteries. Biaxial tensile testing allows full characterization of the anisotropic mechanical behavior of the tissue under well-defined loading conditions, which is essential in order to capture changes in mechanical function with GAG removal. Multiphoton microscopy provides microstructural assessment of elastic and collagen fibers, and offers insightful explanations on the functional and regulatory significance of GAGs in the arterial wall. Overall, our study suggests that despite the relatively low mass fraction of GAGs in arterial tissue, GAGs play an important role in contributing to the structural and mechanical properties of the arterial wall.

The finding of decreased stress relaxation after removing GAGs suggests that GAGs contribute to the viscoelastic behavior of arteries. In cartilage, GAGs attract water and upon tissue deformation, fluid motion flows relative to the collagen-GAG solid phase, creating friction and shear (Mow et al., 1980). This effect, combined with the osmotic swelling due to the ionic charge of GAGs, was assumed to contribute to the viscoelastic and tensile behavior of cartilage based on mixture theory (Ateshian et al., 2009; Lai et al., 1991). More recently, a similar concept was applied to study the GAGs in arteries (Azeloglu et al., 2008). However, in addition to collagen, arteries contain elastin and cells as two other main structural components, so there may be additional interaction effects between these components and GAGs. GAGs not only cross-link collagen fibrils, but also anchor to the cell surface such as hyaluronan anchoring to receptors CD44 or RHAMM (Evanko et al., 2007). Also, the protein cores of biglycan and decorin PGs each have similar yet distinct binding sites on the tropoelastin of elastic fibers (Reinboth et al., 2002).

GAGs have been found to affect the mechanics of other soft tissue, such as tendon, lung, heart valve, and eye, though results are tissue-specific and sometimes contradictory. For example, GAG depletion increased the stress relaxation response of tendon fascicles, perhaps from water movement or collagen sliding (Legerlotz et al., 2013). Indeed, PGs may reduce collagen sliding by forming interfibrillar bridges (Scott, 2003). Alternatively, PGs could promote collagen sliding in tendon by isolating neighboring collagen fibrils (Rigozzi et al., 2013). Additionally, controversial results were obtained in studying the viscoelastic properties of tendon after removing GAGs (Fessel and Snedeker, 2009; Robinson et al., 2004). In parenchymal lung strips, removing GAGs increased hysteresivity independent of frequency from 0.1–10 Hz (Al Jamal et al., 2001). On the other hand, removing GAGs in aortic heart valves reduced hysteresis at low force levels (Eckert et al., 2013). Hysteresis was also decreased in the eye sclera after GAG depletion, along with decreased low-pressure stiffness, but increased high-pressure stiffness and transition point (Murienne et al., 2015). In the present study, removing GAGs decreased stress relaxation and decreased transition point in porcine thoracic aorta. These tissue-specific differences serve as a reminder of the variety of functions and mechanical conditions that the same ECM components serve among different tissues.

GAG removal also results in straighter adventitial collagen fibers even when unloaded (Figures 4.7 and 4.10). Previous histology studies suggest that GAGs fit within wavy collagen fibers perpendicular to the local fiber direction, similar to a laterally supported Euler column (Bellini et al., 2014). Such interactions may contribute to the entanglement of fibers, and provide support to fibers. Moreover GAGs can delay fiber engagement in the direction of mechanical loading. Collagen and elastin fibers are after all, the main load bearing components of arterial tissue experiencing cyclic tension in vivo (Wagenseil and Mecham, 2009). As a result of GAG removal, these fibers can engage earlier in response to mechanical loading. Our earlier study reported a sequential engagement of elastin and collagen fibers in response to mechanical loading. Specifically, the adventitial collagen shows a delayed fiber engagement at about 20% of equibiaxial tissue stretch, while the medial collagen and elastin fibers are engaged immediately upon mechanical loading (Chow et al., 2014). Interestingly, our mechanical study combining transition point (Figure 4.3) with axial cross-coupling analysis (Figure 4.5) together with imaging analysis (Figure 4.10) indicates earlier fiber recruitment due to fiber straightening, but minimal changes to fiber mobility after GAG removal. Such well-defined structural roles of ECM components are crucial for arteries to maintain normal mechanobiological function. The present study demonstrates that the straighter fibers after GAG removal may allow the tension-resisting adventitial collagen fibers to engage at lower levels of mechanical stretch.

After GAG removal, the transition point was significantly lower (Figure 4.3). This suggests that GAGs actually play an important structural and mechanical role in tissue mechanics. Results of multiphoton imaging show that after removing GAGs, medial and adventitial collagen fibers are straighter and recruited at lower levels of strain (Figure 4.8). Thus, the imaging establishes a structure-function relationship supporting the finding of lower transition point from straighter fibers that are recruited at lower levels of strain. The adventitial collagen fibers are straighter even in the unloaded state from straightness parameter analysis (Figure 4.10). In fact, removing GAGs has a similar effect on the waviness of adventitial collagen fibers to applying between 20% (P_s=0.903) and 25% (P_s=0.941) strain to untreated tissue (Chow et al., 2014). A possible explanation is that GAGs inflated from the repulsive charges and swelling pressure may contribute to collagen fiber waviness, so removing GAGs would allow the collagen fibers to be straighter.

Collagen fiber waviness has also been attributed to tensile elastin applying a compressive load on the collagen fibers (Chow et al., 2014; Zeinali-Davarani et al., 2013). Removing elastic fibers with elastase treatment results in straighter collagen fibers, a similar outcome as with mechanical stretching. Zeller and Skalak (1998) also found that the perimeter of arterial rings increased with elastase, interpreted as the removal of tensile elastin that was compressing the tissue resulting in longer tissue (Zeller and Skalak, 1998). Additionally, Lillie and Gosline (2006) found that contour length of elastic lamellae decreased after releasing the residual stress, suggesting that elastin was in tension (Lillie and Gosline, 2006). These experimental findings are supported by modelling that found tensile elastin was offset by compressed GAG-supported collagen and smooth muscle cells (Bellini et al., 2014). However, elastase treatment also removes GAGs, which could also contribute to the straightening of collagen fibers. Our study suggests that GAGs seem to be at least partially responsible for collagen fiber waviness since elastin remains intact after GAG removal and collagen appears to become straighter. Specifically, the inflation of GAGs could cause and fill in collagen waviness, or tensile elastin could compress collagen to make the fibers wavy and GAGs merely fill in the existing waviness.

There are some limitations to studying the effect of GAGs by enzymatically removing them. Removing GAGs while leaving the remaining tissue components visibly unaltered assures that observed effects are due to the absence of GAGs. However, the structural changes can alter attributes such as stress distributions that are not directly observable. Furthermore, it is interesting that the adventitial collagen fiber structure was more affected considering GAGs are generally considered to be more prevalent in the media for rat aorta (Azeloglu et al., 2008). However, our histology showed GAGs throughout the thickness for porcine aorta. Atomic force microscopy showed changes in stiffness to both the adventitia and media after removing GAGs, which was attributed to the observation that even though GAGs are predominantly in the media, GAGs are also present in the adventitia (Beenakker et al., 2012). Another possibility is that, since the ability of GAGs to retain water is well known, removing GAGs might affect tissue and fiber hydration that leads to altered mechanics. However the effect of removing GAGs on hydration and osmotic sensitivity is beyond the scope of this study and would be an interesting subject of future work.

4.6 Summary

This study establishes several new fundamental concepts for the understanding of the role of GAGs in arterial tissue at the structural and functional levels. In summary, removal of GAGs from arterial tissue resulted in the alteration of passive mechanical properties of the tissue. Importantly, GAG removal lowered the transition point of the nonlinear stress-strain curves, which is indicative of altered mechanical function. However, the initial and stiff slopes were not significantly different, suggesting earlier stiffening via recruitment, but not absolute stiffening. Microstructural studies using multiphoton microscopy of the ECM structure revealed the presence of straighter adventitial collagen fibers, and early recruitment of both elastin and collagen fibers. Despite altering fiber recruitment via fiber straightening after removing GAGs, there were minimal changes to fiber mobility during non-equibiaxial loading. Additionally, removing GAGs reduced the per cent stress relaxation in both anatomical directions, in agreement with the idea that GAGs contribute to the viscoelastic behavior of soft tissue. Results from this chapter have clinical and physiological relevance to aging and diabetes altering GAG content, among other mechanisms, in a cascade that leads to accelerated atherosclerosis and arterial stiffening. Overall, this study demonstrates the importance to account for GAGs in addition to elastin and collagen when considering the contribution of ECM components to arterial mechanics.

CHAPTER 5 MODELING THE CONTRIBUTIONS OF GLYCOSAMINOGLYCANS TO FIBER RECRUITMENT IN ARTERIAL MECHANICS

5.1 Overview

The importance of glycosaminoglycans (GAGs) and their contribution to the mechanics of soft tissue has emerged as an important area of research. GAGs provide structural basis for multiple biological functions, such as the organization of ECM assembly and the regulation of cell growth factors. The mechanics of tissue with low GAG content can be indirectly affected by the interaction of GAGs with collagen fibers, which have long been known to be one of the primary contributors to soft tissue mechanics. Our earlier study showed that enzymatic GAG depletion results in straighter collagen fibers that are recruited at lower levels of stretch, resulting in a corresponding shift of nonlinear stiffening at lower levels stretch (Mattson et al., 2016). In this study, the effect of GAGs on collagen recruitment was considered through a structure-based constitutive model. The model incorporates structural information, such as fiber orientation distribution, content, and recruitment for medial elastin, medial collagen, and adventitial collagen fibers. The model was first fit to the planar biaxial tensile stress-stretch data of untreated porcine descending thoracic aorta using the untreated structural information. Changes in elastin and collagen fiber orientation distribution, and collagen fiber recruitment were then incorporated into the model in order to predict the stress-stretch behavior of GAG depleted tissue. Our study shows that incorporating early collagen fiber recruitment into the model predicts the stress-stretch response reasonably well (rms=0.362), while further considering changes of fiber orientation distribution only improves the predicting capability slightly (rms=0.344). Our study further supports the experimental findings that earlier recruitment of straighter collagen fibers plays an important role in the nonlinear stiffening of GAG depleted artery at lower stretch levels, and should be considered in structural based constitutive models.

5.2 Introduction

Pathogenesis of many vascular diseases, including hypertension, atherosclerosis, stenosis, and aneurysms has been associated with ECM disorders in structure and function and its altered interaction with other arterial constituents. Studies of the structural components of arteries are generally focused on elastin and collagen (Boumaza et al., 2001; Brüel and Oxlund, 1996; Campa et al., 1987; Humphrey and Holzapfel, 2012; Martinez-Lemus et al., 2009; Menashi et al., 1987; Vorp, 2007). Once thought of as simply components of connective tissue, over the last decade the functional and regulatory significance of proteoglycans has emerged as a promising field in all aspects of cell biology and human diseases (Halper, 2014). Recent research suggested an important role of GAGs in binding of low-density lipoprotein, or bad cholesterol, to the arterial wall (Little et al., 2007). When proteoglycans are in excess, they play a major role in the formation of atherosclerotic lesions due to the retention of low-density lipoprotein (Huang et al., 2008; Wight and Merrilees, 2004). Localized accumulation/pooling of proteoglycans can cause arterial wall layers to dissect from increased Donnan swelling pressure (Humphrey, 2012; Sorrentino et al., 2015). In contrast, insufficient levels of the proteoglycans reduce the arteries ability to regulate charge/structure and could play a role in diabetes (Jensen, 1997). Proteoglycans deficiency was also suggested lead to aortic rupture by comprising the functionality of other structural components (Heegaard et al., 2007).

The basic proteoglycan unit consists of a “core protein” with one or more covalently attached glycosaminoglycan (GAGs) chains. Proteoglycans are found in all connective tissues. They provide structural basis for multiple biological functions, such as the organization of ECM assembly and the regulation of cell growth factors. Proteoglycans provide appropriate spacing and organization for other ECM components (Gandley et al., 1997). Since GAGs have a high affinity for water molecules, they serve to hydrate the ECM but also can resist deformation (Lee et al., 2001). The highly charged aggregates also interact with other ECM components, for example, decorin is a proteoglycan known to bind to type I collagen (Halper, 2014). Electron microscopy and immunofluorescence studies strongly suggest the association of proteoglycans with specific regions of the banding pattern of collagen fibrils and also indicate that proteoglycans can form bridges between fibrils (Bartholomew and Anderson, 1983; Eisenstein and Kuettner, 1976; Lewis et al., 2010; Scott, 2003). Furthermore, proteoglycans appear to bind to many cell-surface receptors with high specificity, thereby activating signaling pathways that control cell proliferation, differentiation, adhesion, and migration (Schaefer and Schaefer, 2010).

Various models have been developed to consider GAGs in connective tissue mechanics. Bphasic and triphasic theories have been developed to model cartilage mechanics based on the solid collagen-GAG phase and viscous fluid phase, then the addition of a third ionic phase (Lai et al., 1991; Mow et al., 1980). In tendon mechanics, GAGs are modeled as cross-linking collagen to transfer stretch or isolating neighboring collagen fibrils to promote sliding (Rigozzi et al., 2013; Scott, 2003). In lung tissue mechanics, GAGs have been modeled as contributing to a spring network model that maintains stability of alveolar structure (Takahashi et al., 2014). In carotid artery mechanics, a constitutive model demonstrated that GAGs can cause local intramural swelling that affects structural integrity and mechanosensing (Sorrentino et al., 2015). Recently, a multiscale model was developed to incorporate GAGs protecting collagen fibrils from over-stretching (Linka et al., 2016). In a structurally-based constitutive model of porcine aorta, GAGs were considered to transfer load among collagen fibers through the stiffness of collagen-GAG complexes (Polzer et al., 2015).

Our recent work suggests that GAG depletion indirectly affects arterial mechanics by shifting the transition to nonlinear stiffening at lower strain (Mattson et al., 2016). The shift of nonlinear stiffening at lower strain correlated with the structural finding that GAG depletion resulted in straighter collagen fibers being recruited at lower strain, which established a structure-function relationship. In this study, a structure-based constitutive model (Wang et al., 2016) was adapted to consider the contribution of GAGs to collagen fiber recruitment in arterial mechanics.

5.3 Materials and Methods

5.3.1. Determination of fiber recruitment function

ECM fiber orientation before and after GAG depletion were quantified from simultaneously imaging the collagen and elastin fibers in tissue with second harmonic generation and multiphoton excitation fluorescence, respectively (Mattson et al., 2016). Samples were imaged at 0% to 40% grip-to-grip biaxial strain in 5% increments. Fiber orientation was quantified with two-dimensional fast Fourier transform analysis using the Directionality plug-in in FIJI (fiji.sc/Fiji, Ashburn, VA). In this study, the fiber orientation at 40% biaxial strain was used to reveal the fiber orientation distributions when the fibers are straightened.

Straightness parameter and fractal analysis provided insightful information on changes in fiber network structure in response to mechanical loading (Mattson et al., 2016). Straightness parameter provides direct information about the traced straightening and recruitment of adventitial collagen fibers at different increments of strain. Therefore, the distribution of straightness parameter measurements is informative about the proportion of fibers recruited at each strain level. Specifically, a recruitment threshold such as 0.98 can be set and cumulative fiber recruitment can be determined. Fractal analysis determines the self-similarity of images, which shows minimal changes during delayed fiber recruitment as well as after fibers are fully recruited and no longer straightening. Thus, fiber recruitment only occurs over the increments of stretch in which fractal analysis is changing due to straightening of fibers during recruitment. Therefore, adventitial collagen (AC) and medial collagen (MC) fiber recruitment functions were fit to fractal analysis of images before and after enzymatic GAG depletion at 0% to 40% stretch (Chow et al., 2014; Mattson et al., 2016). The fiber recruitment function is defined as (Lanir, 1979):

$$\eta_f^i = \frac{1}{\sqrt{2\pi d_i}} \exp\left[-\frac{(x - m_i)^2}{2d_i^2} \right]$$

where m_i and d_i (i = AC and MC) are the mean and standard deviation of the fiber recruitment function, which were chosen to fit the stretch ranges where the fractal analysis trendline was increasing. The fiber recruitment functions were then incorporated in the model as η_f^i .

5.3.2. Constitutive modeling

In order to consider the contribution of GAGs to fiber recruitment, a structure-based constitutive model that was previous developed by Wang et al. (Wang et al., 2016) were adapted in this study, to which interested readers are referred. Briefly, the model allows direct incorporation of information obtained from quantitative multiphoton imaging analysis and biochemical assays for the prediction of tissue-level mechanical response. The model considers the contribution from medial elastin (ME), medial collagen (MC), and adventitial collagen (AC), incorporating relative collagen and elastin amounts, n_i, fiber orientation distributions, $R_i(\theta)$, and sequential fiber recruitment. The total strain energy function of the arterial wall is the sum of the constituent strain energy:

$$\begin{aligned} W &= n_{ME} \int_{-\pi/2}^{\pi/2} \psi_{ME} R_{ME}(\theta) d\theta \\ &+ n_{MC} \int_{-\pi/2}^{\pi/2} \int_{1}^{\lambda} \psi_{MC}(\lambda - x) \eta_f^{MC} dx R_{MC}(\theta) d\theta \\ &+ n_{AC} \int_{-\pi/2}^{\pi/2} \int_{1}^{\lambda} \psi_{AC}(\lambda - x) \eta_f^{AC} dx R_{AC}(\theta) d\theta \end{aligned}$$

where ψ_i (i = ME, MC, and AC) the fiber level strain energy function. Considering the close association between GAGs and collagen fiber assembly, fiber recruitment function η_f^{MC} and η_f^{AC} are included for medial and adventitial collagen, specifically, and were determined from imaging analysis from Section 2.1.

The fiber level strain energy function is defined by a freely-jointed chain model as (Wang et al., 2016):

$$\psi_i = k\Theta N_i \left(\frac{\rho_i}{N_i} \beta_p^i + \ln \frac{\beta_p^i}{\sinh \beta_p^i} \right) - k\Theta P_i \beta_p^i \ln \lambda_f$$

where $k = 1.38 \times 10^{-23}\,\mathrm{J/K}$ is Boltzmann's constant, $\Theta = 298\mathrm{K}$ is the absolute temperature, N_i is the number of rigid links within each chain, ρ_i is the normalized deformed chain length, P_i is the normalized undeformed length, λ_f is the fiber-level stretch and $\beta_\rho^i = \mathrm{L}^{-1}\left(\rho_i / N_i\right)$, where $\mathrm{L}\left(x\right) = \coth x - 1/x$ is the Langevin function.

The tissue-level Cauchy stress can be expressed as $\sigma = J^{-1} FSF^T$, where $S = \partial W / \partial E$ is the second Piola-Kirchhoff stress, F is the deformation gradient, and $J = \det(F)$.

The model was first fit to the untreated experimental data and then the same parameters were used to predict the GAG depleted experimental mechanics data. To distinguish the relative influence of fiber distribution and recruitment, the first prediction used the untreated fiber distributions with the treated fiber recruitment functions. The second prediction used the treated fiber distributions with the treated fiber recruitment functions. The material parameters were determined by minimizing the objective function with appropriate constraints (Wang et al., 2016):

$$E = \sum_{j=1}^{m} \left[\left(\sigma_{11}^{c} - \sigma_{11}^{e} \right)_j^2 + \left(\sigma_{22}^{c} - \sigma_{22}^{e} \right)_j^2 \right]$$

where m is the number of data points and σ^c and σ^e represent Cauchy stress from the model and biaxial tensile tests, respectively. Subscripts 1 and 2 correspond to the longitudinal and circumferential directions of the aortic sample, respectively. The objective function is minimized using the Nelder–Mead direct search method implemented in the fminsearch subroutine in MATLAB (version R2013b, MathWorks, Inc.). As a measure of goodness of fit, the root mean square error is defined as:

$$e = \frac{\sqrt{\dfrac{E}{m-q}}}{\sigma_{ref}}$$

where q is the number of parameters in the model, and σ_{ref} is determined from the sum of Cauchy stresses for each stress-stretch curve divided by the number of data points m.

5.4. Results

Representative images from multiphoton microscopy show adventitial collagen, medial collagen, and medial elastin (Figure 5.1). The wavy, unstretched bundles of adventitial collagen fibers straighten with stretch (Figures 5.1a,b). The more intricate medial collagen network with tighter crimp is also shown (Figure 5.1c). The medial elastin fiber network is visibly distinguished by lacking the characteristic crimp of collagen (Figure 5.1d).

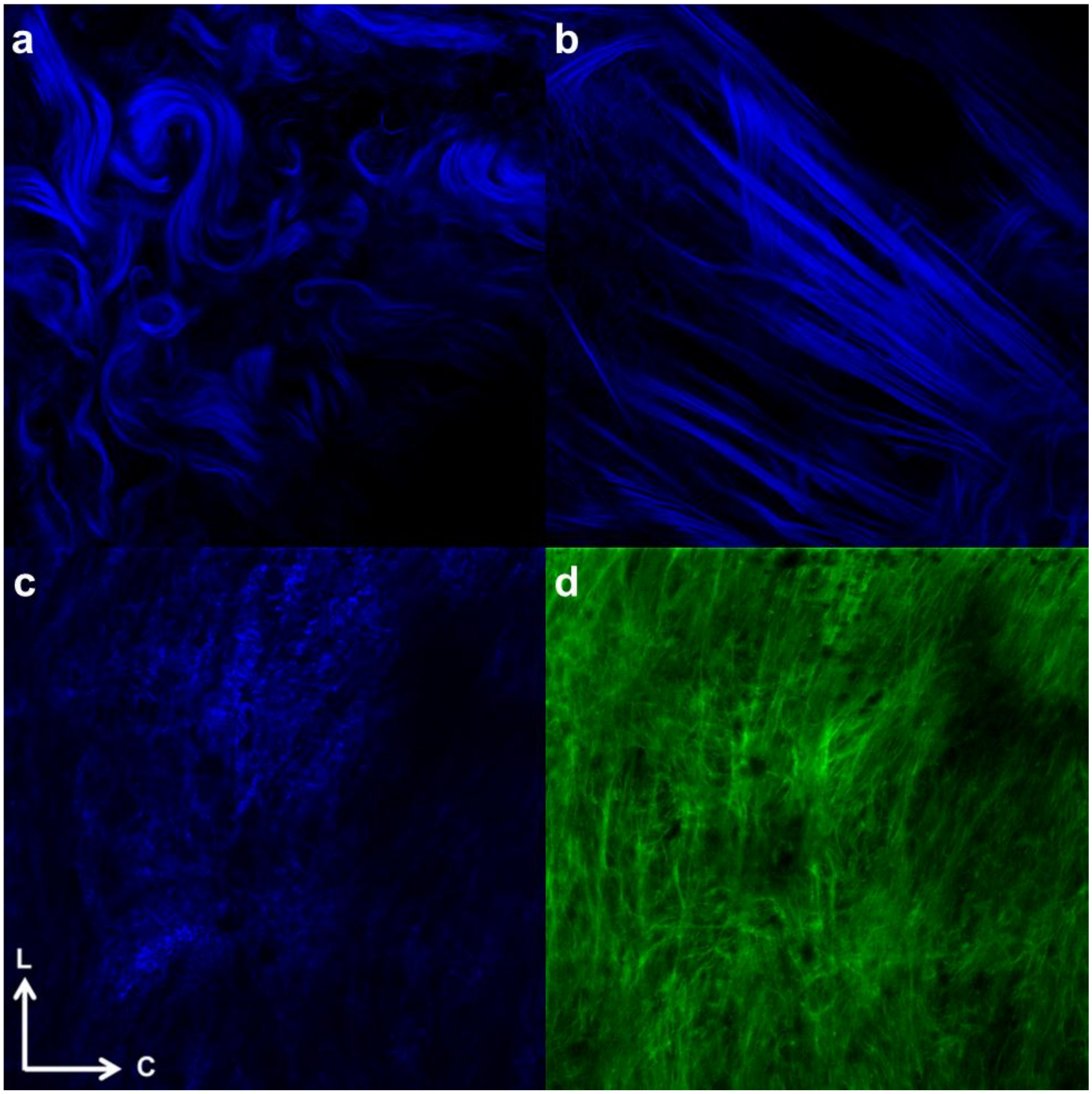

Figure 5.1. Unstretched adventitial collagen fibers are wavy (a), but straighten with stretch (b). Fiber recruitment for the finer medial collagen (c) and medial elastin (d) fiber networks are detectable with fractal analysis. Horizontal is circumferential (C) and vertical is longitudinal (L). Images are 360 µm × 360 µm.

The distributions of straightness parameters for each level of stretch demonstrate that fibers of untreated tissue tend to have a lower straightness parameter compared to treated tissue (Figure 5.2). In general, straightness parameter increases with stretch, visualized by the bar graphs shifting and clustering to the right, asymptotically approaching 1, which represents a straight line. However, at each level, fibers in untreated tissue tend to be wavier and to the left of fibers from treated tissue. To examine adventitial collagen fiber recruitment, cumulative fiber recruitment was determined where fibers with a straightness parameter of at least 0.98 were considered to be recruited (Figure 5.3). Results in Figure 5.3 further shows that there are more recruited fibers for treated versus untreated tissue at each level of stretch until almost all fibers are recruited for both conditions at 1.4 stretch.

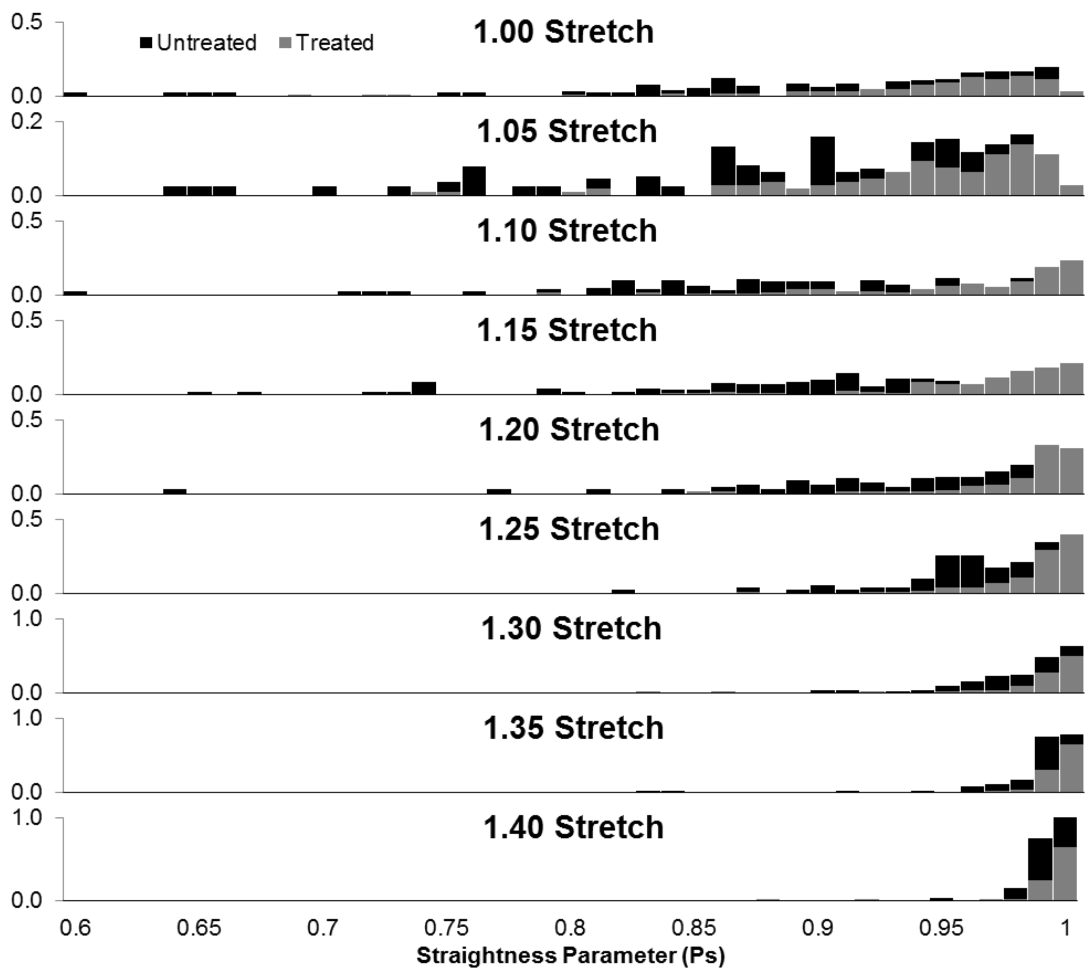

Figure 5.2. Straightness parameter distributions of adventitial collagen for each level of stretch for untreated (black) and treated (gray) tissue from Mattson et al. (Mattson et al., 2016). The number of fibers in each bin were normalized to the total number of fibers traced for each level of stretch for each tissue type.

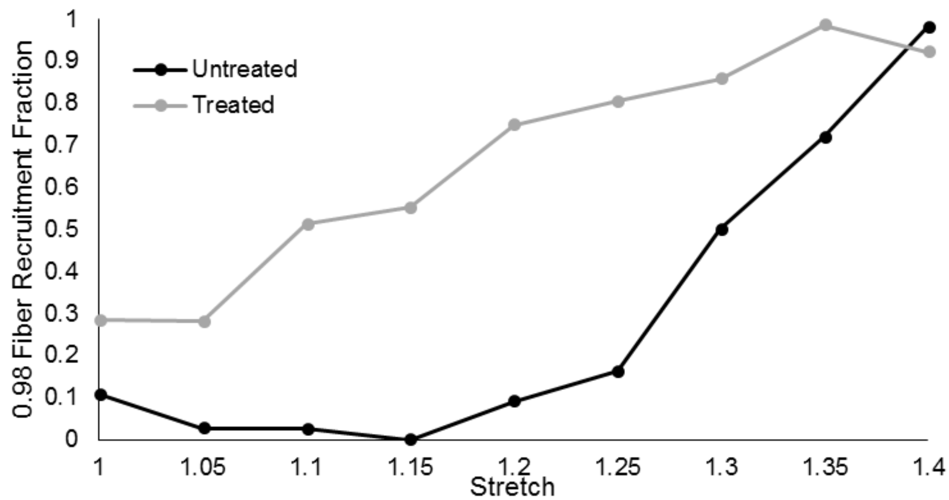

Figure 5.3. Cumulative adventitial collagen fiber recruitment for untreated (black) and treated (gray) tissue, where a straightness parameter of at least 0.98 in Figure 5.2 qualifies a fiber as recruited.

Fiber recruitment functions, h_f^{AC} and h_f^{MC}, were determined for adventitial and medial collagen of untreated and treated tissue (Figure 5.4). Increments of stretch where the fractal analysis trendline is increasing indicates fiber recruitment. Therefore, h_f^{AC} spanned ~1.15 to ~1.35 stretch for untreated tissue (Figure 5.4a), but shifted to a lower stretch range of 1 to ~1.15 after treatment (Figure 5.4b). For medial collagen, h_f^{MC} covered 1 to 1.4 stretch for untreated tissue, but decreased to a stretch range of 1 to ~1.2 after treatment (Figure 5.4d).

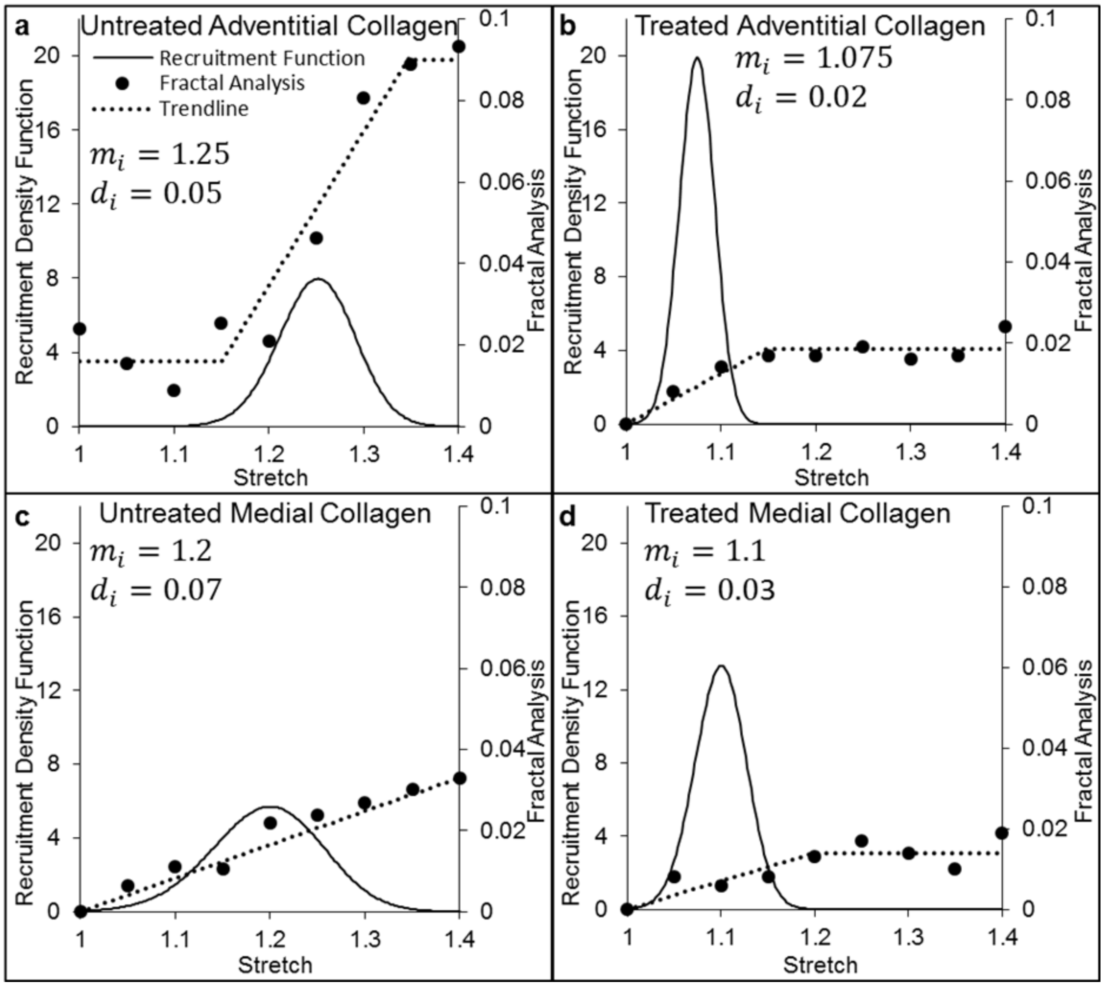

Figure 5.4. Fractal analysis (circles and dashed line) and recruitment functions (solid curve) for adventitial collagen before (a) and after (b) GAG depletion, as well as medial collagen before (c) and after (d) GAG depletion. m_i and d_i are the mean and standard deviation of the fiber recruitment function. Untreated data from (Chow et al., 2014) and treated data from (Mattson et al., 2016).

Figure 5.5 shows the fiber orientation distributions before and after enzymatic GAG depletion at 40% stretch (Figure 5.5). For untreated tissue, adventitial collagen has a preferred longitudinal orientation as well as a minor circumferential oreintation, but after treatement, more peaks emerge with a general shift towards the circumference. Untreated medial collagen is circumferentially oriented and becomes even more so after treatment. Both before and after treatment, medial elastin is relatively uniformly distributed with a slight longitudinal peak as well as a small circumferentialpeak emerging after treatment.

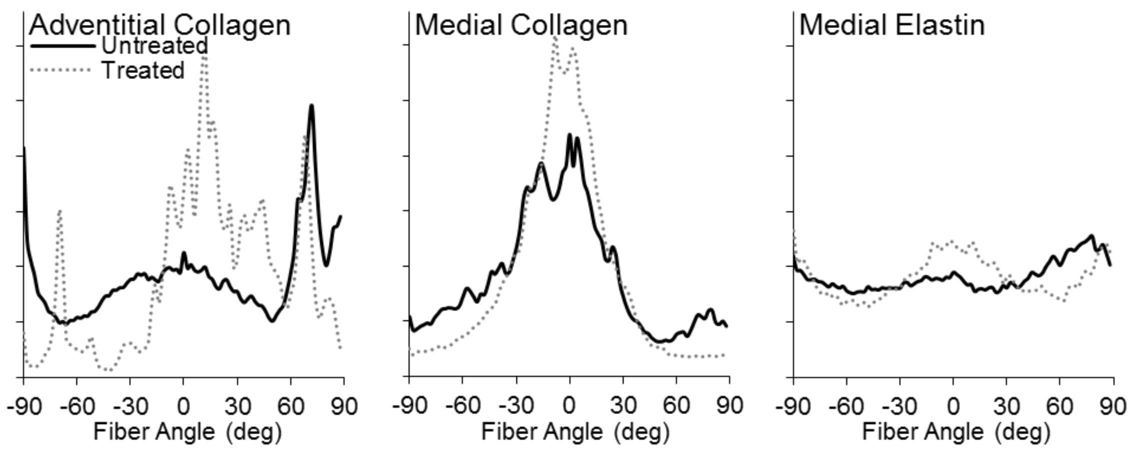

Figure 5.5. Average fiber distributions at 40% stretch for untreated (solid) and treated (dotted) tissue with circumferentially and longitudinally oriented fibers corresponding to 0° and ±90°, respectively. After treatment, adventitial collagen becomes more circumferentially orientated, whereas medial collagen remains circumferentially oriented and medial elastin remains relatively uniformly distributed. Untreated data from (Chow et al., 2014) and treated data from (Mattson et al., 2016).

GAG depletion results in straighter collagen fibers that are recruited at lower levels of stretch with a corresponding earlier transition to nonlinear stiffening (Mattson et al., 2016). Looking at the stress-stretch curves, the treated tissue stiffens more in the circumferential direction in agreement with the primarily circumferentially oriented GAG depleted adventitial and medial collagen fibers (Figures 5.5, 5.6). The model was fit to the untreated biaxial mechanics data to determine the parameter values and fitting error (rms=0.066), then the same parameter values were used to predict the treated stress-stretch mechanics based on the change in fiber orientation distributions and recruitment (Figure 5.6). Overall, the model is able to characterize the nonlinear, anisotropic behavior with a small overestimate in the longitudinal direction at higher stiffness and small underestimate in the circumferential direction. The prediction using the treated fiber orientation distributions and treated fiber recruitment functions was successful (rms=0.344), with a slight overestimate of the nonlinear stiffening in the circumferential direction after GAG depletion. In Figure 5.7, prediction results from using the treated fiber recruitment functions with untreated vs. treated fiber orientation distributions were presented. Considering both the fiber orientation distributions and the fiber recruitment functions after GAG depletion resulted in a slightly better prediction (rms=0.344) than using the untreated fiber orientation distributions (rms=0.362) (Figure 5.7).

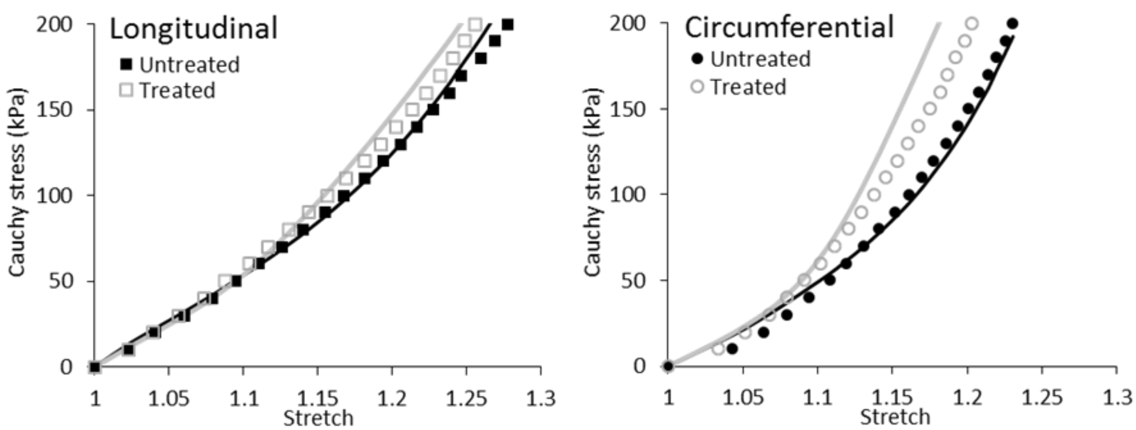

Figure 5.6. Average stress-stretch experimental data (points) and model fit/prediction (lines) for untreated (black) and treated (gray) tissue in the longitudinal and circumferential directions. Chain density ($n_{ME} = 1.61E25, n_{MC} = 5.16E24, n_{AC} = 5.16E23$), rigid links per chain ($N_{ME} = 2.61, N_{MC} = 1.69, N_{AC} = 1.51$), root mean square error of fit (rmsf=0.066), and root mean square error of prediction (rmsp=0.344).

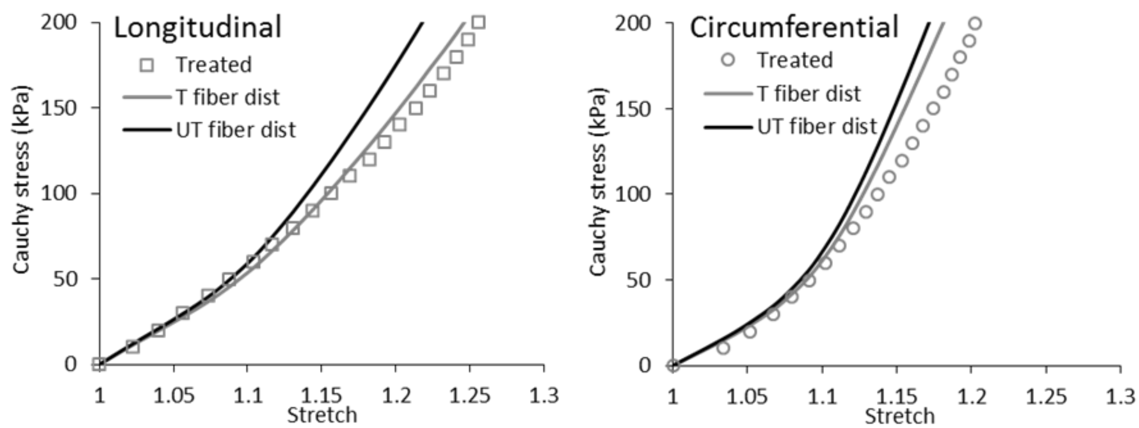

Figure 5.7. Predicting the treated mechanics data (symbols) with treated fiber distributions (T fiber dist, rms=0.344) improved the fit compared to using untreated fiber distributions (UT fiber dist, rms=0.362).

The contribution to biaxial mechanics from each ECM constituent reveals that elastin is dominant over the range tested for both untreated and treated tissue (Figure 5.8). The percent contribution from each ECM constituent at a physiologically relevant level of stretch (20%) is shown in Table 5.1. After treatment, medial collagen and to a lesser extent, adventitial collagen, contributes more to the mechanics, particularly in the circumferential direction. Compared to using the treated fiber distributions, when the untreated fiber distributions were used, the contribution from each ECM constituents to artery mechanics was slightly altered. The percent contribution from longitudinal medial elastin decreased while the contribution of longitudinal medial and adventitial collagen increased. The opposite was true for the circumferential direction, where medial elastin contributed more, but medial and adventitial collagen contributed less.

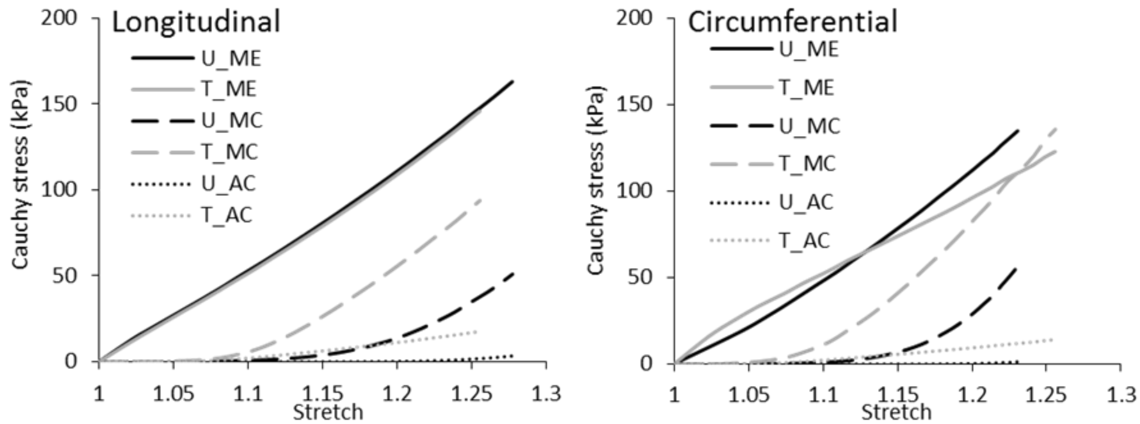

Figure 5.8. Cauchy stress vs. stretch for medial elastin (ME, solid), medial collagen (MC, dashed), and adventitial collagen (AC, dotted) of untreated (U_, black) and treated (T_, gray) tissue in the longitudinal and circumferential directions.

Table 5.1. Percent contribution to mechanics at 1.2 stretch for medial elastin (ME), medial collagen (MC), and adventitial collagen (AC) of untreated and treated tissue in the longitudinal and circumferential directions. U/T uses untreated fiber distributions with treated fiber recruitment functions.

Percent Contribution to Stress-Stretch Curve at 1.2 Stretch

	Longitudinal			Circumferential		
	ME	MC	AC	ME	MC	AC
Untreated	95.39%	4.58%	0.03%	91.13%	8.83%	0.04%
Treated	80.43%	15.79%	3.78%	62.09%	34.32%	3.59%
U/T	74.81%	20.43%	4.76%	78.44%	47.15%	5.70%

5.5 Discussion

GAGs have been found to contribute to the mechanics of soft tissues such as cartilage, tendon, lung, eye sclera, and artery (Halper, 2014; Legerlotz et al., 2013; Mattson et al., 2016; Murienne et al., 2015; Sorrentino et al., 2015; Takahashi et al., 2014). In artery, proteoglycans constitute only a minor component of vascular tissue (2%–5% by dry weight), however these macromolecules are of enormous importance in influencing arterial properties such as viscoelasticity, thrombosis, permeability, lipid metabolism, and hemostasis of the arterial wall (Gerald S Berenson et al., 1984; Camejo, 1982; Mattson et al., 2016; Wight, 1989). Using a structure-based model that incorporates changes in fiber recruitment due to GAG depletion, the present study successfully predicted the earlier mechanical stiffening based on earlier fiber recruitment due to enzymatic GAG depletion. The material parameters are directly based on quantitative analysis of multiphoton microscopy images and biochemical assays. The constitutive model in this study provides new understandings of the structure-function relationship between arterial wall mechanics and ECM constituents, elastin, collagen, and GAGs.

The contribution of GAGs to the mechanics of soft tissue has emerged as an important area of research. Potential mechanisms of GAGs contributing to tensile mechanics are not fully understood. Pressure-controlled inflation testing of eye sclera found that GAG depletion decreased low-pressure stiffness and increased high-pressure stiffness (Murienne et al., 2015). A study of porcine coronary adventitia inflation-extension biaxial mechanics found a negligible GAG contribution (Chen et al., 2016). However, coronary arteries are muscular with lower ECM content compared to aorta, a large elastic artery. Controversial results have been found on the contribution of GAGs to collagen fibril sliding in tendon mechanics (Scott, 2003) (Rigozzi et al., 2013). Findings suggest GAGs either transmit loads between adjacent collagen fibrils by acting as a mechanical crosslink (Scott, 2003), or isolate adjacent fibers from shear friction and do not directly contribute to tensile stiffness (Rigozzi et al., 2013). Building upon the latter and according to the *slide-stuck* theory, a sufficient level of GAGs reduce fibril strain by allowing sliding rather than overstretch (Linka et al., 2016). Though the mechanism may be different, our findings are more consistent with the idea that GAGs protect collagen fibers from over-stretching since enzymatically depleting GAGs results in straighter fibers that are recruited at lower levels of stretch (Figure 5.3). Furthermore, decreased elastin and GAG content from trypsin decellularization reduces fiber waviness (Lin et al., 2016), but since our enzyme treatment specifically targets GAGs, decreasing GAG content alone is sufficient for a loss of collagen fiber waviness (Figure 5.2).

Fiber orientation distributions at 40% stretch were used (Figure 5.5). GAG depletion resulted in more distinct adventitial collagen fiber bundle peaks, perhaps because GAGs are associated with collagen organization, so GAG depletion could lead to less organized fiber bundles with greater variation in orientation (Couchman and Pataki, 2012). Comparing the changes in fiber orientation distributions (Figure 5.5) to changes in fiber contributions to each anatomical direction (Table 5.1) demonstrates that there is a close interplay between fiber recruitment and fiber orientation, and also among different fiber types. For example, the treated fiber orientation distribution for adventitial collagen shows more circumferential peaks (Figure 5.5) and adventitial collagen contributed more to the circumferential direction in treated versus untreated tissue (Table 5.1). However, the fiber orientation distribution for medial elastin showed minimal changes (Figure 5.5), but the contribution of medial elastin decreased in the circumferential direction of treated tissue due to increased collagen recruitment (Table 5.1).

The fiber recruitment function in the present study was obtained based on fractal analysis (Figure 5.4). Fractal analysis serves as a broad measure of fiber recruitment for adventitial collagen as well as medial collagen, which has a finer, more intricate fiber network that cannot be traced with straightness parameter (Chow et al., 2014). In previous studies, collagen fiber recruitment was usually estimated in structure-based constitutive models (Cacho et al., 2007; Weisbecker et al., 2015; Zeinali-Davarani et al., 2015; Zulliger et al., 2004). Hill et al. (Hill et al., 2012) measured medial collagen fiber tortuosity, the inverse of straightness parameter, based on multiphoton images of rabbit carotid artery, and defined fibers as recruited when tortuosity was below 1.02. A gamma cumulative distribution function was then fit to the tortuosity data. In their study, uniaxial loading was used and the model assumes the rest of the arterial structure is an isotropic matrix (Hill et al., 2012). The present study employs biaxial loading, which is important to fully characterize the anisotropic mechanical behavior of aorta. The use of a straightness parameter of at least 0.98 to represent recruited fibers in Figure 5.3 is consistent with the tortuosity of 1.02 by Hill et al. (Hill et al., 2012). The left-skewed straightness parameter distributions in Figure 5.2 complement and support fractal analysis (Figure 5.4), which is a broad measure of fiber recruitment, since both show collagen fibers are being recruited at lower levels of stretch when GAGs are depleted.

Previous work has considered a multiscale structurally-based constitutive model of biaxial porcine aorta, including stiffness of “collagen-GAG complexes” (Polzer et al., 2015). However, GAGs were only considered to transfer load rather than affect fiber recruitment. In addition, the structural parameters were determined from histology analysis, which requires tissue processing. Multiphoton microscopy data used in the present study was simultaneously imaged for collagen and elastin in the same unfixed tissue over a range of stretch levels. Since elastin fibers respond to immediate deformation of the arterial wall, fiber recruitment functions were fit to the fractal analysis of medial and adventitial collagen, which shows changes in fiber recruitment with GAG depletion (Figure 5.4).

The model in the present study provided a good fit to the untreated data as well as prediction of the treated biaxial data (Figure 5.6), Using the treated instead of untreated fiber orientation distributions only slightly affects the model's prediction of overall mechanics (rms=0.344 vs 0.362, Figure 5.7) as well as the relative contribution of each ECM constituent (Table 5.1). This suggests that change to fiber orientation distribution due to GAG depletion has a smaller effect on aorta mechanics than changes to fiber recruitment. An advantage of the constitutive model in this study is that the contribution of individual ECM constituents can be estimated (Figure 5.8 and Table 5.1). At a physiological relevant stretch of 20%, elastin primarily contributes to the total stress, which is expected since collagen, particularly adventitial collagen, is to provide stiffening and prevent arterial rupture during exceptional cases of overextension (Hemmasizadeh et al., 2015; Wagenseil and Mecham, 2009). However, GAG depletion results in collagen being engaged at lower loading levels. As a result, the relative contribution of both medial and adventitial collagen to the total mechanical stress increases, and this change is more prominent in the circumferential direction. Such redistribution of stresses may hold significant implications in alterations of tissue homeostasis, which usually triggers a catastrophic series of events in artery remodeling (Humphrey et al., 2014).

A limitation of the constitutive model in this chapter is that constraints were placed on the six free parameters to ensure a unique solution. However, this is reasonable since the constraints were relatively broad and based on physiologically realistic values.

Furthermore, it is possible that the six parameters of the model overfit the experimental data, but each parameter represents a physical quantity and successfully predicted the treated data set, so overfitting the untreated data set is unlikely. Enzymatic GAG depletion is considered specific and effective, but we cannot entirely rule out an unobservable structural change. In the present model, the changes in mechanical properties were attributed to changes in elastin and collagen fiber distributions as well as in fiber waviness. However, the mechanical properties of elastin and collagen fibers and relative content are assumed to be the same before and after GAG depletion. Multiphoton microscopy z-stacks were conducted from both the adventitial and intimal surfaces, but the middlemost portion of the arterial wall was not captured. Thus, the fiber orientation distributions may not reflect the full structure of arterial wall. Also, averaged data were used, but ultimately subject-specific data will be more clinically relevant. Finally, fiber orientation and recruitment were measured in 2D instead of 3D, but a previous 3D study concluded that a planar assumption is justified since fibers were almost all less than 5° out of plane (Hill et al., 2012).

5.6 Summary

In this chapter, a structure-based constitutive model successfully predicted changes to biaxial arterial mechanics considering the contribution of GAGs to fiber recruitment. The model incorporates medial elastin, medial collagen, and adventitial collagen fiber distributions, recruitment, content, and fiber properties to determine tissue-level biomechanical function. Enzymatic GAG depletion shifts collagen fiber recruitment to lower levels of stretch with a corresponding earlier nonlinear stiffening. Additionally, successful fitting and predicting was accomplished with a small set of physically meaningful material parameters related to the structure and properties of the ECM constituents. This model has clinical and physiological relevance to understanding mechanisms that lead to arterial stiffening with associated alterations in GAG content such as aging, diabetes and atherosclerosis. Our study provides new understandings on the relationship among ECM constituents, elastin, collagen, and GAGs, and how they contribute to mechanics, which may affect vascular homeostasis and mechanobiology.

CHAPTER 6 ONGOING RESEARCH: EFFECT OF AGING AND DIABETES ON HUMAN AORTIC STRUCTURE AND MECHANICS

6.1 Overview

This chapter extends our experimental expertise gained from testing porcine blood vessels and applies our skills to human thoracic aorta from diabetic and age-matched control donors. A framework is established for this research to be continued with a greater sample size and more conclusive findings. Results to date show the aorta thickness increases with age and diabetes seemingly due to intimal thickening and increased, but less organized discontinuous lamellar spacing. With increasing age, collagen/elastin ratio also increases, adventitial collagen fibers are straighter at each level of stretch, and tangent modulus generally increases. Percent stress relaxation and relaxation rate also increased with age, but surprisingly not with diabetes.

6.2 Introduction

As of 2014, an estimated 387 million people have diabetes worldwide, and the number is expected to rise to 592 million by 2035 (WHO, 2004). With the number of people with diabetes rising exponentially, this disease represents one of the greatest medical and socioeconomic challenges worldwide. Diabetic patients are often at high risk of developing cardiovascular diseases (CVDs). In fact, diabetic patients are two to four times more likely to have heart disease or a stroke than nondiabetic subjects (“Cardiovascular Disease & Diabetes,” 2015). Whether in type I or type II diabetes, vascular complications represent the leading cause of morbidity and mortality in diabetic patients. Diabetic patients frequently show signs of accelerated atherosclerosis and age-associated arterial stiffening (Chaturvedi, 2007). Recent studies investigating the association between diabetes and arterial stiffness have consistently shown that diabetic patients have stiffer arteries than nondiabetic subjects (Stehouwer and Ferreira, 2006). Altered extracellular matrix (ECM) structure and composition is identified as one of the main factors attributing to stiffening of the arterial wall in diabetic patients. The structural and biochemical alterations in diabetic vasculature are complex, and the resulted ECM mechanics in and the molecular mechanisms remain poorly understood (Schram et al., 2004; Sun et al., 2009).

There are many biochemical changes in the long-lasting ECM structural proteins with aging and diseases (Lillie and Gosline, 2002; Sell and Monnier, 2012; Zarkovic et al., 2015). Non-enzymatic glycation, the reaction between glucose and the ECM proteins, is magnified in diabetic patients (Lillie and Gosline, 1996; Winlove et al., 1996; Winlove and Parker, 1990). It is one of the main mechanisms of ageing of the long-lived ECM protein, and has been shown to correlate with the severity of diabetic complications (Vishwanath et al., 1986; Vlassara et al., 1986), and to accelerate the age associated stiffening of arteries in diabetic patients (Cameron et al., 2003). Despite the documented biochemical modifications of ECM and their association with CVD, their effect on the biomechanical functionality of ECM remains poorly understood. Such knowledge is integral to understanding the ECM performance in living biological systems. In this Chapter, we build upon our previous work on ECM imaging and mechanical characterization; results from ongoing work on ECM mechanics in diabetes will be presented.

6.3 Materials and Methods

6.3.1 Sample Preparation

Human descending thoracic aortae were obtained from National Disease Research Interchange (NDRI). Duplicate square samples (~30×30 mm) were cut from each donor. Samples were cut with one edge parallel to the longitudinal direction and the other edge parallel to the circumferential direction of the aorta. We have received cylindrical sections (7 cm in length) of human proximal descending thoracic aortas, 15 from non-diabetic donors and 15 from type II diabetic donors. From each of the cylindrical sections, we will obtain 2 samples for a total n=60. To explore the effect of aging, each group will be subdivided into 5 aortas from the following age groups: 18–40, 41–60, 61–100. NDRI harvests the aortas from cadavers within 12 hours of death and snap freezes the specimens in liquid nitrogen, which are then shipped on dry ice overnight and stored in a -80°C freezer upon receipt. Exclusion criteria include: history of cancer, connective tissue diseases, alcoholism, daily tobacco use, intravenous drug use, glucocorticoid treatment, sepsis. In this preliminary study, 8 samples from 4 donors were studied.

6.3.2 Histology

Movat's pentachrome stain was used to compare the overall structural composition of aorta. Refer to Chapter 2.2 for details.

6.3.3 Biochemical assays

For the elastin and collagen assays, adjacent tissue from each blood vessel next to where biaxial samples were cut was used. Refer to Chapter 2.3 for further details. GAG content was quantified with dimethylmethylene blue assay read at 525 nm after using papain digestion of tissue to free GAGs for dye-binding (Stone et al., 1994).

6.3.4 Biaxial Tensile Test

Refer to Chapter 2.4 and 2.4.1 for the biaxial tensile testing protocol. For this experiment, samples were subjected to a 200 N/m equibiaxial loading condition to characterize the anisotropic mechanical behavior.

6.3.5 Multiphoton Microscopy

Refer to Chapter 2.5 for multiphoton microscopy imaging. Samples in this experiment was imaged with a Carl Zeiss LSM 710 NLO microscope system equipped with a Coherent Chameleon Vision–S tunable femtosecond IR pulse laser with an excitation wavelength of 800nm. Power was tuned to approximately 11% of 1900mW, not including attenuation from the optics. Each sample was imaged with a field-of-view of 425 μm at five locations spread over an area of 1 cm^2. Aorta samples were imaged at 0, 5, 10, 20, and 30% equibiaxial grip-to-grip strain. The images were then used in the analysis of fiber straightening and recruitment in response to mechanical loading.

Samples were also embedded in optimal cutting temperature (OCT) compound and sliced in 100 μm increments on a microtome-cryostat for through-thickness medial imaging. Intimal and medial thickness were determined from histology and images were collected at five evenly spaced locations from the inner media, mid1, mid2 (middle), mid3, and outer media.

6.3.6 Imaging analysis

Fiber orientation and frequency of fiber angle were determined from two-dimensional fast Fourier transform analysis using the Directionality plug-in in FIJI (fiji.sc/Fiji, Ashburn, VA) following the developer's instructions. Adventitial collagen fiber waviness was quantified with NeuronJ (imagescience.org/meijering/ software/neuronj) by measuring the end-to-end distance (L_o) and total fiber length (L_f), to define a straightness parameter:

$$P_s = L_o / L_f$$

which is equal to 1 for a straight line (Chow et al., 2014).

6.3.7 Statistical Analysis

Blood vessel thickness, collagen and elastin assay results, mechanics data, and straightness parameter are summarized and plotted with mean ± standard error of the mean. Two-tailed independent t-tests were used for analysis with $p<0.05$ considered as statistically significant.

6.4 Results

Donor data is summarized in Table 6.1. In general, arterial thickness increases with age and diabetes, though 08315 and 10618 had hypertension, which also contributes to arterial wall thickening.

Table 6.1. Summary of donor data. Thickness is mean ± SEM of the duplicate samples.

NDRI #	Age	Sex	Height	Weight	Thickness (mm)	Diabetes	Hypertension
09486	24	F	64"	176 lbs.	1.25 ± 0.01	N	N
08315	44	F	62"	209 lbs.	1.53 ± 0.03	N	Y
08484	57	F	66"	115 lbs.	1.48 ± 0.05	N	N
10618	58	M	72”	165 lbs.	1.96 ± 0.12	Y	Y

Movat's histological stain for each nondiabetic donor is shown in Figure 6.1. 09486 is a young, healthy aorta. Similar to what we have seen in porcine aorta (Figure 4.2): the intima makes up a small portion of the thickness and the media has regularly spaced elastic lamellae (black) with an adventitial collagen (yellow) outer layer. The older donors are thicker overall with thicker intima, and less regular continuity but increased spacing of the elastic lamellae.

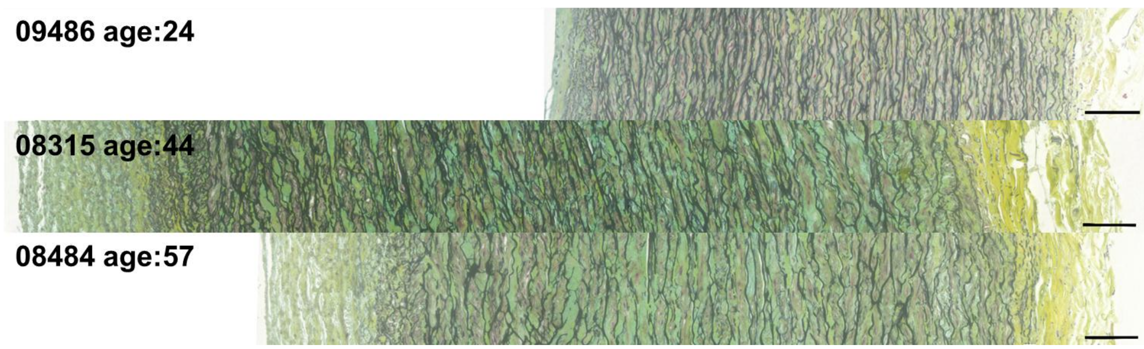

Figure 6.1. Movat's histological stain of through-thickness aorta for different ages. Intima is to the left of the image and adventitia is to the right. Adventitia is mostly collagen (yellow), and media has layers of elastic lamellae (black) interspersed with GAGs (blue) and smooth muscle cells (dark red). Scale bars are 100 µm.

Biochemical assays complement the histology of ECM structure with relative ECM content of collagen, elastin, and GAGs (Figure 6.2). Collagen and elastin comprise most of the ECM, while GAGs make up a smaller fraction for all donors. The collagen/elastin ratio increases significantly ($p<0.0.5$) with age.

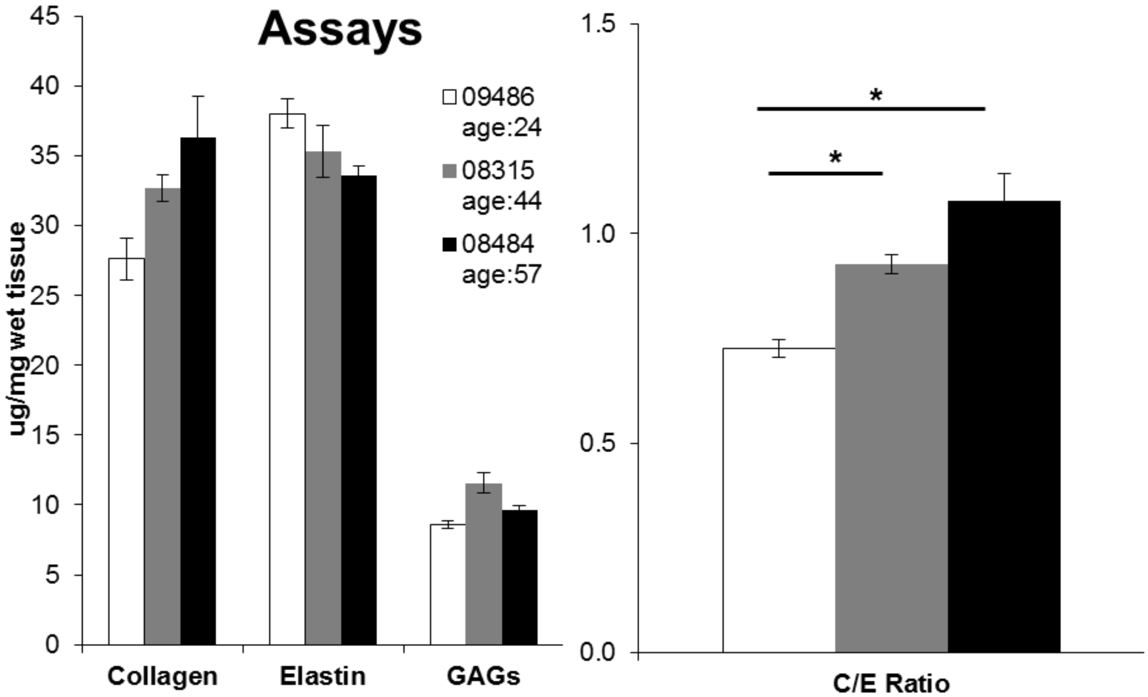

Figure 6.2. Biochemical assays for collagen, elastin, and GAG content for each donor. The collagen/elastin (C/E) ratio significantly ($p<0.05$) increases with age.

Results from mechanical testing show that the younger donor has less inter sample variability and is generally more compliant than older donors, except 08315 in the circumferential direction (Figure 6.3). Tangent modulus was obtained by taking the derivative of a 5^{th} order polynomial fit to the stress-stretch data. Samples from the diabetic donor had similar stiffness to the age-matched nondiabetic donor.

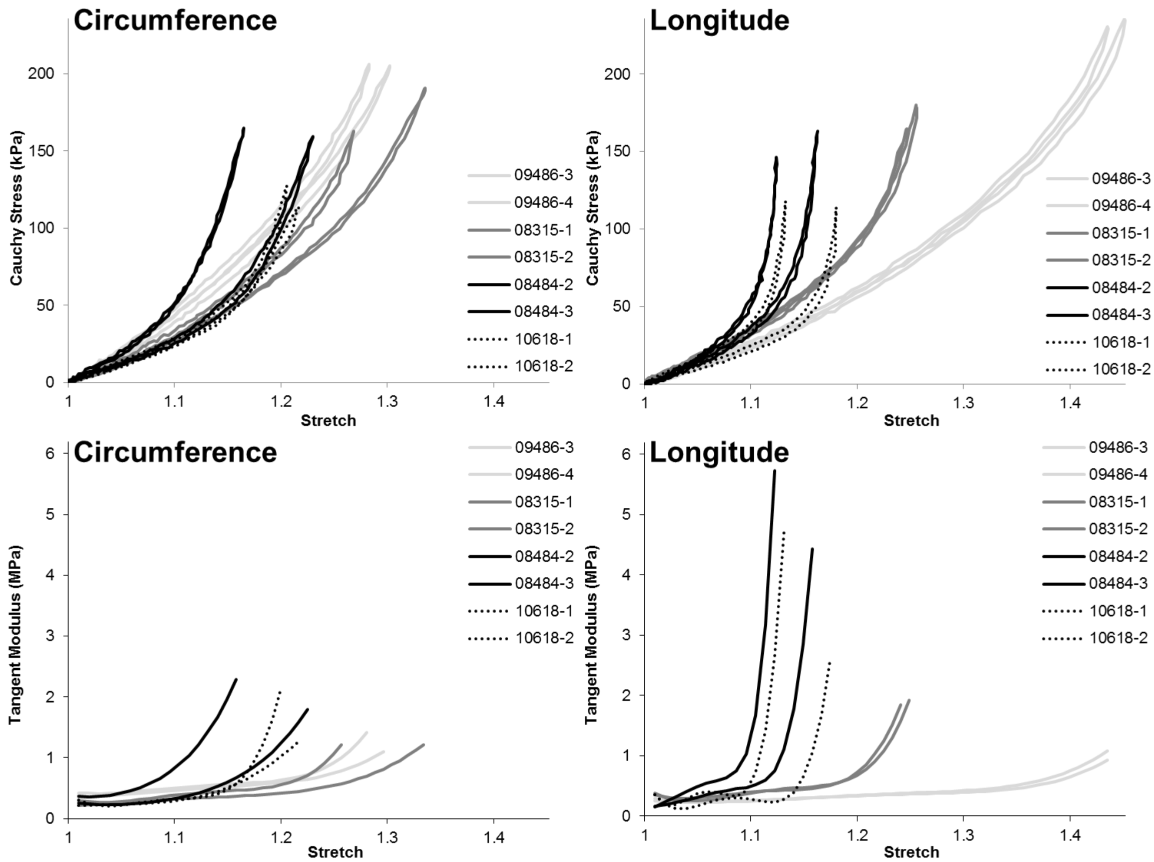

Figure 6.3. Stress-stretch data and corresponding tangent moduli of the circumferential and longitudinal directions for each sample.

Stress relaxation data also provide insight into the effect of aging and diabetes on viscoelastic behavior of aorta (Table 6.2). The rate of relaxation was obtained from the semi-log plot. The first time point used was at 20 s, ten times larger than the rise time to prevent transient effects from a loading that it not truly a step function (Provenzano et al., 2001). The oldest nondiabetic donor had the fastest relaxation rate and highest percent stress relaxation. Surprisingly, the diabetic samples were similar to the young donor with slower relaxation rate and less percent relaxation, but this may be due to the low initial stress.

Table 6.2. Stress relaxation rate and percent relaxation for each sample.

		Circumference		Longitude	
Sample	Initial σ (kPa)	Relaxation Rate	% Relaxation	Relaxation Rate	% Relaxation
09486-3	160	1.36	8.90	1.53	9.14
09486-4	155	1.23	8.01	1.77	10.74
08315-1	135	1.81	13.16	2.10	13.37
08315-2	140	1.96	13.80	2.22	12.28
08484-2	150	5.90	25.26	7.54	36.28
08484-3	140	4.31	21.48	5.21	28.15
10618-1	95	1.08	10.29	1.05	10.09
10618-2	115	1.33	9.17	1.34	10.14

Quantitative analysis of the multiphoton images provides information about adventitial collagen fiber recruitment (Figures 6.4, 6.5). The oldest donor had significantly ($p<0.05$) straighter adventitial collagen fibers (Figure 6.4), which supports the mechanics data that 08484 has higher tangent moduli than the younger donors (Figure 6.3). Straightness parameter distributions at each level of stretch show that the older donors tend to have straighter adventitial collagen fibers that get recruited at lower levels of stretch (Figure 6.5).

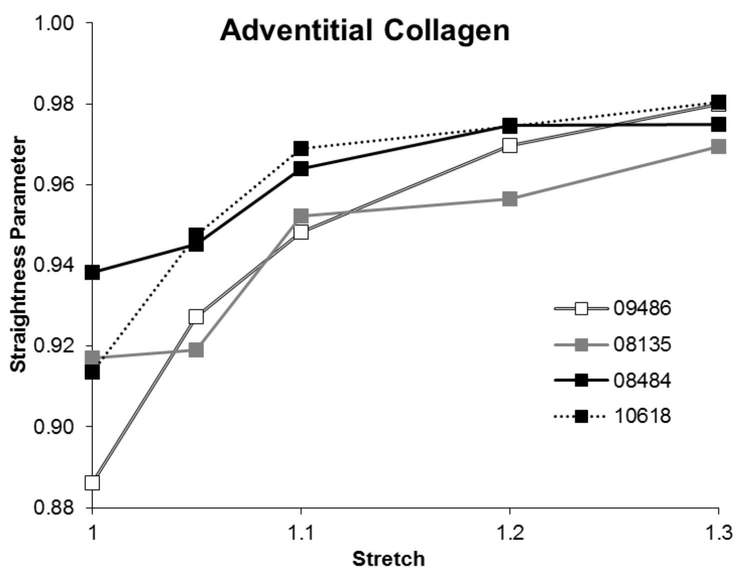

Figure 6.4. Straightness parameter of each donor. For undeformed samples, the oldest donor (08484) has significantly (p<0.05) straighter adventitial collagen fibers than the younger donors.

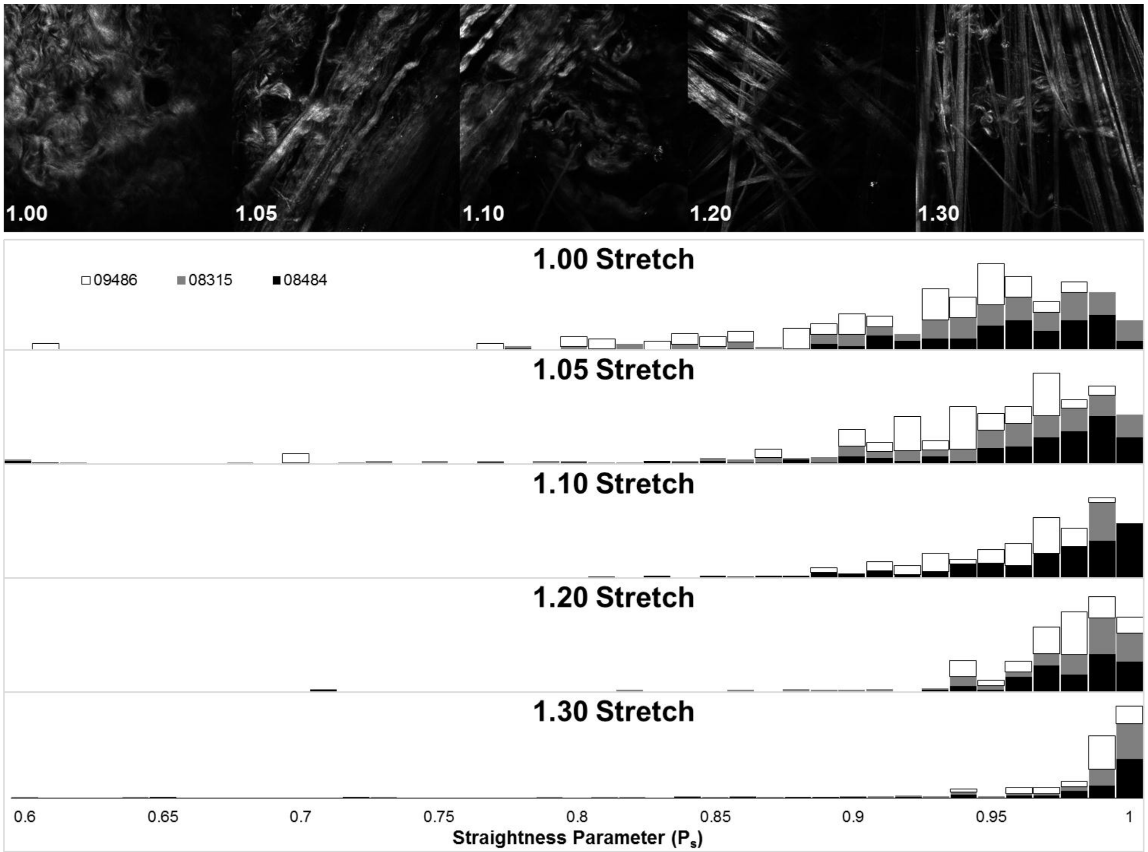

Figure 6.5. Straightness parameter distributions of adventitial collagen for each level of stretch for each donor. The number of fibers in each bin were normalized to the total number of fibers traced for each level of stretch for each donor.

Fiber orientation distributions were quantified from the multiphoton images using fast Fourier transform analysis for adventitial collagen, medial collagen, and medial elastin from nondiabetic and diabetic samples (Figure 6.6).

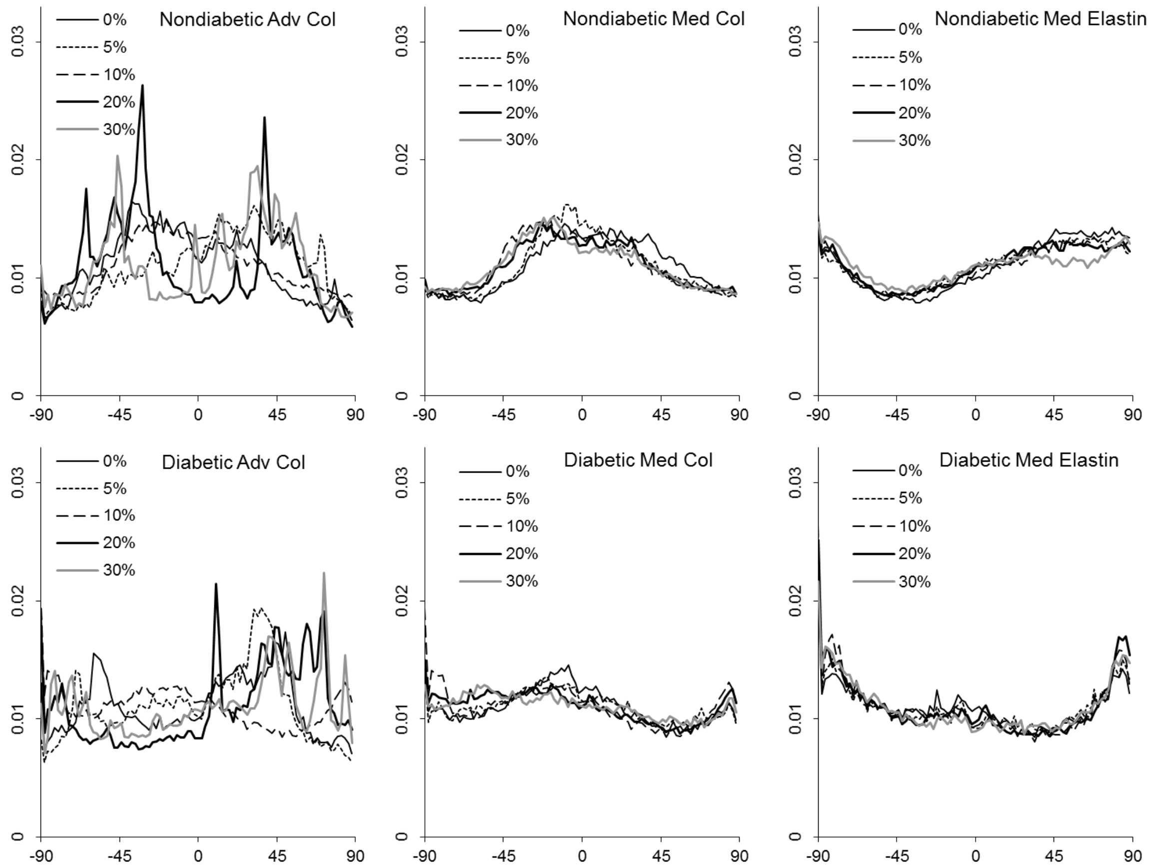

Figure 6.6. Fiber orientation distributions for adventitial collagen, medial collagen, and medial elastin for nondiabetic and diabetic donors at each level of stretch.

Due to the thickened intimal layer, it is likely that the “medial collagen” and “medial elastin” presented in Figure 6.6 are actually from the intimal layer. Detailed structural information are provided from multiphoton imaging throughout the medial thickness (Figures 6.7, 6.8). For each donor, collagen and elastin were imaged at five locations throughout the medial thickness. Representative images from the inner media (Figure 6.7) are shown. Donor 08315 with hypertension was lacking the shift from circumferentially to longitudinally oriented fibers at the inner media observed in the normotensive donors (Figure 6.8).

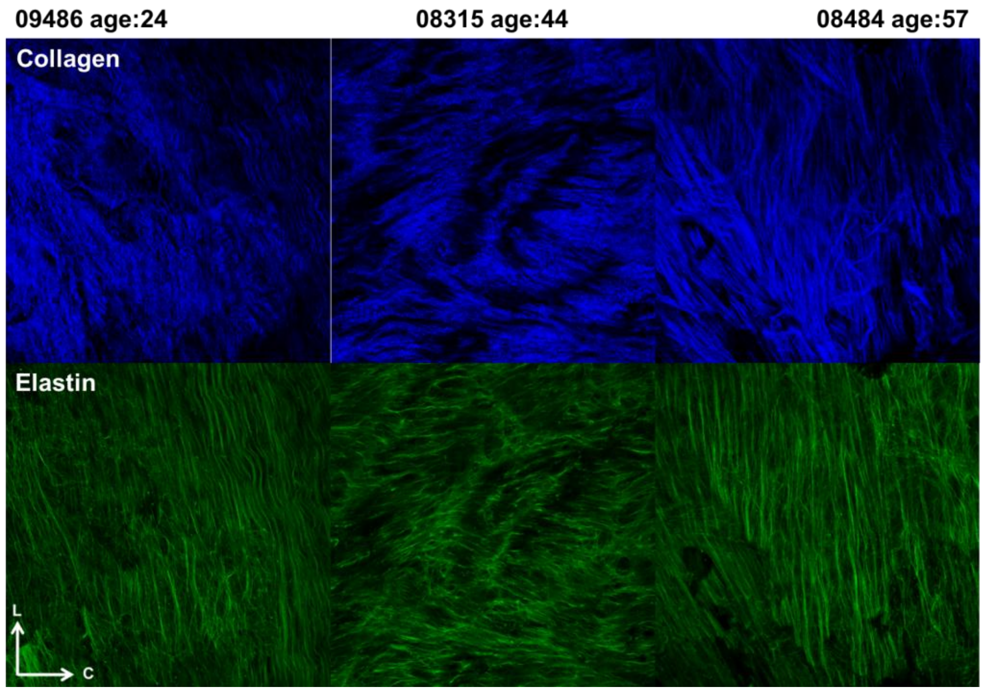

Figure 6.7. Multiphoton images of collagen and elastin at the inner media for each donor. Horizontal is circumferential (C) and vertical is longitudinal (L). Images are 425x425 µm.

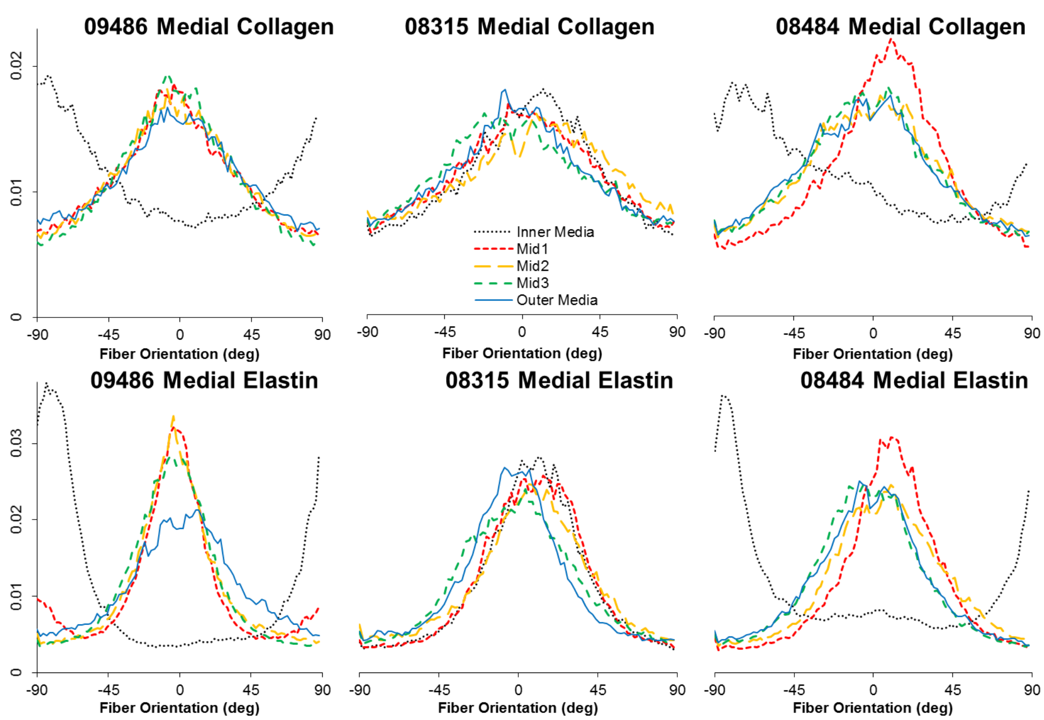

Figure 6.8. Fiber orientation distributions medial collagen and elastin at five locations throughout the thickness of the media for each donor. The circumferential direction is 0° and the longitudinal direction is ±90°.

6.5 Discussion

Aging and disease can have profound effects on the mechanical properties of blood vessels. In this study, human donors were divided into age groups of 18–40, 41–60, and 61–100 with age-matched controls for diabetes. Compared to younger arteries, older arteries generally have a thicker intima, larger interlamellar spacing, with less organized, discontinuous lamellae (Figure 6.1). Increasing arterial thickness with age (Schriefl et al., 2012) and the thickness range of 1.25 to 1.96 mm is consistent with other research (Roccabianca et al., 2014; Schriefl et al., 2012). Consistent with existing literature (Tsamis et al., 2013), the collagen/elastin ratio also significantly ($p<0.05$) increases with age (Figure 6.2), However, GAG content was not significantly different.

Older arteries are generally stiffer, but the diabetic aorta was not stiffer than the age-matched control (Figure 6.3). Our results support a similar previous study of descending aorta planar biaxial mechanics for ages 0–30, 31–60, and 61+ (Haskett et al., 2010). A cyclic tension of 120 N/m was used compared to 200 N/m in the present study and our range of tangent moduli overlap, but also contain higher values due to higher loading (Table 6.3). Our results are also in general agreement with previous data sets of descending thoracic aorta mechanics compiled and standardized by the authors (Roccabianca et al., 2014). A recent study also found that descending thoracic aorta from donors older than 55 years generally had stiffer biaxial mechanics compared to donors younger than 40 years (Taghizadeh and Tafazzoli-Shadpour, 2017). Furthermore, despite using uniaxial tension, previous studies found a similar range of stretch for nonlinear stiffening as well as the longitudinal direction generally being stiffer than the circumference (García-Herrera et al., 2012; Pierce et al., 2015).

Table 6.3. A comparison of stiffness from the four samples in the present study to age groups of a previous study (Haskett et al., 2010).

Age	Circumference Stiffness (MPa)	Longitude Stiffness (MPa)
24	0.35-1.41	0.25-1.10
44	0.21-1.41	0.36-1.92
57	0.25-2.29	0.16-5.73
58	0.21-2.12	0.35-4.70
0-30	0.60-0.75	0.60-0.70
31-60	1.05-1.55	1.50-2.60
61+	1.25-1.65	3.7-4.85

The total percent and rate of stress relaxation generally increase with age, but surprisingly, the diabetic aorta, had less total percent stress relaxation than the age-matched control (Table 6.2). The percent stress relaxation was in the range of other studies such as ~15% for ascending aorta of 42–51 year olds (Craiem et al., 2008) and ~20% for cerebral artery of 28–32 year olds (Li et al., 2013). Some of this difference may be attributed to the fact that the diabetic samples were thicker and because the test is tension-controlled, the initial stress level was lower, which can result in less relaxation (Zou and Zhang, 2011).

The straightness parameter results (Figures 6.4, 6.5) suggest that aging results in straighter adventitial collagen fibers that get recruited at lower levels of stretch and correspond with the nonlinear stiffening of stress-stretch data in Figure 6.3. However, there weren't any obvious differences in fiber orientation distribution between nondiabetic and diabetic donors (Figure 6.6). A previous study used small-angle light scattering validated with multiphoton imaging to suggest a general circumferential fiber orientation of descending aorta for all ages, but increasing alignment with age (Haskett et al., 2010). However, another study used polarized light histology and found diagonally oriented fiber families throughout the thickness (Schriefl et al., 2012). Through-thickness analysis in the present study revealed that the nondiabetic hypertensive aorta (08315) seemed to lack a longitudinally oriented inner media observed in the other donors (Figures 6.7, 6.8). It is possible that the through-thickness sectioning missed the internal lamina, but looking at the histology, the location of where the lamina could be expected is less organized and blends more with the thickened intima (Figure 6.1).

6.6 Summary

This ongoing study has revealed interesting results combining microstructure quantification with biaxial mechanics. Standard techniques of histology and biochemical assays show typical changes with aging such as thicker aorta with higher collagen/elastin ratio. Multiphoton imaging allows for quantification of medial elastin, medial collagen and adventitial collagen fiber orientation as well as adventitial collagen fiber recruitment. Samples from the oldest donor showed fiber recruitment at lower levels of stretch, consistent with the biaxial mechanics showing the same samples having higher stiffness at lower levels of stretch. Rate of stress relaxation and total percent stress relaxation also seem to increase with age, but not with diabetes. However, increasing the sample size is necessary before drawing conclusions of clinical and physiological relevance.

CHAPTER 7 CONCLUSIONS AND OUTLOOK

7.1 Conclusions

Elastin and collagen fibers are the major load-bearing ECM constituents of the vascular wall. Our research compared the relationship between biaxial mechanical function and ECM structure of porcine thoracic aorta and inferior vena cava. Our study suggests that aorta contains slightly more elastin than collagen due to the cyclical extensibility, but vena cava contains almost four times more collagen than elastin to maintain integrity. In addition to differences in relative ECM content, ECM fiber orientation and recruitment varied between vena cava and aorta. In vena cava, elastin is longitudinally oriented while collagen is primarily circumferentially oriented and recruited at supraphysiologic stress, but low levels of strain. However in aorta, elastin is distributed uniformly and the primarily circumferentially oriented collagen is recruited at higher levels of strain than vena cava. These structural differences support the highly anisotropic mechanics of vena cava with the longitude being more compliant than the stiff circumferential direction.

While studies often focus on the contribution of elastin and collagen fibers to the mechanics of blood vessels, we also considered the role of GAGs. Although GAGs represent only a small component of the vessel wall ECM, they are considerably important because of their diverse functionality and their role in pathological processes. Our research found that GAGs also affect arterial mechanics by influencing ECM fiber recruitment. Enzymatic GAG depletion results in straighter fibers that are recruited at lower levels of stretch, which corresponds to a shift in nonlinear stiffening to lower levels of stretch for arterial mechanics. A structure-based constitutive model that incorporated relative ECM content with fiber orientation and recruitment successfully predicted the changes in mechanics due to structural changes after GAG depletion. The model parameters were determined using the untreated structural measurements to fit the untreated biaxial stress-stretch data. Then using the same parameters with GAG depleted structural measurements, the GAG depleted stress-stretch data was successfully predicted for porcine thoracic aorta.

Our research coupling multiphoton structure quantification with rigorous biaxial mechanical testing and structure-based constitutive modeling has been expanded to study human thoracic aorta from diabetic and age-matched control donors. Aging correlates with thicker aorta, higher collagen/ratio, straighter adventitial collagen fibers, stiffer mechanics, and more stress relaxation at a faster rate. Whether it is due to differences in blood vessel type, GAG depletion, aging or disease, straighter collagen fibers strongly correlate with stiffer mechanics in the direction that the fibers are oriented. Differences due to diabetes will need to be established with a larger sample size.

7.2 Outlook

The contribution of each structural aspect (e.g., relative ECM content, fiber orientation, fiber recruitment) to mechanics can be intuitive, but a more complex relationship emerges when necessarily considering all aspects together due to interaction effects. A reductionist approach is useful for establishing a framework, but it can be difficult to isolate effects of each component from interactions among components. Using new technology is helpful and maintaining rigorous quantification and characterization is necessary. It is important to pair validated structure-based models with experimental mechanics and test predictions in a continually improving cycle.

Our structure-based constitutive model could be expanded to include changes in elastin recruitment or through-thickness structural variations. Analysis of microstructure can be continued in 3-D and ECM volume can be mapped. Furthermore, our research could incorporate residual stress or be applied to growth and remodeling. Additionally, the relationship between GAGs and hydration or osmotic conditions can be explored, potentially with GAG-specific depletion or a mouse GAG-knockout model. Fundamental research is essential, but because there are endless possibilities of research questions, it is important to be guided towards translational research.

Our robust techniques can be applied to other arteries and veins, possibly from different animal models or different diseases. There is a need to establish a baseline characterization to understand native, healthy tissue to be able to understand pathologic changes and how to restore vital conditions. This same knowledge can provide essential benchmarks for the emerging field of tissue engineering, opening the way for more collaboration with tissue engineers and considering the mechanobiological effect of ECM multiscale strain transfer on cellular activity.

BIBLIOGRAPHY

Aikawa, J., Munakata, H., Isemura, M., Ototani, N., Yosizawa, Z., 1984. Comparison of Glycosaminoglycans from Thoracic Aortas of Several Mammals. Tohoku Journal of Experimental Medicine. 143, 107–112.

Akhtar, R., Schwarzer, N., Sherratt, M.J., Watson, R.E.B., Graham, H.K., Trafford, A.W., Mummery, P.M., Derby, B., 2009. Nanoindentation of histological specimens. Journal of Materials Research. 24, 638–646. doi:10.1557/JMR.2009.0130

Al Jamal, R., Roughley, P.J., Ludwig, M.S., 2001. Effect of glycosaminoglycan degradation on lung tissue viscoelasticity. American Journal of Physiology. Lung Cellular and Molecular Physiology. 280, L306–L315.

Alastrué, V., Peña, E., Martínez, M.A., Doblaré, M., 2008. Experimental study and constitutive modelling of the passive mechanical properties of the ovine infrarenal vena cava tissue. Journal of Biomechanics. 41, 3038–3045. doi:10.1016/j.jbiomech.2008.07.008

Alkhalili, E., Greenbaum, A., Langsfeld, M., Marek, J., Rana, M.A., Glew, R., Nir, I., 2016. Leiomyosarcoma of the Inferior Vena Cava: A Case Series and Review of the Literature. Annals of Vascular Surgery. 33, 245–251. doi:10.1016/j.avsg.2015.10.016

Ateshian, G.A., Rajan, V., Chahine, N.O., Canal, C.E., Hung, C.T., 2009. Modeling the matrix of articular cartilage using a continuous fiber angular distribution predicts many observed phenomena. Journal of Biomechanical Engineceering. 131, 61003. doi:10.1115/1.3118773

Azeloglu, E.U., Albro, M.B., Thimmappa, V. a, Ateshian, G. a, Costa, K.D., 2008. Heterogeneous transmural proteoglycan distribution provides a mechanism for regulating residual stresses in the aorta. American Journal of Physiology. Heart and Circulatory Physiology 294, H1197–H1205. doi:10.1152/ajpheart.01027.2007.

Baker, A.B., Chatzizisis, Y.S., Beigel, R., Jonas, M., Stone, B. V., Coskun, A.U., Maynard, C., Rogers, C., Koskinas, K.C., Feldman, C.L., Stone, P.H., Edelman, E.R., 2010. Regulation of heparanase expression in coronary artery disease in diabetic, hyperlipidemic swine. Atherosclerosis 213, 436–442. doi:10.1016/j.atherosclerosis.2010.09.003

Baker, A.B., Groothuis, A., Jonas, M., Ettenson, D.S., Shazly, T., Zcharia, E., Vlodavsky, I., Seifert, P., Edelman, E.R., 2009. Heparanase alters arterial structure, mechanics, and repair following endovascular stenting in mice. Circulation Research. 104, 380–387. doi:10.1161/CIRCRESAHA.108.180695

Bartholomew, J.S., Anderson, J.C., 1983. Investigation of relationships between collagens, elastin and proteoglycans in bovine thoracic aorta by immunofluorescence techniques. Histochemical Journal. 15, 1177–90.

Beenakker, J.-W.M.W.M., Ashcroft, B.A.A., Lindeman, J.H.N.H.N., Oosterkamp, T.H.H., 2012. Mechanical properties of the extracellular matrix of the aorta studied by enzymatic treatments. Biophysical Journal. 102, 1731–1737. doi:10.1016/j.bpj.2012.03.041

Bellini, C., Ferruzzi, J., Roccabianca, S., Di Martino, E.S., Humphrey, J.D., 2014. A microstructurally motivated model of arterial wall mechanics with mechanobiological implications. Annals of Biomedical Engineering. 42, 488–502. doi:10.1007/s10439-013-0928-x

Berenson, G.S., Radhakrishnamurthy, B., Srinivasan, S.R., Vijayagopal, P., Dalferes, E.R., Sharma, C., 1984. Recent advances in molecular pathology. Carbohydrate-protein macromolecules and arterial wall integrity–a role in atherogenesis. Experimental and Molecular Pathology. 41, 267–287. doi:10.1016/0014-4800(84)90043-1

Boumaza, S., Arribas, S.M., Osborne-Pellegrin, M., McGrath, J.C., Laurent, S., Lacolley, P., Challande, P., 2001. Fenestrations of the carotid internal elastic lamina and structural adaptation in stroke-prone spontaneously hypertensive rats. Hypertension. 37, 1101–1107.

Brüel, A., Oxlund, H., 1996. Changes in biomechanical properties, composition of collagen and elastin, and advanced glycation endproducts of the rat aorta in relation to age. Atherosclerosis 127, 155–165. doi:10.1016/S0021-9150(96)05947-3

Burton, A.C., 1954. Relation of structure to function of the tissues of the wall of blood vessels. Physiological Reviews. 34, 619–42.

Cacho, F., Elbischger, P.J., Rodríguez, J.F., Doblaré, M., Holzapfel, G.A., 2007. A constitutive model for fibrous tissues considering collagen fiber crimp. International Journal of Non-Linear Mechanics. Special Issue in Honour of Dr Ronald S. Rivlin 42, 391–402. doi:10.1016/j.ijnonlinmec.2007.02.002

Camejo, G., 1982. The interaction of lipids and lipoproteins with the intercellular matrix of arterial tissue: its possible role in atherogenesis. Advances in Lipid Research. 19, 1–53.

Camejo, G., Hurt-Camejo, E., Wiklund, O., Bondjers, G., 1998. Association of apo B lipoproteins with arterial proteoglycans: Pathological significance and molecular basis. Atherosclerosis. 139(2), 205–222. doi:10.1016/S0021-9150(98)00107-5

Cameron, J.D., Bulpitt, C.J., Pinto, E.S., Rajkumar, C., 2003. The aging of elastic and muscular arteries: a comparison of diabetic and nondiabetic subjects. Diabetes Care 26, 2133–2138.

Campa, J.S., Greenhalgh, R.M., Powell, J.T., 1987. Elastin degradation in abdominal aortic aneurysms. Atherosclerosis 65, 13–21.

Cardiovascular Disease & Diabetes [WWW Document], 2015. URL http://www.heart.org/HEARTORG/Conditions/Diabetes/WhyDiabetesMatters/Cardiovascular-DiseaseDiabetes_UCM_313865_Article.jsp

Cavalcante, F.S.A., Ito, S., Brewer, K., Sakai, H., Alencar, A.M., Almeida, M.P., Andrade, J.S., Majumdar, A., Ingenito, E.P., Suki, B., 2005. Mechanical interactions between collagen and proteoglycans: implications for the stability of lung tissue. Journal of Applied Physiology. 98, 672–679. doi:10.1152/japplphysiol.00619.2004

Chaturvedi, N., 2007. The burden of diabetes and its complications: Trends and implications for intervention. Diabetes Research and Clinical Practice. 76(Suppl. 1), S3–12. doi:10.1016/j.diabres.2007.01.019

Chen, H., Guo, X., Luo, T., Kassab, G.S., 2016. A validated 3D microstructure-based constitutive model of coronary artery adventitia. Journal of Applied Physiology. 121, 603–603. doi:10.1152/japplphysiol.zdg-1941.corr.2016

Chow, M.-J., Zou, Y., He, H., McGowan, F.X., Zurakowski, D., Zhang, Y., 2011. Obstruction-induced pulmonary vascular remodeling. Journal of Biomechanical Engineering. 133, 111009. doi:10.1115/1.4005301

Chow, M.-J.J., Turcotte, R.R., Lin, C.P.P., Zhang, Y., 2014. Arterial extracellular matrix: A mechanobiological study of the contributions and interactions of elastin and collagen. Biophysical Journal. 106, 2684–2692. doi:10.1016/j.bpj.2014.05.014

Chow, M.J., Mondonedo, J.R., Johnson, V.M., Zhang, Y., 2013. Progressive structural and biomechanical changes in elastin degraded aorta. Biomechanics and Modeling in Mechanobiology. 12, 361–372. doi:10.1007/s10237-012-0404-9

Couchman, J.R., Pataki, C.A., 2012. An introduction to proteoglycans and their localization. Journal of Histochemistry and Cytochemistry. 60, 885–897. doi:10.1369/0022155412464638

Craiem, D., Rojo, F.J., Atienza, J.M., Armentano, R.L., Guinea, G. V, 2008. Fractional-order viscoelasticity applied to describe uniaxial stress relaxation of human arteries. Physics in Medicine and Biology. 53, 4543–54. doi:10.1088/0031-9155/53/17/006

Davies, M.G., Fulton, G.J., Svendsen, E., Hagen, P.O., 1999. Time course of the regression of intimal hyperplasia in experimental vein grafts. Cardiovascular Pathology. 8, 161–168. doi:10.1016/S1054-8807(98)00029-5

Desai, M., Mirzay-Razzaz, J., von Delft, D., Sarkar, S., Hamilton, G., Seifalian, A.M., 2010. Inhibition of neointimal formation and hyperplasia in vein grafts by external stent/sheath. Vascular Medicine. 15, 287–97. doi:10.1177/1358863X10366479

Desch, G.W., Weizsäcker, H.W., 2007. A model for passive elastic properties of rat vena cava. Journal of Biomechanics. 40, 3130–3145. doi:10.1016/j.jbiomech.2007.03.028

Dingemans, K.P., Teeling, P., Lagendijk, J.H., Becker, A.E., 2000. Extracellular matrix of the human aortic media: an ultrastructural histochemical and immunohistochemical study of the adult aortic media. Anatomical Record. 258, 1–14. doi:10.1002/(SICI)1097-0185(20000101)258:1<1::AID-AR1>3.0.CO;2-7

Disease Statistics - NHLBI, NIH [WWW Document], 2012. NIH Natl. Hear. Lung, Blood Inst. URL http://www.nhlbi.nih.gov/about/documents/factbook/2012/chapter4 (accessed 6.1.16).

Dobrin, P.B., Littooy, F.N., Endean, E.D., 1989. Mechanical factors predisposing to intimal hyperplasia and medial thickening in autogenous vein grafts. Surgery 105, 393–400.

Eckert, C.E., Fan, R., Mikulis, B., Barron, M., Carruthers, C.A., Friebe, V.M., Vyavahare, N.R., Sacks, M.S., 2013. On the biomechanical role of glycosaminoglycans in the aortic heart valve leaflet. Acta Biomaterialia. 9, 4653–4660. doi:10.1016/j.actbio.2012.09.031

Eisenstein, R., Kuettner, K., 1976. The ground substance of the arterial wall Part 2. Electron-microscopic studies. Atherosclerosis 24, 37–46. doi:10.1016/0021-9150(76)90062-9

Evanko, S.P., Tammi, M.I., Tammi, R.H., Wight, T.N., 2007. Hyaluronan-dependent pericellular matrix. Advanced Drug Delivery Reviews 59, 1351–1365. doi:10.1016/j.addr.2007.08.008

Fann, J.I., Sokoloff, M.H., Sarris, G.E., Yun, K.L., Kosek, J.C., Miller, D.C., 1990. The reversibility of canine vein-graft arterialization. Circulation 82, IV9–18.

Fessel, G., Snedeker, J.G., 2009. Evidence against proteoglycan mediated collagen fibril load transmission and dynamic viscoelasticity in tendon. Matrix Biology. 28, 503–510. doi:10.1016/j.matbio.2009.08.002

Gandley, R.E., McLaughlin, M.K., Koob, T.J., Little, S.A., McGuffee, L.J., 1997. Contribution of chondroitin-dermatan sulfate-containing proteoglycans to the function of rat mesenteric arteries. American Journal of Physiology. 273, H952–960.

García-Herrera, C.M., Celentano, D.J., Cruchaga, M. a., Rojo, F.J., Atienza, J.M., Guinea, G. V., Goicolea, J.M., 2012. Mechanical characterisation of the human thoracic descending aorta: experiments and modelling. Computer Methods in Biomechanics and Biomedical Engineering. 15, 185–193. doi:10.1080/10255842.2010.520704

Gineyts, E., Cloos, P. a, Borel, O., Grimaud, L., Delmas, P.D., Garnero, P., 2000. Racemization and isomerization of type I collagen C-telopeptides in human bone and soft tissues: assessment of tissue turnover. Biochemical Journal. 345 Pt 3, 481–5. doi:10.1042/0264-6021:3450481

Grashow, J.S., Yoganathan, A.P., Sacks, M.S., 2006. Biaixal stress-stretch behavior of the mitral valve anterior leaflet at physiologic strain rates. Annals of Biomedical Engineering. 34, 315–325. doi:10.1007/s10439-005-9027-y

Halper, J., 2014. Proteoglycans and diseases of soft tissues, in: Halper, J. (Ed.), Advances in Experimental Medicine and Biology. Springer Netherlands, pp. 49–58. doi:10.1007/978-94-007-7893-1_4

Haskett, D., Johnson, G., Zhou, A., Utzinger, U., Geest, J. Vande, Vande Geest, J., 2010. Microstructural and biomechanical alterations of the human aorta as a function of age and location. Biomechanics and Modeling in Mechanobiology. 9, 725–736. doi:10.1007/s10237-010-0209-7

Hayes, A.J., Lord, M.S., Smith, S.M., Smith, M.M., Whitelock, J.M., Weiss, A.S., Melrose, J., 2011. Colocalization in vivo and association in vitro of perlecan and elastin. Histochemistry and Cell Biology. 136, 437–454. doi:10.1007/s00418-011-0854-7

Heegaard, A.-M.M., Corsi, A., Danielsen, C.C., Nielsen, K.L., Jorgensen, H.L., Riminucci, M., Young, M.F., Bianco, P., 2007. Biglycan deficiency causes spontaneous aortic dissection and rupture in mice. Circulation 115, 2731–2738. doi:10.1161/CIRCULATIONAHA.106.653980

Hemmasizadeh, A., Tsamis, A., Cheheltani, R., Assari, S., D'Amore, A., Autieri, M., Kiani, M.F., Pleshko, N., Wagner, W.R., Watkins, S.C., Vorp, D., Darvish, K., 2015. Correlations between transmural mechanical and morphological properties in porcine thoracic descending aorta. Journal of the Mechanical Behavior of Biomedical Materials. 47, 12–20. doi:10.1016/j.jmbbm.2015.03.004

Hill, M.R., Duan, X., Gibson, G.A., Watkins, S., Robertson, A.M., 2012. A theoretical and non-destructive experimental approach for direct inclusion of measured collagen orientation and recruitment into mechanical models of the artery wall. Journal of Biomechanics, Special Issue on Cardiovascular Solid Mechanics 45, 762–771. doi:10.1016/j.jbiomech.2011.11.016

Huang, F., Thompson, J.C., Wilson, P.G., Aung, H.H., Rutledge, J.C., Tannock, L.R., 2008. Angiotensin II increases vascular proteoglycan content preceding and contributing to atherosclerosis development. Journal of Lipid Research. 49, 521–530. doi:10.1194/jlr.M700329-JLR200

Huang, Y.-K.K., Lin, C.-C.C., Lin, H.-S.S., 2015. Peritonitis as presentation of aorto-caval fistula with Salmonella choleraesuis-associated abdominal aortic aneurysm. Surgical Infections 16, 108–109. doi:10.1089/sur.2014.056

Humphrey, J.D., 2012. Possible mechanical roles of glycosaminoglycans in thoracic aortic dissection and associations with dysregulated transforming growth factor-β. Journal of Vascular Research. 50(10), 1–10 doi:10.1159/000342436

Humphrey, J.D., 2002. Cardiovascular Solid Mechanics. Springer: New York, NY. doi:10.1007/978-0-387-21576-1

Humphrey, J.D., Dufresne, E.R., Schwartz, M.A., 2014. Mechanotransduction and extracellular matrix homeostasis. Nature Reviews. Molecular Cell Biology. 15, 802–812. doi:10.1038/nrm3896

Humphrey, J.D., Eberth, J.F., Dye, W.W., Gleason, R.L., 2009. Fundamental role of axial stress in compensatory adaptations by arteries. Journal of Biomechanics. 42(1), 1–8. doi:10.1016/j.jbiomech.2008.11.011

Humphrey, J.D., Holzapfel, G.A., 2012. Mechanics, mechanobiology, and modeling of human abdominal aorta and aneurysms. Journal of Biomechanics. 45, 805–814. doi:10.1016/j.jbiomech.2011.11.021

Jensen, T., 1997. Pathogenesis of diabetic vascular disease: evidence for the role of reduced heparan sulfate proteoglycan. Diabetes 46(Suppl 2), S98–100. doi:10.2337/diab.46.2.S98

John, L.C.H., 2009. Biomechanics of coronary artery and bypass graft disease: potential new approaches. Annals of Thoracic Surgery. 87, 331–338. doi:10.1016/j.athoracsur.2008.07.023

Kim, J., Baek, S., 2011. Circumferential variations of mechanical behavior of the porcine thoracic aorta during the inflation test. Journal of Biomechanics. 44, 1941–1947. doi:10.1016/j.jbiomech.2011.04.022

Lai, W.M., Hou, J.S., Mow, V.C., 1991. A triphasic theory for the swelling and deformation behaviors of articular cartilage. Journal of Biomechanical Engineering. 113, 245–258. doi:10.1115/1.2894880

Lanir, Y., 1979. A structural theory for the homogeneous biaxial stress-strain relationships in flat collagenous tissues. Journal of Biomechanics. 12, 423–436. doi:10.1016/0021-9290(79)90027-7

Lee, R.T., Yamamoto, C., Feng, Y., Potter-Perigo, S., Briggs, W.H., Landschulz, K.T., Turi, T.G., Thompson, J.F., Libby, P., Wight, T.N., 2001. Mechanical Strain Induces Specific Changes in the Synthesis and Organization of Proteoglycans by Vascular Smooth Muscle Cells. Journal of Biological Chemistry. 276, 13847–13851. doi:10.1074/jbc.M010556200

Lee, Y.U., Naito, Y., Kurobe, H., Breuer, C.K., Humphrey, J.D., 2013. Biaxial mechanical properties of the inferior vena cava in C57BL/6 and CB-17 SCID/bg mice. Journal of Biomechanics. 46, 2277–2282. doi:10.1016/j.jbiomech.2013.06.013

Legerlotz, K., Riley, G.P., Screen, H.R.C., 2013. GAG depletion increases the stress-relaxation response of tendon fascicles, but does not influence recovery. Acta Biomaterialia. 9, 6860–6866. doi:10.1016/j.actbio.2013.02.028

Lewis, P.N., Pinali, C., Young, R.D., Meek, K.M., Quantock, A.J., Knupp, C., 2010. Structural Interactions between Collagen and Proteoglycans Are Elucidated by Three-Dimensional Electron Tomography of Bovine Cornea. Structure 18, 239–245. doi:10.1016/j.str.2009.11.013

Li, D., Xu, D., Li, P., Wei, J., Yang, K., Zhao, C., 2013. Viscoelastic evaluation of fetal umbilical vein for reconstruction of middle cerebral artery. Neural Regeneration Research. 8, 3055–3062. doi:10.3969/j.issn.1673-5374.2013.32.009

Lillie, M.A., Gosline, J.M., 2006. Tensile residual strains on the elastic lamellae along the porcine thoracic aorta. Journal of Vascular Research. 43, 587–601. doi:10.1159/000096112

Lillie, M.A., Gosline, J.M., 2002. Effects of lipids on elastin’s viscoelastic properties. Biopolymers 64, 127–38. doi:10.1002/bip.10154

Lillie, M.A., Gosline, J.M., 1996. Swelling and viscoelastic properties of osmotically stressed elastin. Biopolymers 39, 641–52. doi:10.1002/(SICI)1097-0282(199611)39:5<641::AID-BIP3>3.0.CO;2-W

Lin, C.H., Kao, Y.C., Lin, Y.H., Ma, H., Tsay, R.Y., 2016. A fiber-progressive-engagement model to evaluate the composition, microstructure, and nonlinear pseudoelastic behavior of porcine arteries and decellularized derivatives. Acta

Biomaterialia. 46, 101–111. doi:10.1016/j.actbio.2016.09.025

Linka, K., Khiêm, V.N., Itskov, M., 2016. Multi-scale modeling of soft fibrous tissues based on proteoglycan mechanics. Journal of Biomechanics. 49, 2349–2357. doi:10.1016/j.jbiomech.2016.02.049

Little, P.J., Ballinger, M.L., Osman, N., 2007. Vascular wall proteoglycan synthesis and structure as a target for the prevention of atherosclerosis, Vascular Health and Risk Management. 3(1), 117–124.

Lovekamp, J.J., Simionescu, D.T., Mercuri, J.J., Zubiate, B., Sacks, M.S., Vyavahare, N.R., 2006. Stability and function of glycosaminoglycans in porcine bioprosthetic heart valves. Biomaterials 27, 1507–1518. doi:10.1016/j.biomaterials.2005.08.003

Lu, D.Y., Chen, E.Y., Wong, D.J., Yamamoto, K., Protack, C.D., Williams, W.T., Assi, R., Hall, M.R., Sadaghianloo, N., Dardik, A., 2014. Vein graft adaptation and fistula maturation in the arterial environment. Journal of Surgical Research. 188(1), 162–173. doi:10.1016/j.jss.2014.01.042

Lüscher, T.F., Predel, H.G., Yang, Z., Bühler, F.R., von Segesser, L., Turina, M., 1992. Implications of pulsatile stretch on growth of saphenous vein and mammary artery smooth muscle. Lancet 340, 878–879. doi:10.1016/0140-6736(92)93287-W

Maroudas, A., 1976. Balance between swelling pressure and collagen tension in normal and degenerate cartilage. Nature 260, 808–809. doi:10.1038/260808a0

Martinez-Lemus, L.A., Hill, M.A., Meininger, G.A., 2009. The plastic nature of the vascular wall: a continuum of remodeling events contributing to control of arteriolar diameter and structure. Physiology. 24, 45–57. doi:10.1152/physiol.00029.2008

Mattson, J.M., Turcotte, R., Zhang, Y., 2016. Glycosaminoglycans contribute to extracellular matrix fiber recruitment and arterial wall mechanics. Biomechanics and Modeling in Mechanobiology. 16, 1–13. doi:10.1007/s10237-016-0811-4

McGilvray, K.C., Sarkar, R., Nguyen, K., Puttlitz, C.M., 2010. A biomechanical analysis of venous tissue in its normal and post-phlebitic conditions. Journal of Biomechanics. 43, 2941–2947. doi:10.1016/j.jbiomech.2010.07.012

Menashi, S., Campa, J.S., Greenhalgh, R.M., Powell, J.T., 1987. Collagen in abdominal aortic aneurysm: typing, content, and degradation. Journal of Vascular Surgery. 6, 578–582.

Miyake, T., Aoki, M., Morishita, R., 2008. Inhibition of anastomotic intimal hyperplasia using a chimeric decoy strategy against NFkappaB and E2F in a rabbit model. Cardiovascular Research. 79, 706–714. doi:10.1093/cvr/cvn139

Monos, E., Berczi, V., Nadasy, G., Bérczi, V., Nádasy, G., 1995. Local control of veins: biomechanical, metabolic, and humoral aspects. Physiological Reviews. 75, 611–666. doi:10.1007/BF00980145

Mow, V.C., Kuei, S.C., Lai, W.M., Armstrong, C.G., 1980. Biphasic Creep and Stress Relaxation of Articular Cartilage in Compression: Theory and Experiments. Journal of Biomechanical Engineering. 102, 73–84. doi:10.1115/1.3138202

Murienne, B.J., Jefferys, J.L., Quigley, H.A., Nguyen, T.D., 2015. The effects of glycosaminoglycan degradation on the mechanical behavior of the posterior porcine sclera. Acta Biomaterialia. 12, 195–206. doi:10.1016/j.actbio.2014.10.033

Ng, S., Tan, K.A.L., Anil, G., 2015. The role of interventional radiology in complications associated with liver transplantation. Clinical Radiology. 70(12), 1323–1335. doi:10.1016/j.crad.2015.07.005

O'Connell, M.K., Murthy, S., Phan, S., Xu, C., Buchanan, J.A., Spilker, R., Dalman, R.L., Zarins, C.K., Denk, W., Taylor, C.A., 2008. The three-dimensional micro- and nanostructure of the aortic medial lamellar unit measured using 3D confocal and electron microscopy imaging. Matrix Biology. 27, 171–181. doi:10.1016/j.matbio.2007.10.008

Owens, C.D., Gasper, W.J., Rahman, A.S., Conte, M.S., 2015. Vein graft failure. Journal of Vascular Surgery. 61, 203–216. doi:10.1016/j.jvs.2013.08.019

Pierce, D.M., Maier, F., Weisbecker, H., Viertler, C., Verbrugghe, P., Famaey, N., Fourneau, I., Herijgers, P., Holzapfel, G.A., 2015. Human thoracic and abdominal aortic aneurysmal tissues: Damage experiments, statistical analysis and constitutive modeling. Journal of the Mechanical Behavior of Biomedical Materials. 41, 92–107. doi:10.1016/j.jmbbm.2014.10.003

Polzer, S., Gasser, T.C., Novak, K., Man, V., Tichy, M., Skacel, P., Bursa, J., 2015. Structure-based constitutive model can accurately predict planar biaxial properties of aortic wall tissue. Acta Biomaterialia. 14, 133–145. doi:10.1016/j.actbio.2014.11.043

Provenzano, P., Lakes, R., Keenan, T., Vanderby, R., 2001. Nonlinear ligament viscoelasticity. Annals of Biomedical Engineering. 29, 908–914. doi:10.1114/1.1408926

Quint, C., Kondo, Y., Manson, R.J., Lawson, J.H., Dardik, A., Niklason, L.E., 2011. Decellularized tissue-engineered blood vessel as an arterial conduit. Proceedings of the National Academy of Sciences of the United States of America. 108, 9214–9219. doi:10.1073/pnas.1019506108

Reinboth, B., Hanssen, E., Cleary, E.G., Gibson, M.A., 2002. Molecular Interactions of Biglycan and Decorin with Elastic Fiber Components. Journal of Biological Chemistry. 277, 3950–3957. doi:10.1074/jbc.M109540200

Rigozzi, S., Müller, R., Stemmer, A., Snedeker, J.G., 2013. Tendon glycosaminoglycan proteoglycan sidechains promote collagen fibril sliding-AFM observations at the nanoscale. Journal of Biomechanics. 46, 813–818. doi:10.1016/j.jbiomech.2012.11.017

Robinson, P.S., Lin, T.W., Reynolds, P.R., Derwin, K.A., Iozzo, R. V., Soslowsky, L.J., 2004. Strain-rate sensitive mechanical properties of tendon fascicles from mice with genetically engineered alterations in collagen and decorin. Journal of Biomechanical Engineering. 126, 252–257. doi:10.1115/1.1695570

Roccabianca, S., Ateshian, G.A., Humphrey, J.D., 2014. Biomechanical roles of medial pooling of glycosaminoglycans in thoracic aortic dissection. Biomechanics and Modeling in Mechanobiology. 13, 13–25. doi:10.1007/s10237-013-0482-3

Roccabianca, S., Bellini, C., Humphrey, J.D., 2014. Computational modelling suggests good, bad and ugly roles of glycosaminoglycans in arterial wall mechanics and mechanobiology. Journal of the Royal Society, Interface 11, 20140397. doi:10.1098/rsif.2014.0397

Roccabianca, S., Figueroa, C.A., Tellides, G., Humphrey, J.D., 2014. Quantification of regional differences in aortic stiffness in the aging human. Journal of the Mechanical Behavior of Biomedical Materials. 29, 618–634. doi:10.1016/j.jmbbm.2013.01.026

Rossmann, J.S., 2010. Elastomechanical properties of bovine veins. Journal of the Mechanical Behavior of Biomedical Materials. 3, 210–215. doi:10.1016/j.jmbbm.2009.06.003

Sacks, M.S., Chuong, C.J., 1998. Orthotropic Mechanical Properties of Chemically Treated Bovine Pericardium. Annals of Biomedical Engineering. 26, 892–902. doi:10.1114/1.135

Safar, M.E., London, G.M., 1985. Venous system in essential hypertension. Clinical Science. 69, 497–504.

Schaefer, L., Schaefer, R.M., 2010. Proteoglycans: from structural compounds to signaling molecules. Cell and Tissue Research. 339, 237–246. doi:10.1007/s00441-009-0821-y

Schram, M.T., Henry, R.M.A., Van Dijk, R.A.J.M., Kostense, P.J., Dekker, J.M., Nijpels, G., Heine, R.J., Bouter, L.M., Westerhof, N., Stehouwer, C.D.A., 2004. Increased Central Artery Stiffness in Impaired Glucose Metabolism and Type 2 Diabetes: The

Hoorn Study. Hypertension 43, 176–181. doi:10.1161/01.HYP.0000111829.46090.92

Schriefl, A.J., Zeindlinger, G., Pierce, D.M., Regitnig, P., Holzapfel, G.A., 2012. Determination of the layer-specific distributed collagen fibre orientations in human thoracic and abdominal aortas and common iliac arteries. Journal of the Royal Society. Interface 9, 1275–1286. doi:10.1098/rsif.2011.0727

Scott, J.E., 2003. Elasticity in extracellular matrix “shape modules” of tendon, cartilage, etc. A sliding proteoglycan-filament model. Journal of Physiology. 553, 335–343. doi:10.1113/jphysiol.2003.050179

Seidel, C.L., Lewis, R.M., Bowers, R., Bukoski, R.D., Kim, H.S., Allen, J.C., Hartley, C., 1984. Adaptation of canine saphenous veins to grafting. Correlation of contractility and contractile protein content. Circulation Research. 55, 102–109.

Sell, D.R., Monnier, V.M., 2012. Molecular basis of arterial stiffening: Role of glycation-a mini-review. Gerontology 58, 227–237. doi:10.1159/000334668

Silver, F.H., Snowhill, P.B., Foran, D.J., 2003. Mechanical behavior of vessel wall: A comparative study of aorta, vena cava, and carotid artery. Annals of Biomedical Engineering. 31, 793–803. doi:10.1114/1.1581287

Sohn, S., Rothman, A., Shiota, T., Luk, G., Tong, A., Swensson, R.E., Sahn, D.J., 1994. Acute and follow-up intravascular ultrasound findings after balloon dilation of coarctation of the aorta. Circulation 90, 340–347. doi:10.1161/01.cir.90.1.340

Sokolis, D.P., 2013. Experimental investigation and constitutive modeling of the 3D histomechanical properties of vein tissue. Biomechanics and Modeling in Mechanobiology. 12, 431–451. doi:10.1007/s10237-012-0410-y

Sokolis, D.P., 2007. Passive mechanical properties and structure of the aorta: Segmental analysis. Acta Physiologica. 190, 277–289. doi:10.1111/j.1748-1716.2006.01661.x

Sorrentino, T.A., Fourman, L., Ferruzzi, J., Miller, K.S., Humphrey, J.D., Roccabianca, S., 2015. Local Versus Global Mechanical Effects of Intramural Swelling in Carotid Arteries. Journal of Biomechanical Engineering. 137, 041008–041008. doi:10.1115/1.4029303

Stehouwer, C.D.A., Ferreira, I., 2006. Diabetes, lipids and other cardiovascular risk factors, in: Arterial Stiffness in Hypertension. Elsevier, p. 427.

Stone, J.E., Akhtar, N., Botchway, S., Pennock, C.A., 1994. Interaction of 1,9-Dimethylmethylene Blue with Glycosaminoglycans. Annals of Clinical Biochemistry. 31, 147–152. doi:10.1177/000456329403100206

Sun, H., Zhong, M., Miao, Y., Ma, X., Gong, H.P., Tan, H.W., Zhang, Y., Zhang, W., 2009. Impaired elastic properties of the aorta in fat-fed, streptozotocin-treated rats: Cardiology 114, 107–113. doi:10.1159/000219211

Taghizadeh, H., Tafazzoli-Shadpour, M., 2017. Characterization of mechanical properties of lamellar structure of the aortic wall: Effect of aging. Journal of the Mechanical Behavior of Biomedical Materials. 65, 20–28. doi:10.1016/j.jmbbm.2016.08.011

Takahashi, A., Majumdar, A., Parameswaran, H., Bartolák-Suki, E., Suki, B., 2014. Proteoglycans maintain lung stability in an elastase-treated mouse model of emphysema. American Journal of Respiratory Cell and Molecular Biology. 51, 26–33. doi:10.1165/rcmb.2013-0179OC

Tan, X., Sanderson, M.J., 2014. Bitter tasting compounds dilate airways by inhibiting airway smooth muscle calcium oscillations and calcium sensitivity. British Journal of Pharmacology. 171, 646–662. doi:10.1111/bph.12460

Tovar, a. M.F., Cesar, D.C.F., Leta, G.C., Mourao, P. a. S., 1998. Age-Related Changes in Populations of Aortic Glycosaminoglycans : Species With Low Affinity for Plasma Low-Density Lipoproteins, and Not Species With High Affinity, Are Preferentially Affected. Arteriosclerosis, Thrombosis, and Vascular Biology. 18, 604–614. doi:10.1161/01.ATV.18.4.604

Tsamis, A., Krawiec, J.T., Vorp, D. a, 2013. Elastin and collagen fibre microstructure of the human aorta in ageing and disease: a review. Journal of the Royal Society, Interface 10, 20121004. doi:10.1098/rsif.2012.1004

Turcotte, R., Mattson, J., Wu, J., Zhang, Y., Lin, C., 2016. Molecular order of arterial collagen using circular polarization second-harmonic generation imaging. Biophysical Journal. 110(3), 530–533. doi: 10.1016/j.bpj.2015.12.030

Vishwanath, V., Frank, K.E., Elmets, C.A., Dauchot, P.J., Monnier, V.M., 1986. Glycation of skin collagen in type I diabetes mellitus. Correlation with long-term complications. Diabetes 35, 916–921.

Vlassara, H., Brownlee, M., Cerami, A., 1986. Nonenzymatic glycosylation: role in the pathogenesis of diabetic complications. Clinical Chemistry. 32, B37–41.

Vorp, D.A., 2007. Biomechanics of abdominal aortic aneurysm. Journal of Biomechanics. 40, 1887–1902. doi:10.1016/j.jbiomech.2006.09.003

Wachtel, H., Jackson, B.M., Bartlett, E.K., Karakousis, G.C., Roses, R.E., Bavaria, J.E., Fraker, D.L., 2015. Resection of primary leiomyosarcoma of the inferior vena cava (IVC) with reconstruction: A case series and review of the literature. Journal of Surgical Oncology. 111, 328–333. doi:10.1002/jso.23798

Wagenseil, J.E., Mecham, R.P., 2009. Vascular Extracellular Matrix and Arterial Mechanics. Physiological Reviews. 89, 957–989. doi:10.1152/physrev.00041.2008

Wang, F., Kim, M.S., Puthanveetil, P., Kewalramani, G., Deppe, S., Ghosh, S., Abrahani, A., Rodrigues, B., 2009. Endothelial heparanase secretion after acute hypoinsulinemia is regulated by glucose and fatty acid. American Journal of Physiology. Heart and Circulatory Physiology. 296, H1108–1116. doi:10.1152/ajpheart.01312.2008

Wang, Y., Zeinali-Davarani, S., Zhang, Y., 2016. Arterial mechanics considering the structural and mechanical contributions of ECM constituents. Journal of Biomechanics. 49, 2358–2365. doi:10.1016/j.jbiomech.2016.02.027

Weisbecker, H., Unterberger, M.J., Holzapfel, G.A., 2015. Constitutive modelling of arteries considering fibre recruitment and three-dimensional fibre distribution. Journal of the Royal Society, Interface 12, 20150111-. doi:10.1098/rsif.2015.0111

WHO, 2004. International Diabetes Federation 2015, 2040.

Wight, T.N., 1989. Cell biology of arterial proteoglycans. Arteriosclerosis 9, 1–20. doi:10.1161/01.ATV.9.1.1

Wight, T.N., 1980. Vessel proteoglycans and thrombogenesis. Progress in Hemostasis and Thrombosis. 5, 1–39.

Wight, T.N., Merrilees, M.J., 2004. Proteoglycans in atherosclerosis and restenosis: Key roles for versican. Circulation Research. 94, 1158–1167. doi:10.1161/01.RES.0000126921.29919.51

Winlove, C.P., Parker, K.H., 1990. Influence of solvent composition on the mechanical properties of arterial elastin. Biopolymers 29, 729–35. doi:10.1002/bip.360290407

Winlove, C.P., Parker, K.H., Avery, N.C., Bailey, A.J., 1996. Interactions of elastin and aorta with sugars in vitro and their effects on biochemical and physical properties. Diabetologia 39, 1131–1139.

Zarkovic, K., Larroque-Cardoso, P., Pucelle, M., Salvayre, R., Waeg, G., N?gre-Salvayre, A., Zarkovic, N., 2015. Elastin aging and lipid oxidation products in human aorta. Redox Biology. 4, 109–117. doi:10.1016/j.redox.2014.12.008

Zeinali-Davarani, S., Chow, M.-J., Turcotte, R., Zhang, Y., 2013. Characterization of Biaxial Mechanical Behavior of Porcine Aorta under Gradual Elastin Degradation. Annals of Biomedical Engineering. 41, 1528–1538. doi:10.1007/s10439-012-0733-y

Zeinali-Davarani, S., Wang, Y., Chow, M.-J., Turcotte, R., Zhang, Y., 2015. Contribution of collagen fiber undulation to regional biomechanical properties along porcine thoracic aorta. Journal of Biomechanical Engineering. 137, 51001. doi:10.1115/1.4029637

Zeller, P.J., Skalak, T.C., 1998. Contribution of individual structural components in determining the zero-stress state in small arteries. Journal of Vascular Research. 35, 8–17. doi:10.1159/000025560

Zhu, W., Iatridis, J.C., Hlibczuk, V., Ratcliffe, A., Mow, V.C., 1996. Determination of collagen-proteoglycan interactions in vitro. Journal of Biomechanics. 29, 773–783. doi:10.1016/0021-9290(95)00136-0

Zou, Y., Zhang, Y., 2011. The orthotropic viscoelastic behavior of aortic elastin. Biomechanics and Modeling in Mechanobiology. 10, 613–625. doi:10.1007/s10237-010-0260-4

Zulliger, M.A., Fridez, P., Hayashi, K., Stergiopulos, N., 2004. A strain energy function for arteries accounting for wall composition and structure. Journal of Biomechanics. 37, 989–1000. doi:10.1016/j.jbiomech.2003.11.026

CURRICULUM VITAE

[redacted]

[redacted]

[redacted]

[redacted]